POLITECNICO DI MILANO

SCUOLA DI INGEGNERIA INDUSTRIALE E DELL'INFORMAZIONE
Dipartimento di Elettronica, Informazione e Bioingegneria
Corso di Laurea Magistrale in Ingegneria Elettrica

A Grid-Connected Inverter controller with PMU capability

Tesi di laurea di:
Roberto NICOLOSI
Matricola 818153

Relatore:
Prof. Luigi PIEGARI

Correlatore:
Dott. Andrea BENIGNI

Anno Accademico 2014-2015

Alla mia famiglia
che mi sostiene in ogni lotta,
che mi aiuta oggi a diventare la persona che sarò domani.

—

A tutte le persone che stimo,
passate, presenti e future,
che arricchiscono la mia vita

Contents

Introduction 1

1 Phasor Measurement Unit 5
- 1.1 Historical Overview . . . 5
- 1.2 Synchrophasors . . . 6
- 1.3 Time Synchronization Systems . . . 9
  - 1.3.1 Global Positioning System . . . 10
  - 1.3.2 Global Navigation Satellite System (GLONASS) . . . 12
  - 1.3.3 GALILEO . . . 13
  - 1.3.4 Synchronization Distribution Methods . . . 13
- 1.4 IEEE Standards . . . 15
  - 1.4.1 Birth and progresses . . . 15
  - 1.4.2 Standard C37.118-2011 . . . 18
- 1.5 Algorithms for synchrophasor estimation . . . 24
- 1.6 Applications and Deployment . . . 28

2 Grid-Connected converters 33
- 2.1 Grid integration of renewable resources . . . 33
  - 2.1.1 Wind turbine systems . . . 36
  - 2.1.2 Photovoltaic systems . . . 38
  - 2.1.3 Role of converters in renewable energy systems . . . 41
- 2.2 Grid-tied converter control . . . 47
  - 2.2.1 Current control . . . 49
  - 2.2.2 DC bus control . . . 57
  - 2.2.3 Grid synchronization . . . 61

3 Auxiliary Services in RES 67
- 3.1 Auxiliary services . . . 69
  - 3.1.1 Frequency regulation . . . 71
  - 3.1.2 Voltage regulation . . . 72
  - 3.1.3 Reserves . . . 73
  - 3.1.4 Black start capability . . . 74
  - 3.1.5 Other services . . . 75
- 3.2 Grid Requirements . . . 77
  - 3.2.1 Static requirements . . . 77
  - 3.2.2 Dynamic requirements . . . 80
- 3.3 Converter control for ancillary services . . . 82

3.3.1 Voltage grid support 82
3.3.2 Harmonic Compensation 87
3.3.3 Anti-islanding Detection 91

4 Smart Controller **99**
4.1 Hardware and design 100
4.1.1 Control design 102
4.1.2 PMU design 107
4.2 Implementation 109
4.2.1 FPGA and sampling process 109
4.2.2 Control system 113
4.3 Experimental validation with HIL 118
4.3.1 Results 120

Conclusion **131**

Bibliography **135**

List of Figures

1.1 First PMU prototype . . . 6
1.2 Generic sinusoid and its phasor representation . . . 7
1.3 Block diagram of a Phasor Measurement Unit . . . 8
1.4 Synchrophasor Data Network . . . 9
1.5 GNSS working principle . . . 10
1.6 Synchronization time sources . . . 14
1.7 Convention for synchrophasor representation . . . 18
1.8 Phase evaluation . . . 19
1.9 The TVE criterion . . . 20
1.10 TVE limited values for compliance test . . . 21
1.11 Required PMU reporting rates . . . 22
1.12 Phasor Timetagging . . . 23
1.13 Dynamic test example . . . 24
1.14 Qualitative behaviour of dynamic phasor model in the frequency domain . . . 27
1.15 PMU deployment for WISP project . . . 29

2.1 IRENA LCOE . . . 34
2.2 Grid-connected RES . . . 35
2.3 Basic power conversion wind turbine system . . . 36
2.4 WT with synchronous or induction generator . . . 38
2.5 PV system . . . 39
2.6 Grid-connected PV systems . . . 40
2.7 General control function blocks for wind turbine systems . . . 42
2.8 Three-phase back-to-back converter for wind turbines . . . 42
2.9 Three-phase back-to-back converter for wind turbines . . . 43
2.10 Multicell converter with paralleled 2L-VSC converter cells with multi-winding generator . . . 43
2.11 General control function blocks for photovoltaic systems . . . 44
2.12 H5 inverter by SMA . . . 45
2.13 HERIC inverter . . . 46
2.14 qZSI inverter with battery for PV power generation . . . 47
2.15 Overall scheme of the LCL filter grid converter control . . . 48
2.16 Reference scheme for DC voltage control . . . 49
2.17 PI current control . . . 50
2.18 PR current control . . . 53
2.19 Deadbeat controller block diagram . . . 55

2.20 Reference scheme for DC voltage control . . . 59
2.21 DC voltage control block diagram . . . 60
2.22 Phase-locked loop structure . . . 62
2.23 Block diagram of basic PLL in Laplace domain . . . 63
2.24 Block diagram of a PLL with quadrature signal generator . . . 64

3.1 Wind Power Global Capacity trend from 2004 to 2014 . . . 68
3.2 Solar Power Global Capacity trend from 2004 to 2014 . . . 68
3.3 Simplified block diagram for frequency regulation . . . 71
3.4 Characteristic curves $cos\phi = f(P)$ . . . 79
3.5 Standard characteristic curves Q=f(V) . . . 79
3.6 Active power limiting ramp for over frequency occurrences . . . 80
3.7 LVRT requirements in italian power system . . . 81
3.8 V-t voltage profile for static generating units . . . 82
3.9 Power flow through a line and its relative phasor diagram . . . 83
3.10 Voltage droop characteristic . . . 84
3.11 . . . 86
3.12 PCC connection of a DG resource in distribution line . . . 87
3.13 Compensating algorithm block diagram . . . 90
3.14 Alternative harmonic detector . . . 90
3.15 Representative scheme for converter connection in LV lines . . . 91
3.16 ADF current signal . . . 94
3.17 Converter equivalent model . . . 95
3.18 PLL block model . . . 96
3.19 PLL submodels . . . 96

4.1 NI-9035 hardware configuration . . . 101
4.2 Control System . . . 103
4.3 Voltage control by varying m_a . . . 106
4.4 Prototype block diagram . . . 107
4.5 Dataframe organization according to C37.118 . . . 109
4.6 Prototype Block Diagram . . . 110
4.7 FPGA clock synchronization in LabVIEW . . . 112
4.8 Direct Memory Access FIFO . . . 113
4.9 Control system Simulink model . . . 114
4.10 Detail of the control subsystem . . . 114
4.11 Step change in current reference with steady-state error . . . 116
4.12 FPGA user interface . . . 117
4.13 CPU user interface . . . 118
4.14 CPU user interface . . . 119
4.15 Simulink model for real time simulation with Hardware in the Loop 120
4.16 Hardware In the Loop testing set-up . . . 120
4.17 Laboratory configuration . . . 121
4.18 NI-cRIO connections to lab testbench . . . 121
4.19 PWM generated signal . . . 122
4.20 Controlled three-phase steady state current . . . 122
4.21 DFT algorithm testing . . . 123

4.22 Power step change P=5 and 10kW and Q costant 123
4.23 Power step change Q=5 and 10kW and P constant 124
4.24 Current responses to power step changes: P:3kW and Q=3kVar and P=6kW and Q=6kVar 124
4.25 Current responses to power step changes: P:1kW and Q=1kVar and P=8kW and Q=8kVar 124
4.26 Power responses to power step changes: P:1kW and Q=1kVar and P=8kW and Q=8kVar 124
4.27 Current transient response 125
4.28 Open PDC interface with real-time phasor datastreaming 126
4.29 Real time phasor visualization for injected power P=10kW and Q=0KW 126
4.30 Real time phasor visualization for injected power P=3kW and Q=-3KW 127
4.31 Real time phasor visualization for injected power P=3kW and Q=3KW 127
4.32 Phasor magnitude transient evolution 128
4.33 Phasor angle transient evolution 128

Sommario

Durante gli ultimi dieci anni, in seguito alla liberarizzazione del mercato dell'energia, la configurazione del sistema elettrico è mutata sempre di più grazie soprattutto alla crescente penetrazione di sistemi di generazione diffusa che, allacciandosi alle reti di media e bassa tensione, stanno cambiando le caratteristiche del flusso di potenza all'interno della rete da una condizione di unidirezionalità ad una di bidirezionalità. Questo sostanziale cambiamento sta mettendo a repentaglio la stabilità del sistema elettrico e ha fatto nascere nuove problematiche nella gestione della rete. Per questo motivo, la comunità scientifica internazionale ha da qualche anno proposto un nuovo concetto di rete elettrica che tramite un cambio di paradigma possa superare queste nuove difficoltà: le smart grid. Una smart grid è una rete elettrica che si appoggia su un sistema di comunicazione affidabile tra i vari punti della rete e su un sistema di controllo distribuito capillarmente su vaste aree. Basandosi su logiche di controllo automatiche e locali, le smart grid permettono di migliorare le capacità di gestione del sistema elettrico garantendo una più facile integrazione della generazione diffusa, di cui le risorse rinnovabili fanno parte. La transizione verso un concetto di rete intelligente passa tramite l'installazione delle PMU, dispositivi in grado di effettuare misure fasoriali universalmente sincronizzate tramite segnale GPS, che garantiscono, tramite opportuni canali di comunicazione, le necessarie informazioni sulla rete per operare sistemi di controllo e analisi. Tuttavia, la diffusione delle PMU nelle reti di media e bassa tensione sta riscontrando delle difficoltà legate prevalentemente alle caratteristiche delle reti e dai costi superiori che ne derivano. In questo lavoro si propone dunque l'implementazione di una PMU in un controllore per convertitori di potenza, dispositivi sempre presenti e necessari negli impianti di generazione distribuita. Il convertitore di potenza d'interfaccia con la rete elettrica è infatti dotato di un'unità di calcolo che, a parte qualche modifica, presenta tutti i requisiti per la realizzazione di una PMU e potrebbe dunque fungere da veicolo per una maggiore diffusione di tali unità di misura. Questa tesi tratta dunque del funzionamento e delle caratteristiche delle PMU e del controllo dei convertitori di potenza per l'interfacciamento di sorgenti distribuite alla rete, evidenziando in particolare la fornitura di servizi ausiliari che al giorno d'oggi è richiesta sempre di più. Infine, nell'ultimo capitolo, viene discussa l'implementazione di un prototipo di controllore intelligente con funzione di PMU su una scheda NI-cRIO 9035, al fine di individuare le problematiche ingegnerestiche che potrebbero sorgere durante il progetto di un tale dispositivo. Il sistema è infine testato usando tecniche con Hardware in the Loop.

Abstract

During the last ten years, following the energy market liberalization, the electrical system configuration has been changing continuously mainly due to the increasing penetration level of distributed generating systems. Those systems, connected to the medium and low voltage grid, are modifying the network power flow from unidirectional to bidirectional. This remarkable change is threatening the electrical system stability and it has brought about new challenges in the network management. For this reason, in the past few years, the international scientific community has proposed a new concept of electrical grid capable of overcoming these new difficulties: the smart grids. A smart grid is an electrical grid that leans on a reliable communication system connecting different points of the network and on a wide area control system. Based on local and automatic control logics, the smart grids would allow an improvement of the management capacity of the electrical system, ensuring an easier integration of distributed generating units, to which renewable resources belong. The transition to a smart grid concept goes through the installation of the PMUs, devices able to perform phasorial measurement universally synchronized by means of a GPS signal. The PMUs would provide, through proper communication channels, the necessary information about the grid to enable the operation of analysis and control systems. Nevertheless, the diffusion of the PMUs in medium and low voltage networks is facing some difficulties caused mainly by different grid characteristics and, by consequence, increased costs. Considering the necessary presence of power conversion systems into distributed generating units, the implementation of a PMU into a power converter controller is proposed in this work. A grid-connected power converter is, indeed, provided of almost all that is needed to implement a PMU and, therefore, can be used as a mean to enhance the diffusion of these measurement units. This thesis deals with the operation and the characteristics of PMUs and with the grid-connected power converters control systems for distributed resources, highlighting in particular ancillary services provision that nowadays is more and more requested. In the last chapter, the implementation of a smart controller prototype with PMU capabilities in a NI-cRIO 9035 board is discussed to address the main problems that may arise during the design process of such a device. The device is eventually tested using Hardware in the Loop techniques.

Out-of-control emotions can make smart people stupid.
Emotional aptitude is a "meta-ability" that determines how well we can use whatever other skills we possess, including raw intellect.

— Daniel Goleman

Ringraziamenti

Un sentito ringraziamento va al Chiar.mo Prof. Luigi Piegari che mi ha aiutato ad ampliare il mio bagaglio sia scientifico che umano, dandomi la grande opportunità di svolgere questo lavoro di ricerca all'estero. Con la sua grande disponibilità e correttezza mi ha seguito e indirizzato durante questo lavoro di tesi, garantendomi sempre saggi e opportuni suggerimenti che hanno contribuito ad innalzare il livello del mio lavoro.

Una profonda gratitudine è dedicata verso il Dott. Andrea Benigni sotto la cui costante supervisione ho svolto questo lavoro presso la *University of South Carolina, Columbia*. Egli non solo mi ha guidato durante il mio studio ma ha costituito un punto di riferimento essenziale dentro e fuori il laboratorio.

Palermo, Italia, Aprile 2016 R. N.

Introduction

Since the early diffusion of electrical energy, grid topology has always been considered as the composition of two distinct structures, the transmission grid and the distribution grid. The transmission grid is a meshed structure, covering long distances, used to bring the power generated by a small number of large production plants, to electrical substations spread in those areas where the energy needs to be delivered. Complementary, the distribution grid is a radial system that capillary connects the transmission substations to the various sites where the energy is really needed and consumed. The power flow of this type of network has always been mainly unidirectional, from big power plants to the customers, leading to certain system characteristics that have been exploited to design the majority of equipment and protection devices and to plan management strategies to make the whole power system reliable.

However, the beginning of the 21st century is distinguished by an ongoing social paradigm shift that is characterized by a growing sensitivity of the world population towards the preservation of the planet and sustainable development. This ongoing change, together with the energy market liberalization, has led the international electrical engineering community to focus its attention towards new technological developments, regarding transmission and distribution grids, aiming to increase the penetration in the system of renewable resources at distribution level.

The general trend is directed to the application of an innovative approach to manage the actual electrical grid, addressed to take advantage and to be compliant with cutting-edge technologies and to answer to changing market demands of the actual era. In line with the recent innovations in the field of telecommunication, the acknowledged name for this new idea of electrical network is "smart grid", a name that by itself helps to highlight the difference with a traditional concept of grid.

The term "smart grid" generally refers to all those devices and technological achievements used to bring electricity delivery systems into the 21st century, using computer-based remote control and automation systems. Such innovation is made possible by two-way communication technology and computer processing that have been used for decades in other industries and that only now are beginning to be used on electricity networks, from the power plants, all the way to the consumers of electricity in homes and businesses[1].

Due to the new regulations concerning liberalization of the energy market, aiming to replace a monopoly with a competition regime, the increasing penetration level of Distributed Generation(DG) is another reason to bring such a revolution into the power system. DG indicates all those small and medium size power sources that are spread in different points of the distribution network and are

capable of injecting electrical power in the opposite direction with respect to the traditional unidirectional stream. Hence, other than renewable power sources, such as photovoltaic panels and wind turbines, DG units include other types of generation such as fuel cells, small diesel generators and, in the near future, also vehicle-to-grid connections. Typically, DG produces local changes in network configuration that leads to problems concerning protection coordination and energy dispatching. Hence, if wind farms and photovoltaic power plants become a considerable source of electrical power, it is necessary to no longer consider the distribution grid as a static system but as a dynamic one, in order to not compromise system reliability.

It appears clear now that, in order to achieve a more sustainable energy production and to encourage a further diffusion of green power sources, a development of the electrical network is imperative. It is in this scenario that smart grids are the most reasonable solution to these problems, having automation technology as their main feature that lets the utility adjust and control each individual device or millions of devices from a central location. The system, therefore, becomes "smart" like the brain controlling every part of the body.

The possibility of such grids, the smart ones, are several and they may change entirely the way the human being can handle its life. They offer many benefits to utilities and consumers such as big improvements in energy efficiency and in reliability of the whole power system[2].

The main challenge that smart grids have to face consists in a massive architecture transformation of the electrical network that ensures high communication capabilities, increased measurement accuracy and faster reporting rates. In light of this, a device such the Phasor Measurement Unit(PMU), capable of providing time synchronized measurements of voltage and current phasors, along with frequency and rate of change of frequency, becomes a fundamental tool to move a step closer towards the grid of the future.

Due to the wide range of possible applications, to encourage PMU's deployment, many Transmission System Operators have developed pilot projects that have led to the installation of hundreds of PMUs. Furthermore, several Intelligent Electronic Devices used in electric substations, mainly for protection purposes or other measurement instruments, have been updated to introduce PMU functionalities. However, the performance offered by current PMUs, which are normally suitable for applications in transmission grids, can be in some cases insufficient for the distribution systems. By consequence, considering also that distribution grids would require an higher number of units to be correctly observed, their deployment in these type of grids seems to be limited by the increasing costs and hardware.

On the other hand, in the past years, the increasing penetration level of distributed generating units and storage devices in distribution networks, has enhanced the development of power electronics source-to-grid interfaces. Nowadays, grid-connected power converters are no more limited to extract and inject active power from the source to the grid but, due to a growing need of system flexibility, they are also asked to provide auxiliary services for the power system. Hence, these converters require multi-functional control systems, implemented in powerful and performing computational units, that feed to their control loops voltage and current

measurements acquired at the point of connection.

In this thesis, to reduce the costs and the hardware required for PMUs deployment in distribution network, the implementation of PMU function into a grid-connected power converter controller is proposed. This work analyses the various functions of the proposed system, namely the PMU, the grid-interface control systems and the provision of auxiliary services. Lastly, the design and the implementation on real hardware of a prototype of the controller including the PMU function is described. Grid-connected converters have almost all that is needed to implement the PMU function and only a few additional pieces of hardware are needed. A converter of the proposed kind would fit perfectly into the scenario of smart grids, both as a tool to improve the system stability and as a monitoring device, becoming eventually a "smart converter".

This work is organized as follow:

The first chapter introduces the Phasor Measurement Units. In particular, the analysis focuses on the tasks that a PMU must accomplish, namely synchrophasor estimation and time synchronization. The IEEE standards for synchrophasor estimation is also presented and discussed. Lastly, an overview of the current state of PMU deployment process is provided.

The second chapter deals with the integration of the main renewable systems into the power grid by means of grid-connected converters. The role of the power electronic section is stressed, as well as the basic control function that allows a correct grid connection of these systems.

The third chapter discusses the provision of ancillary services in the network. In particular, the main ancillary services are defined and the requirements of the grid codes are presented. In the last section of this chapter the converter control for the main ancillary services provision is analysed.

The last chapter presents the experimental part of this thesis. The design and the implementation of a prototype of the proposed "smart controller" is described in detail. In particular in the first part of the chapter the hardware employed and the design process are discussed; in the second part the implementation of the system is described; in the third part the results of the experimental validation are shown and commented.

Concluding remarks are given at the end, enhancing the most interesting findings of this work and addressing possible future investigation.

Chapter 1

Phasor Measurement Unit

1.1 Historical Overview

Modern Phasor Measurement Unit systems can trace their origins to the development of the Symmetrical Component Distance Relay (SCDR) in the early 1970s. The computational power of that period was not capable of handling the requirements of a distance relay algorithm. This led to the invention of the SCDR in which the main novelty was that the relaying algorithm was based upon the measurement of positive, negative and zero sequence voltages and currents at the transmission line terminal. The advantage of this new algorithm was that it required processing of only one equation to determine fault location of all fault types that may occur on the system. Over time it became clear that microcomputers had become sufficiently capable so that this innovation was no longer required for line relaying. However, the fact that SCDR utilized efficient methods of measuring symmetrical components of voltages and currents proved to be very interesting for other applications. Indeed, positive sequence voltages and currents of an electrical network can be considered as the backbone of most power system analysis programs: stability, load flow, state estimation, short circuit detection, optimum power flow, contingency analysis, etc.[3].

To enable further developments for this technology it was necessary to synchronize in time the measurements retrieved in different part of the system for the main purpose of make them comparable between each others and, therefore, to allow further analysis. In the early 1980s some prototypes including a common time reference had been built and designed using different synchronization technique such as HBG radio transmissions(in Europe) and LORAN-C, GOES satellite transmissions. However, at that time these solutions lacked both in accuracy and in economic feasibility since the cost of receivers was still too high [4]. During the same years, at Virginia Tech University, another prototype of such measurement system was crafted. The difference with its likes was that it used a Global Positioning System(GPS) signal as time reference. This is now considered the first Phasor Measurement Unit in the world (see 1.1 on the following page). In fact, in the next years, GPS satellites network would have grown more letting the cost of the devices dropping down and, in the meanwhile, improving the accuracy of the reference time signal. Today, with the satellite system complete and fully deployed, a chip set

of the GPS receivers could be obtained for just a few hundred dollars. [5] It can be said that, nowadays, the technology of synchronized phasor measurements has finally come of age and most modern power systems around the world are in the process of implementing wide-area measurement systems consisting of the phasor measurement units.

Figure 1.1: First PMU prototype built and designed at Virginia Tech in 1980s

1.2 Synchrophasors

In the previous paragraph an historical overview of PMU evolution has been given but any technical aspect regarding the device has been considered. In this part of the elaborate, the device's working principle will be introduced as well as synchrophasor network elements and their interconnection.

A Phasor Measurement Unit is basically a device aimed to compute the main tone phasor (RMS value and phase) of three-phase voltages and currents at the point of measure using a standard synchronization signal as time reference for the measurement. Considering a generic sinusoidal signal, its mathematical expression in the continuous time domain is:

$$\begin{aligned} x(t) &= X_m \cos(2\pi f t + \phi) \\ &= \mathrm{Re}\{X_m e^{j(\omega t+\phi)}\} \\ &= \mathrm{Re}\{[e^{j\omega t}]X_m e^{j\phi}\}. \end{aligned} \tag{1.1}$$

By convention, the term $e^{j\omega t}$ is suppressed in the expression above, with the common understanding that the angular frequency is ω. The sinusoid of eq. (1.1) is represented by a complex number $\bar{X}$ known as its phasor representation:

$$x(t) \leftrightarrow \bar{X} = (X_m/\sqrt{2})e^{j\phi} = X_{\text{rms}}[\cos\phi + j\sin\phi] = X_r + jX_i \tag{1.2}$$

where X_{rms} is the root mean square value of the sinusoid and ϕ its phase angle expressed in radiants. The absolute value of this last quantity is dependent on the time instant t_0 at which the considered sinusoid is acquired. In order to have a comparable set of measurements related to different sites of the network, time synchronization is necessary. This implies that every comparable measurement must be referred to the same time instant t_0. This task can be carried out using several synchronization signal sources, however GPS, thanks to its precision and reliability, is nowadays the most employed system .

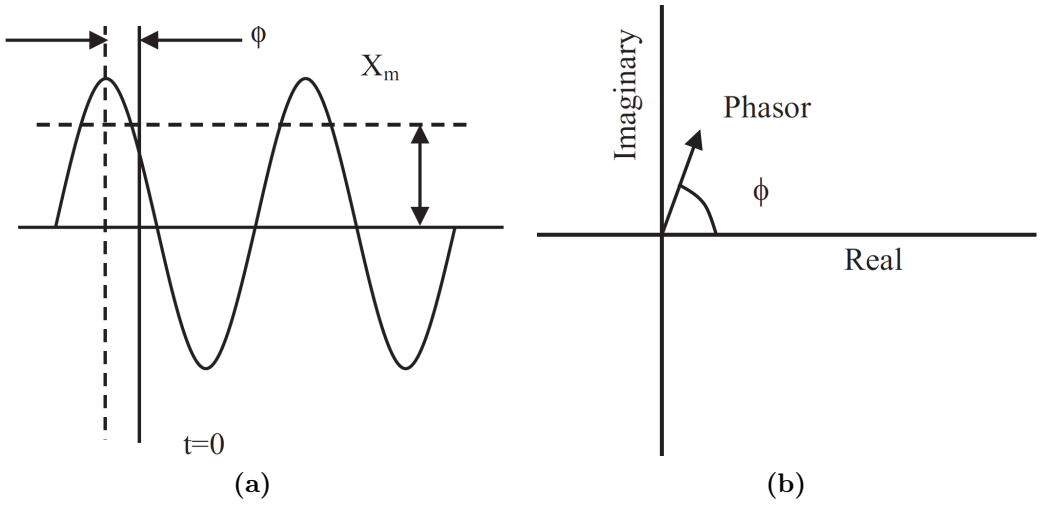

Figure 1.2: Generic sinusoid and its phasor representation

In figure 1.2 the relation between a generic sinusoid and its phasor representation is shown. As previously mentioned, since the phase angle depends on the considered time instant, the phasor can be seen as a static representation of the sinusoid. Hence, in general, given $t_1 > t_0$ the angle ϕ_1 will be different than ϕ_0. The current existing methods and architecture to obtain a synchrophasor measurement system are many and different. At present there are about 24 commercial manufacturers of Phasor Measurement Units but among all the solutions available today the majority proposes the working principle expressed by the block diagram in figure 1.3 on the following page.

The GPS receiver provide a signal synchronized with the Coordinated Universal Time(UTC) with an accuracy in the order of microseconds. This is the Pulse-per-second signal(PPS), a train pulse in which every rising edge coincides with the occurrence of a second. The analog signals coming from the electrical network can be three,six or more, depending on the quantities of interest (the three-phase voltages only or also the currents) and on how many buses of the substation the PMU is monitoring. In the modern PMUs the typical number of inputs coming from the grid is 12.

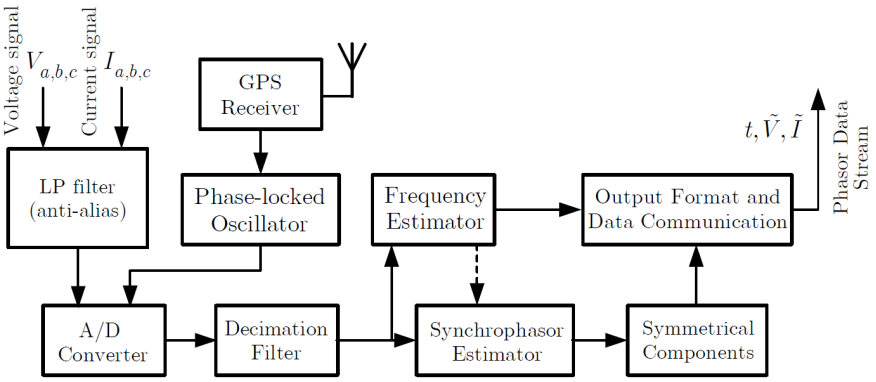

Figure 1.3: Block diagram of a Phasor Measurement Unit

The sampling process is synchronized to the reference time signal through an internal Phase-Locked-Loop(PLL) algorithms. This solution ensures a quality synchronization far above the one required by this application, but in some cases other solutions with a similar accuracy are adopted. The evaluation of amplitudes and phases for each phasor is achieved with Discrete Fourier Transform(DFT) algorithm but also for this purpose other means can be found in literature. Once the phasors are computed, a label with all the time information such as UTC time, second of century(SOC) and synchronization status is assigned to each of them. This process is called timestamping and it allows comparison of phasors measured with different PMUs. Thanks to this process, therefore, all the phasors are synchronized and they become synchrophasors[6]. Contemporary to phasor estimation, the samples are processed to obtain two other measures of interest: the frequency of the acquired signal and the rate of change of frequency(ROCOF).

The ability of measuring in real-time meaningful quantities of an electrical power system makes Phasor Measurement Units a paramount device of future smart grids. Thanks to their architecture they also proved to be the most up-and-coming tool towards the implementation of Wide Area Monitoring Systems(WAMS): utilizing PMUs, information can be recorded and monitored to detect disturbances and improve knowledge of network behavior under dynamic conditions, enabling system operators to maximize power flow and network stability. For this reason, other than improve their performances, in the last years it has been necessary to design an upper level structure to collect and analyse data coming from different PMUs.

Each device streams the measurements to a local Phasor Data Concentrator(PDC) often installed at the same substation of the PMU itself. The Phasor Data Concentrator consists of three important parts. The first part is a central unit. The central unit is a computer based server that receives and collects data from the Phasor Measurement Unit through User Datagrama Protocol(UDP). The software application in the PDC is to manage, display and record data received from the PMU. The second part is a data storage unit, that collects all the incoming data and stores them in the database. The last part is the Human Machine Interface (HMI) that functions as a displays unit and controls the whole system. Hence, data are collected, sorted by time and then sent again to further analysis to another Phasor Data Concentrator of higher hierarchical level(regional or national). Each

PDC is configured to communicate either upstream and downstream according to a radial network architecture letting data to flow in both direction(1.4).

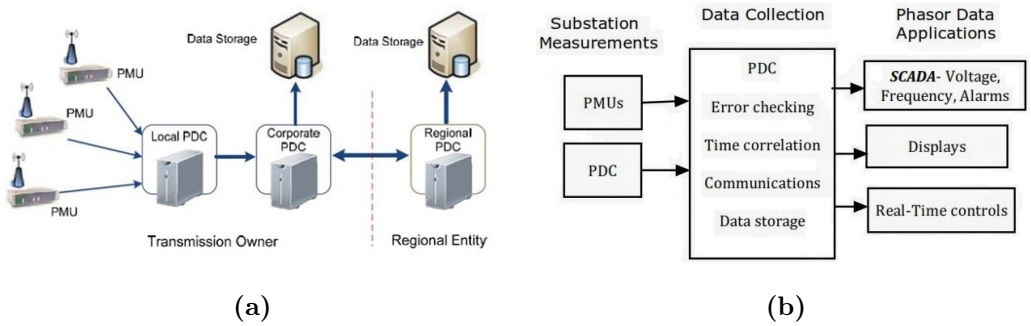

(a) **(b)**

Figure 1.4: Synchrophasor Data Network

The exploitation of the various measurements for real-time state estimation, control and protection coordination takes place at PDCs of highest level, indeed at the top of the hierarchy there are strategic control stations for monitoring, data analysis and control purposes that can guarantee higher computational power and better performances[7].

1.3 Time Synchronization Systems

At this point, it should be clear that providing a common reference time to measurements taken in different points of the system is the only way to make them exploitable for higher level applications such as control, state estimation and protection coordination. Wide-area measurement system can reach remarkable size and extension and it is,therefore, necessary that the available data aren't significantly affected by a loss of synchronization between each other. Among the different systems that can be used in order to obtain a common time reference, satellite systems are surely those that provide the best performances in terms of accuracy although they usually imply an higher installation cost.

Global Navigation Satellite System(GNSS) is a generic term to identify a system of satellites that provides autonomous geo-spatial positioning with global coverage. It allows electronic receivers to determine their location and also to calculate current local time with high precision. Not all GNSS systems are equivalent in terms of time accuracy and satellite orbits. Before analysing different types of GNSS, it is useful to understand their general functioning.

Satellite system's working principle is based on the measure of the amount of time that a signal, sent by the satellite, spends before arriving to a whatsoever terrestrial receiver. Receivers are equipped with an internal clock, so they are able to measure the time interval between the transmission instant and the reception instant. Given this quantity and knowing the electromagnetic propagation speed, it is possible to calculate the distance between the receiver and the satellite. The locus of points at the same distance from the emitter is a sphere whose intersection with the earth surface origins a circumference. If the satellites are three, as well

three circumferences can be originated by means of which is possible to identify a triangular area that depends on the accuracy of the measures. Therefore, knowing the altitude of the receiver it is possible to track its position (see figure 1.5).

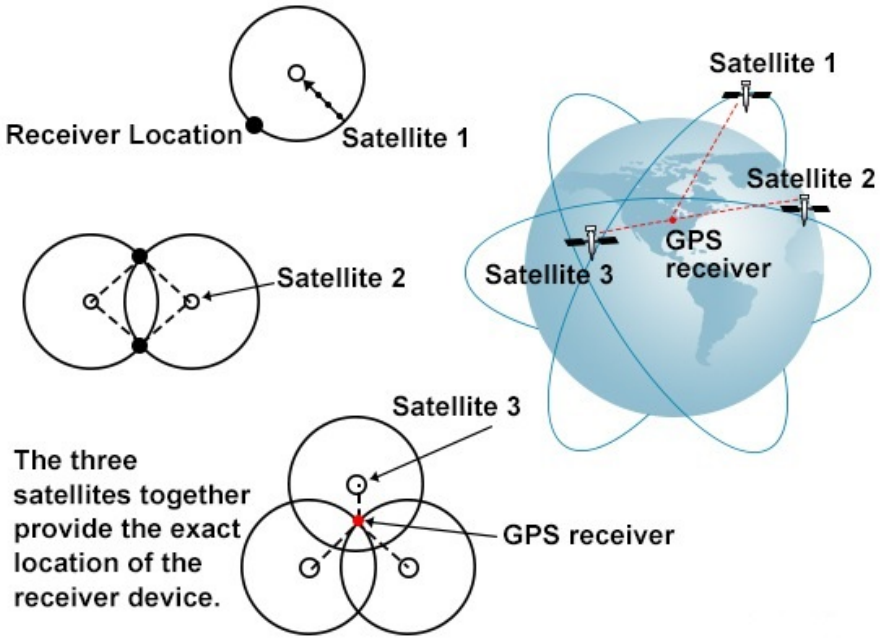

Figure 1.5: GNSS working principle

In addition, every satellite is equipped with an high precision clock, controlled and monitored through apposite terrestrial monitoring stations. Receivers, instead, are provided with traditional clocks to avoid an excessive increasing of the costs. Nevertheless, it is possible to retrieve their deviation from the time signal provided by the satellites solving a system of four equations in the 4 unknowns latitude, longitude, altitude and time.

1.3.1 Global Positioning System

Navigation System Time And Ranging Global Position System (NAVSTAR GPS), usually called GPS, is a U.S. Department of Defense satellite-based radio navigation system, used nowadays for several tasks, civil and military both[8]. It represents today the most complete and exploited GNSS in the world. Its design and creation began in 1960s for military purposes. Due to high costs of implementation and to lack of development in technology, the first group of satellites has been launched only after more than ten years. In 1978, the first eleven satellites were in orbit and they were called "Block one". During the 80s and 90s the system has been expanded and obsolete satellites have been substituted. The access and the utilisation of the whole infrastructure, since it had been made, have always been restricted to military only. In may 2000, unexpectedly the restriction has been removed and the system made accessible to everyone without any limitation.

The overall configuration of the system can be seen as three subsystems together, called segments:

- space segment
- control segment
- user segment

Space segment is constituted by a set of 24 satellites, plus 8 back-up units, ready for use in case of failure of other units or for ensure better performance in particular cases. The constellation of 24 satellites was designed in order to guarantee visibility for at least 4 units from every location in the world having an inclination of more than five degrees. The 24 units are distributed on six different orbital planes that are 60 degrees distant from each others and with an inclination of 55 degrees with respect to the equatorial plane. This yield to have 4 satellites on each plane that are normally uniformly distributed on it. However, if some circumstance requiring a different deployment of the satellites occurs, their positions can be controlled by means of the terrestrial control system. On board each satellite there are two cesium and two rubidium oscillators, having the function of atomic clock. They are constantly monitored by the control segment. GPS satellites transfer information on two different carrier frequencies, both of them multiples of the oscillators' fundamental frequency $f_0 = 10.23$ MHz. In details, carrier frequency $L_1 = 1575.42$ MHz transfer a signal useful for a rough geographical localization whilst carrier frequency $L_2 = 1227.60$ MHz transfers a signal aimed to a more accurate geolocalization [9].

The GPS control segment consists of a global network of ground facilities that track the GPS satellites, monitor their transmissions, perform analyses, and send commands and data to the constellation. For instance, they monitor and correct the functioning of atomic onboard clock. It is constituted by five monitor stations, located in Kwajalein, Ascension Island, Diego Garcia, Hawaii e Colorado Springs in the United States. Master control station dwells in this latter location. It is the operation center for the whole segment. Each monitor station receives continuously data from satellites such as clock signals, UTC corrections, status and location units information. This set of information is gathered and analysed in control sections that send feedback information to the space segment. In particular Master control station has the task of estimating daily offset time and orbit of each satellite. As a consequence, orbits are continuously recalculated and adjusted. For better performances, control stations are equipped with hydrogen atomic clocks with high stability performances; they represent a time reference for all other clocks, terrestrial and satellite both.

Lastly, user segment is represented by all those people able to exploit the services globally provided by GPS. Users are furnished with receiving devices, available on the market at different costs and performances, that allow to retrieve information on position and time. In the last few years, thanks to technological strides, simplification of the exercise and an overall reduction in costs, GPS receivers have been through a wide diffusion and they are today employed in omnifarious civil applications. GPS receivers can be considered as a special radio receiver, tuned on system's characteristic frequencies, furnished with decoding and signal elaboration devices and also with an internal memory for data storage. A common receiver is composed by: an antenna, a microprocessor, an oscillator(generally made of quartz),

a decoding signal system, an internal physical memory and software for controlling data acquisition process. It is possible to classify satellite receivers in three families:

- sequential receivers: they have a single channel for tracking at least four satellites and for sequential position determination. These receivers are usually fairly cheap but they can't be used in cases where the computational speed is a critical parameter such as in real-time applications

- multichannel receivers: they have different channels for tracking satellites, all independent on each other.A microprocessor provides the data analysis for the whole dataset and furnish an estimate for position, time and speed. Usually they are more expensive than the sequential ones and are more suitable for high dynamic applications.

- multiplex receivers: they have a single channel but it is used to track a different satellites every 20ms. With this solution is possible to have a trade-off in terms of performances between the previous mentioned receivers [10].

1.3.2 Global Navigation Satellite System (GLONASS)

GLONASS is a satellite system developed from the Soviet Union and it is currently managed by the Russian government through the Russian Space Forces [11]. The development of the system had began in 1976, during the Cold War, for military purposes. First satellites were launched in space in 1982 and only in 1997 the whole structure had been completed with the deployment of 24 units. In the following years, due to difficult economic conditions, the Russian government had not been able to maintain the system on, indeed, in 2002, only eight of the 24 satellites were still operating. In the last decade, thanks to improvements of the Russian economy, a restoring program has taken place. In 2012 the constellation has become again fully operative and it is now provided with 24 satellites plus 4 backups. The Russian Global Navigation Satellite System provides similar capabilities to GPS. Sporadic funding, and the resulting inconsistent satellite coverage, have hampered widespread acceptance of the GLONASS system, although it is in some ways superior to GPS, as the accuracy. The space segment of this system is managed by the System Control Center(SCC) located in Krasnoznamensk, while tracking, telemetry and control station are placed in San Petersburg, Schelkovo, Yenisseisk e Komsomolsk-Na-Amure. Satellites are placed at an altitude of 19000 km and positioned, grouped by eight, on three orbital planes 64.8 degrees tilted with respect to the equatorial plane; each satellite spend 11 hours and 15 minutes to complete its orbit[12]. The working principle of GLONASS system, as well as GPS, is based on time and distance measurements using the signals transmitted from the satellites to the receivers. Differently from GPS system, each satellite transmit signals on its own frequencies. Thanks to its deployment, GLONASS has made possible a further improvement of synchronization time sources both in availability and in performances [9].

1.3.3 GALILEO

GALILEO is a navigation and position satellite system issued in Europe as an alternative to GPS and GLONASS systems that are controlled by their respective governments, american and russian one, and it will be characterized by civil only purposes[13]. This initiative, proposed by the European Union, is born in 1994 with the intent of realizing an independent and autonomous satellite system that can guarantee a full signal availability, contrary to what takes place with GPS and GLONASS where their respective governments have the right to shut down the system whenever they have the need. GALILEO's deployment should have started in 2011 but consequently to bureaucratic and economic problems it is started on august 22nd, 2014 with the launch of two satellites. From an operative point of view, GALILEO is designed to have in its final configuration 30 satellites, where 27 are operative and 3 for backup function. They are positioned on three orbits at an altitude of 23616 km and with a tilting angle of 56 degrees with respect to equatorial plane. The higher number of satellites enables a bigger satellite coverage, above all for locations sited at high altitudes. GALILEO satellites are designed to transmit signals on four carrier frequencies that are respectively $E_5A = 1176.45$ MHz $E_5B = 1207.14$ MHz $E_6 = 1278.75$ MHz and $L_1 = 1575.42$ MHz. When fully deployed, the system will be able to manage an high range of data at high transmission speed, ranging from a minimum of 250 bit/s up to 1500 bit/s. The control segment (Ground Control System) is composed by a control center for the navigation system NSCC (Navigation System Control Center), by a global network for orbitography and synchronization OSS(Orbitography and Synchronization System) and by a set of stations for tracking, telemetry and command (TT&C). Each station OSS carries out distance measurements that are subsequently sent to NSCC, together with data coming from satellites. Internally to NSCC there are three structures indicated by the acronyms SCF, OSPF, PTS. Satellite Control Facility(SCF) monitors the orbits and provides maintenance for satellites through a control action executed by means of TT&C. Orbitography and Synchronisation Processing Facility(OSPF) is intended to compute orbital positions for each satellite together with offset for onboard clocks. Finally, Precision Timing Station(PTS) includes high performance atomic clocks able to provide the so called Galileo System Time(GST) which is the time reference for the whole system. Total deployment of GALILEO system is forecasted for late 2019.

1.3.4 Synchronization Distribution Methods

A PMU requires a source of UTC time synchronization. UTC time synchronization may be delivered to the PMU by using different systems: this may be supplied directly from a time broadcast such as GPS or from a local clock using a standard time code. The main time synchronization sources are:

- PPS signal: a one pulse per second positive pulse with the rising edge on time with the second change. Even if it provides precise time synchronization, since each pulse is identical there is no way of knowing which second a pulse is associated with. Resolving this ambiguity requires a simultaneous data channel.he IRIG-B tim

- IRIG-B signal: it has been created by the TeleCommunications Working Group of the U.S. military's Inter-Range Instrumentation Group (IRIG) in 1960 and it is commonly used for local time dissemination. It repeats each second and has a total of 100 bits per second. Some of these are framing (sync) bits, some are assigned for time, and some are available for control functions. IRIG-B code may be used in either logic-level (unmodulated) format or as an amplitude-modulated signal with a 1 kHz carrier frequency [12]. If the amplitude modulation is used, it may need to be supplemented with a 1 PPS pulse train to achieve the required accuracy. The IRIG-B amplitude modulated format is commonly available and hence is the most readily implemented. Moreover IRIG-B may be also used in Manchester format: this newer format is more compatible with fiber optic and digital systems and provides complete synchronization without additional signals(see figure 1.6)[14].

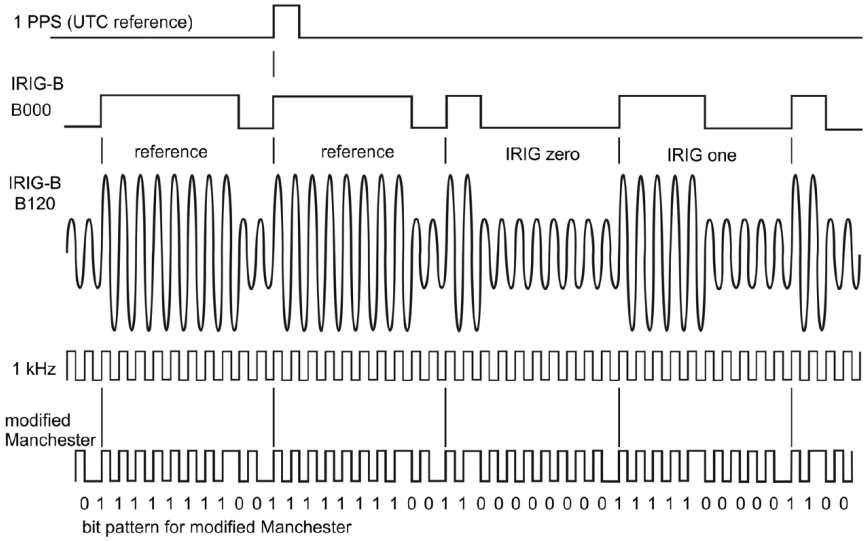

Figure 1.6: Synchronization time sources: in order we find a)PPS b)unmodulated IRIG-B c)amplitude-modulated IRIG-B d)Manchester format

- IEEE 1588: IEEE Std 1588-2008 specifies a Precision Time Protocol(PTP) that can be used for power system applications, such as PMU. PTP distributes precise time over Ethernet-based networks and requires special hardware support at each Ethernet port to achieve high time accuracy. Messages containing precise actual time are transmitted once per second. By adding dedicated timing hardware to each port in a data network, the time of transmission and reception of certain messages can be determined with an accuracy sufficient to transfer time with performance comparable to that of an IRIG-B or 1 PPS signal. The protocol needs to be supported by all devices in time distribution chain to achieve $1\mu s$ time accuracy. Thanks to this level of accuracy, the same communication infrastructure(Ethernet) for PMU/PDC data and time distribution and reduced use of GPS connectivity whenever possible, a rapid adoption of this technology is expected in the following years[15].

Satellite-based timing signals are particularly suitable for PMU applications since they make possible accurate synchronization without requiring the PMU user to deploy the user's own primary time and time dissemination systems. At the same time, GNSS systems provide intrinsic advantages such as wide area coverage, easy access to remote sites, and adaptability to changing network patterns. Synchronizing signals may also be disseminated using terrestrial systems (e.g., radio broadcasts, microwave, and fiber-optic systems).

1.4 IEEE Standards

1.4.1 Birth and progresses

Phasor Measurement Units represents today one of the most interesting approach to study and analyse electric power system and, for this reason, in the last years they have spread more and more on the market and their technological progress has been evident. For the purpose of evaluating phasor quantities, omnifarious algorithms are used, based mostly on Fourier analysis utilisation. Indeed, although the main elements for phasor computation are the same, the implementation of measurement algorithm can change dramatically depending on the particular system that is considered[16]. Therefore, to allow interoperability between different manufacturers and comparison among data, it is imperative to define common definition and rules for synchrophasor evaluation.

Until a few years ago, PMU manufacturers were completely free to chose not only the phasor evaluation process but also a set of critical parameters such as the length of the observation interval, the sampling frequency, the computational speed of the algorithm, adapting those characteristics to their particular hardware setup. Standard IEEE 1344 [17], introduced for the first time in 1995 and valid until 2005, stated some measures to adopt in order to ensure interoperability between PMUs of different manufacturers. However, this standard provided some guidelines regarding only some of the aspects concerning synchrophasors estimation, like time synchronization and the format of the output dataframe, without any specification regarding measurement techniques, accuracy limits or transmission rate and it considered only communication between the PMU and one another device only.

Synchrophasor definition given by the standard [17] was by itself not satisfying being that the possibility, far from unreal, of dealing with off-nominal frequency quantities wasn't even taken into account. In particular, the instruction given to manufacturers in case of off-nominal frequency voltages and currents was to find ad-hoc solution. For the purpose to avoid measurement problems due to lack of precision in synchrophasor definition, Standard 1344 has been improved and substituted in 2005 by Standard IEEE C37.118 [18]. In this review, for the first time, a method of evaluating measurement performance was introduced together with a messaging system that was usable for synchrophasor systems. The novelty of an evaluation criterion shifted the focus from the measurement method to measurement results, allowing the use of any algorithm that produces good results. Standard IEEE C37.118-2005 had a great success and allowed the compatibility of different PMUs in the same system for the first time. The concept of different classes of

performance was introduced as well. Classes were differentiated as performance levels 0 and 1, respectively for applications insensitive to small signals but needed minimum latency and for use by controls and applications that are sensitive to harmonics and to small signals. Compared to the requirements for level 1, level 0 had relaxed requirements for harmonics and out-of-band signal rejection, and narrowed frequency and magnitude ranges for measurement performance.

As described above, the IEEE standards has been redacted with the goal of introducing and supporting the development of synchrophasor measurements and their associated systems. Up to a dozen of years ago, there were no suitable standards available for synchrophasor measurement and the real-time data communication for this type of measurement. The standards addressed the measurement, data communication, and timing to facilitate development of the technology. However technology has undergone major development in the years since the first standard was released, it is sufficient to think about telecommunication developments that have undergone major strides from channel based serial into digital and fiber-optic based systems. In response to the changes in technology, IEEE explored changes in C37.118-2005. It was recognized that in addition to specifying steady state error, the Standard C37.118-2005 needed further specifications for dynamic performance. Moreover, there was a need to better define frequency measurement. Nevertheless, a big quantity of systems, that were already deployed and installed, adhered to the C37.118-2005 Standard, although many others units followed the IEEE 1344 or other proprietary protocols. Hence, in order to minimize disruption of existing systems, the revision of the standard was carried out with a guideline of backward compatibility.[19]

In order to gain a wider international acceptance, they proposed dual logo status, a process between IEEE and IEC(International Electrotechnical Commission)to adapt standards made by one body into a standard by the other. After investigation, it was found that a dual-logo adoption was not practical. Indeed the IEC separates measurements and communications into different standards. To facilitate the adoption of synchrophasor measurement into IEC and support C37.118 communications, the IEEE decided to split the current C37.118 standard into two standards. In 2009 the IEEE and IEC made an agreement to create a joint standard that includes C37.118 and IEC61850. One standard has the measurement definitions and requirements, and the other deal with data communication.From this collaboration in 2011 a new IEEE standard was published.

C37.118.1-2011 [14] is the IEEE standard for synchrophasor measurements. It is based on the portion of C37.118-2005 that covered synchrophasor measurements. It includes definitions that have been expanded to cover synchrophasors in dynamic conditions as well as frequency and ROCOF. The steady state performance requirements have become more strict and requirements have been added for dynamic conditions. Both frequency and rate of change of frequency performance requirements were added.

C37.118.2-2011[20] is the IEEE standard for synchrophasor data transfer. It is based on the portion of C37.118-2005 that covered data communication. While some improvements over the 2005 version were possible, most of the possible extensions and enhancements were not included in order to maintain backward compatibility. Consequently it is essentially unchanged from the 2005 standard, but it includes

a new configuration message that will handle large data sets as well as improved naming, scaling and PMU parameter reporting. The standard actually defines a messaging system rather than a communication system. This allows using any communication system to carry the messages. An annex in the Standard describes the current implementation that is commonly used[21].

After its publication, it was recognized that in [14] some of the requirements specified in the text were too strict and difficult to be met. Therefore, to not jeopardize the desired spreading of Phasor Measurement Units, the standard was amended by IEEE Standard C37.118.1a-2014 [22] to ensure that the performance requirements can be met. The amendment relaxes the relevant parameters and clarifies a few requirements. It is worth to mention, for example, that the 2014 amendment suspended the ROCOF error requirement for harmonic testing of M class(level 0) PMUs, following different tests of actual PMUs that showed as it was a driving factor in PMU design which could compromise the phasor measurement capability. Also, the equations for frequency and ROCOF estimation were revised to eliminate a time offset in these estimates, thereby better aligning them with the synchrophasor estimates. Today, IEC tecnhical committe 95 and IEEE Power Systems Relaying Committee WGH11, which authored the IEEE standards, have joined the forces to revise and publish a new joint standard IEC/IEEE 60255-118-1. The key elements of this new version are:

- reduction of the required number of reporting rates;
- considering adding and higher reporting rates;
- further clarification of latency requirements;
- resolve several ambiguities in clause 5.5:
  - relative phase of harmonics;
  - step-response time interpolation;
  - step overshoot reference level;
  - phase-angle test is redundant with the frequency range test;
  - increments in the out-of-band interfering signals test;
  - maximum PMU reporting latency might not be found with only 1000 reports.
- temperature tests are the only requirement that make the standard a “device standard” rather than a “function standard;” consider the reference to other environmental test standards and suggest how to test the PMU function under those standards;
- consider testing a PMU function with test signals in digital form (as from a merging unit);
- consider either new, higher accuracy classes, or setting performance levels within the M and P class;

- reconsider the definition of frequency.

The joint working group estimates this effort will take until 2017 to complete[23].

1.4.2 Standard C37.118-2011

Standard C37.118-2011, called "IEEE Standard for Synchrophasors for Power Systems", besides of providing an exhaustive definition of synchrophasor, describes in details synchronization specifications, format for output dataframe and, above all, measurements requirements. The intent of the standard is to provide to users requirements and guidelines to implement Phasor Measurement Units and to ensure an adequate comparison between the measurements coming from different systems.

Considering equation 1.2 on page 7, Standards [14] define the synchrophasor as "the value $\bar{X}$ where ϕ is the instantaneous phase angle relative to a cosine function at the nominal system frequency synchronized to UTC." The convention to define the angle ϕ is shown in figure 1.7:

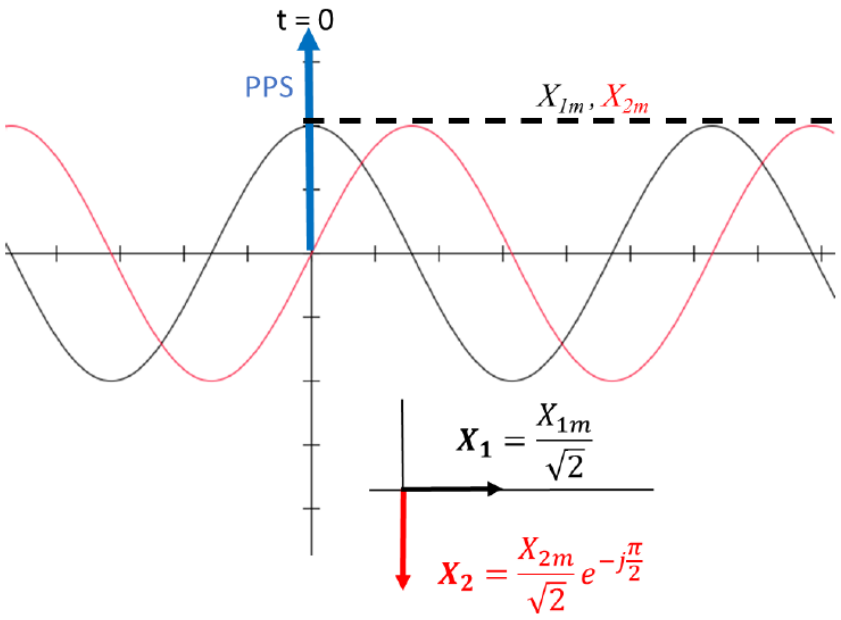

Figure 1.7: Convention for synchrophasor representation

Phasor representation of a signal $x(t)$ is independent on its frequency value. In fact, by observing the sinusoid in correspondence of time intervals that are multiples of the base interval T_0 $\{0, T_0, 2T_0, 3T_0, .., nT_0\}$, it's possible to compute the related phasors $\{X_0, X_1, X_2, X_3, .., X_n\}$ evaluated considering as starting time the beginning of each interval. If the observation interval T_o is chosen to be an integer multiple of the nominal period T_n of the considered signal, the phasor representation will be characterized by the same values of magnitude and phase, supposing of course a steady-state working point. Instead, if the value T_o is not an integer multiple of T_n, the phase angle of the phasor will be continuously varying by an amount in radiants expressed by $2\pi\frac{f_n - f_o}{f_o}$ for each observation interval(see picture 1.8 on the facing page).

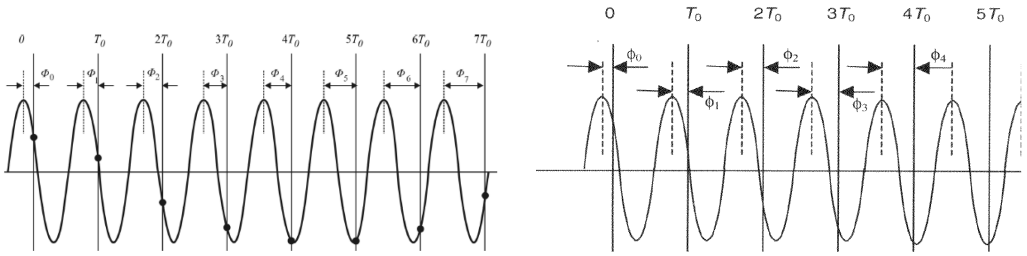

(a) $T_o = kT_n$ **(b)** $T_o \neq kT_n$

Figure 1.8: Phase evaluation

The standard also defines the frequency and its ROCOF. Considering the following expression of a sinusoidal signal:

$$x(t) = X_m \cos\theta(t) \tag{1.3}$$

its frequency and ROCOF are defined respectively by the following expressions:

$$f(t) = \frac{1}{2\pi}\frac{\mathrm{d}\theta(t)}{\mathrm{d}t} \tag{1.4}$$

$$ROCOF(t) = \frac{\mathrm{d}f(t)}{\mathrm{d}t} \tag{1.5}$$

If the argument of the cosine in 1.3 is represented as:

$$\theta(t) = 2\pi f_0 t + \psi \tag{1.6}$$

the previous definitions can be expressed by:

$$f(t) = f_0 + \frac{\mathrm{d}(\frac{\psi(t)}{2\pi})}{\mathrm{d}t} = f_0 + \Delta f(t) \tag{1.7}$$

$$ROCOF(t) = \frac{\mathrm{d}^2(\frac{\psi(t)}{2\pi})}{\mathrm{d}t^2} = \frac{\mathrm{d}\Delta f(t)}{\mathrm{d}t} \tag{1.8}$$

The reference time considered in the Standard for synchrophasor evaluation is the Coordinated Universal Time. As previously mentioned, the time signal must comply with a series of requirements for ensure accuracy and reliability. As far as reliability is concerned, it is worth to notice that one of the fundamental aspects for these systems, characterized by a continuous operating condition, is the availability of the synchronization time source. The time source can be provided directly by a satellite broadcast (such as the GPS system) or by means of a local clock, internal or external to the device. In those cases in which the PMU lays on an internal clock, the standard C37.118-2011 imposes a maximum timing error E_t given by the following relation:

$$E_t = E_s + R_i A_c \tag{1.9}$$

where E_s represents the maximum error related to the synchronization signal(typically in the order of microseconds), R_i is the repetition interval and A_c is the accuracy of the clock used to perform the measure. For instance, using a GPS receiver with a PPS as synchronization signal characterized by a maximum error $E_s = 1\ \mu s$ and an internal clock with an accuracy $A_c = 10^{-6}$, the maximum timing error would be $E_t = 2\ \mu s$. Reliability is a paramount feature for synchrophasor measurements, for this reason the Standard orders to every PMU system to insert in the output dataframe information about loss of synchronization: not only a digital flag indicating whether synchronization is occurring or not but also data about the unlocked time. As far as synchronization is concerning, even if any specific requirement is given, the Standard states that the required limits for the parameter TVE (defined in next paragraph) must be always verified.

Steady state requirements

The TVE (Total Vector Error) is an important index to evaluate the performance of synchrophasor estimation, and for many years it has been the only parameter to asses the accuracy of a measure both in steady state and in dynamic conditions. The TVE is an aggregated index, which represents the vector error between the theoretical synchrophasor and the estimated one, given by the unit under test at the same instant of time.

The formula of TVE is:

$$TVE = \sqrt{\frac{(X_r(n) - X_r)^2 + (X_i(n) - X_i)^2}{{X_r}^2 + {X_i}^2}} \tag{1.10}$$

where $X_r(n)$ and $X_i(n)$ are respectively the real and the imaginary part of the estimated synchrophasor at the n^{th} sampling instant whilst X_r and X_i indicate the theoretical component of the signal.

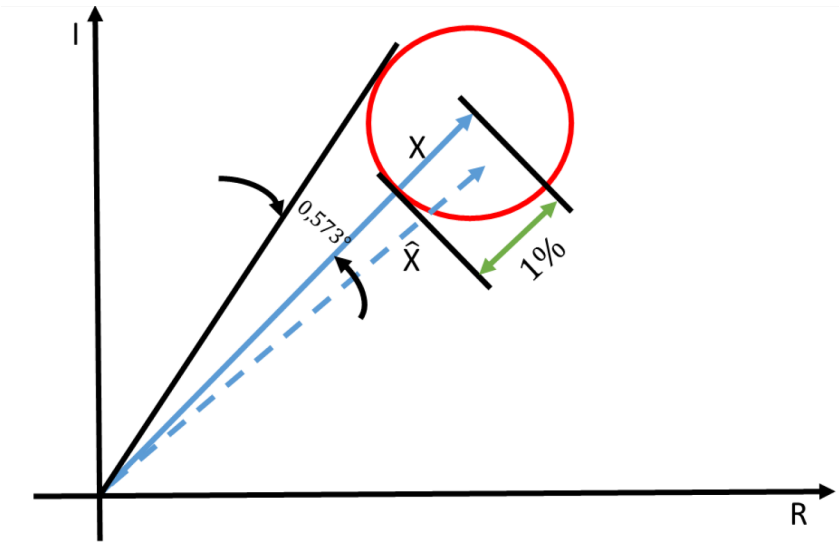

Figure 1.9: The TVE criterion shown on the end of phasor. For example, when the maximum TVE error is 1 % and the magnitude error is zero, the maximum error in angle is just under 0.573°.

Influence quantity	Reference condition	Minimum range of influence quantity over which PMU shall be within given TVE limit			
		P class		M class	
		Range	Max TVE (%)	Range	Max TVE (%)
Signal frequency range—f_{dev} (test applied nominal + deviation: $f_0 \pm f_{dev}$)	$F_{nominal}$ (f_0)	± 2.0 Hz	1	± 2.0 Hz for F_s<10 ± F_s/5 for 10 ≤ F_s < 25 ± 5.0 Hz for F_s ≥25	1
The signal frequency range tests above are to be performed over the given ranges and meet the given requirements at three temperatures: T = nominal (~23 °C), T = 0 °C, and T = 50 °C					
Signal magnitude—Voltage	100% rated	80% to 120% rated	1	10% to 120% rated	1
Signal magnitude—Current	100% rated	10% to 200% rated	1	10% to 200% rated	1
Phase angle with $\lvert f_{in} - f_0 \rvert$ <0.25 Hz (See NOTE 1)	Constant or slowly varying angle	±π radians	1	±π radians	1
Harmonic distortion (single harmonic)	<0.2% (THD)	1%, each harmonic up to 50th	1	10%, each harmonic up to 50th	1
Out-of-band interference as described below (See NOTES 2 and 3)	<0.2% of input signal magnitude		None	10% of input signal magnitude for $F_s \geq 10$. No requirement for $F_s < 10$.	1.3
Out-of-band interference testing: The passband at each reporting rate is defined as $\lvert f - f_0 \rvert < F_s/2$. An interfering signal outside the filter passband is a signal at frequency f where: $\lvert f - f_0 \rvert \geq F_s/2$ For test the input test signal frequency f_{in} is varied between f_0 and ± (10%) of the Nyquist frequency of the reporting rate. That is: $f_0 - 0.1\,(F_s/2) \leq f_{in} \leq f_0 + 0.1\,(F_s/2)$ where F_s = phasor reporting rate f_0 = nominal system frequency f_{in} = fundamental frequency of the input test signal					
NOTE 1—The phase angle test can be performed with the input frequency f_{in} offset from f_0 where $\lvert f_{in} - f_0 \rvert$<0.25 Hz. This provides a slowly varying phase angle that simplifies compliance verification without causing significant other effects. NOTE 2—A signal whose frequency exceeds the Nyquist rate for the reporting rate F_s can alias into the passband. The test signal described for the out-of-band interference test verifies the effectiveness of the PMU anti-alias filtering. The test signal shall include those frequencies outside of the bandwidth specified above that cause the greatest TVE. NOTE 3—Compliance with out-of-band rejection can be confirmed by using a single frequency sinusoid added to the fundamental power signal at the required magnitude level. The signal frequency is varied over a range from below the passband (at least down to 10 Hz) and from above the passband up to the second harmonic ($2 \times f_0$). If the positive sequence measurement is being tested, the interfering signal is a positive sequence.					

Figure 1.10: TVE limited values for compliance test

TVE combines magnitude and phase errors (see figure 1.9 on the facing page) and it is computed relative to measurement magnitude and phase at the given system frequency. Time synchronization errors will result in different TVE depending on the actual system frequency. For instance 1 cycle of the signal is 20 ms at 50 Hz and 16.67 ms at 60 Hz. One degree of phase angle at 50 Hz is 55.6 μs and at 60 Hz is 46.3 μs. Therefore the timing error that will cause a 1% TVE error are ±31.7 μs at 50 Hz and ±26 μs at 60 Hz. In figure 1.10 limited values for TVE parameter are shown. The 2005 standard required 1% TVE over a range of frequency variation of 0.5 Hz for P class and 5 Hz for M class. The 0.5 Hz variation was deemed too narrow for many applications, so the new range for P class is now 2 Hz, independently on the reporting rate F_s. Moreover, it was found that the 5Hz range created difficult filtering requirements because it exceeds the Nyquist criterion for $F_s = 10$ frames/s. The ranges of frequency performance for the M class are ±2 Hz for $F_s < 10$ frames/s, $F_s/5$ for $[10 \leq F_s < 25]$ frames/s and ±5 Hz for $F_s \geq 25$ frames/s[21]. The effects produced by the different quantities are considered cumulative and the TVE value must not exceed the limit imposed by a given compliance level.

It is worth to notice that in IEEE C37.118 there isn't any specification about

the type of algorithm that should be used for synchrophasor estimation; this means that each manufacturer is completely free to adopt its own method to accomplish this task. However, the norm has precise indications concerning data transmission and management, in order to ensure complete correlation of big amount of data coming from different Phasor Measurement Units.

Since phase angle is measured in relation to a time reference, angles from different measurements can only be compared if they are made at the same time. Fixed reporting times and rates allows ready angle comparisons. Reports can be sent with various specified rates, evenly spaced in time. The allowed reporting rates are shown in figure 1.11 and they depends on the nominal frequency of the system in which the PMU is installed (50 Hz or 60 Hz). As specified in the 2014 amendment, higher and lower rates are also possible. Lower rates may be useful for Supervisory Control and Data Acquisition(SCADA) systems reporting, such as power flow and state estimation. A user may request compliance with the appropriate sections of the standard at these additional rates, but this is not required for compliance with the standard. Low reporting rate measurements are intended as a snapshot with which the system as a whole can be assessed. Unfiltered lower sample rates could be obtained by selecting a subset of sample from a higher rate stream. On the other hand, higher rates may be useful for control systems or system dynamic analysis.

Rates for a 50 Hz power system (fps)					
10		25		50	
Rates for a 60 Hz power system (fps)					
10	12	15	20	30	60

Figure 1.11: Required PMU reporting rates in frames per second

As far as the timetagging is concerning, once the number N of frame per second is chosen, a time label is assigned to every frame to univocally identify each synchrophasor. Therefore, timetags and synchrophasor are related through a number, called frame number, ranging from 0, in correspondence of the Pulse-per-second rising edge occurrence, to $(N-1)$. For better clarity in figure 1.12 on the next page an example of timetagging is reported.

In figure 1.12 on the facing page is also possible to notice the difference in phase evaluation in two different cases: when the actual frequency of the system is equal to the nominal one(60Hz) the phase angle is constant; when the system is operating with an off-nominal frequency the phase angle is varying and the related synchrophasor is rotating in the imaginary plane as mentioned at the beginning of this section.

Only in the last revision of the standard two more performance index were added: frequency measurement error(FE) and ROCOF measurement error(RFE). They are defined as follow:

$$\begin{cases} FE = |f_{true} - f_{measured}| = |\Delta f_{true} - \Delta f_{measured}| \\ RFE = |(\frac{\mathrm{d}f(t)}{\mathrm{d}t})_{true} - (\frac{\mathrm{d}f(t)}{\mathrm{d}t})_{measured}| \end{cases} \tag{1.11}$$

they are both estimated for the same time instant.

Time	Fractional time		Synchrophasor—60 Hz		Synchrophasor—61 Hz	
Second	Frame number	Fractional second	Synchro-phasor (0°)	Synchro-phasor (–90°)	Synchro-phasor (0°)	Synchro-phasor (–90°)
k–1	9	0.900000	$X_m/\sqrt{2}, \angle 0°$	$X_m/\sqrt{2}, \angle -90°$	$X_m/\sqrt{2}, \angle -36°$	$X_m/\sqrt{2}, \angle -126°$
k	0	0.000000	$X_m/\sqrt{2}, \angle 0°$	$X_m/\sqrt{2}, \angle -90°$	$X_m/\sqrt{2}, \angle 0°$	$X_m/\sqrt{2}, \angle -90°$
k	1	0.100000	$X_m/\sqrt{2}, \angle 0°$	$X_m/\sqrt{2}, \angle -90°$	$X_m/\sqrt{2}, \angle 36°$	$X_m/\sqrt{2}, \angle -54°$
k	2	0.200000	$X_m/\sqrt{2}, \angle 0°$	$X_m/\sqrt{2}, \angle -90°$	$X_m/\sqrt{2}, \angle 72°$	$X_m/\sqrt{2}, \angle -18°$
k	3	0.300000	$X_m/\sqrt{2}, \angle 0°$	$X_m/\sqrt{2}, \angle -90°$	$X_m/\sqrt{2}, \angle 108°$	$X_m/\sqrt{2}, \angle 18°$
k	4	0.400000	$X_m/\sqrt{2}, \angle 0°$	$X_m/\sqrt{2}, \angle -90°$	$X_m/\sqrt{2}, \angle 144°$	$X_m/\sqrt{2}, \angle 54°$
k	5	0.500000	$X_m/\sqrt{2}, \angle 0°$	$X_m/\sqrt{2}, \angle -90°$	$X_m/\sqrt{2}, \angle 180°$	$X_m/\sqrt{2}, \angle 90°$
k	6	0.600000	$X_m/\sqrt{2}, \angle 0°$	$X_m/\sqrt{2}, \angle -90°$	$X_m/\sqrt{2}, \angle -144°$	$X_m/\sqrt{2}, \angle 126°$
k	7	0.700000	$X_m/\sqrt{2}, \angle 0°$	$X_m/\sqrt{2}, \angle -90°$	$X_m/\sqrt{2}, \angle -108°$	$X_m/\sqrt{2}, \angle 162°$
k	8	0.800000	$X_m/\sqrt{2}, \angle 0°$	$X_m/\sqrt{2}, \angle -90°$	$X_m/\sqrt{2}, \angle -72°$	$X_m/\sqrt{2}, \angle -162°$
k	9	0.900000	$X_m/\sqrt{2}, \angle 0°$	$X_m/\sqrt{2}, \angle -90°$	$X_m/\sqrt{2}, \angle -36°$	$X_m/\sqrt{2}, \angle -126°$
k+1	0	0.000000	$X_m/\sqrt{2}, \angle 0°$	$X_m/\sqrt{2}, \angle -90°$	$X_m/\sqrt{2}, \angle 0°$	$X_m/\sqrt{2}, \angle -90°$

Figure 1.12: Phasor Timetagging

Dynamic requirements

A principal use for synchrophasor measurements is observing power system dynamics. Consequently, requirements for PMU performance under dynamic conditions are specified in the Standard, and verifying conformance is important. The TVE is not able to asses correctly the performance under step change conditions because in a fast variation it is important to evaluate the transition time between two steady-state measurements, before and after a step change is applied to the input. To evaluate if two different measurements are comparable characteristics such as bandwidth, response time, linearity, frequency tracking, settling time, overshoot,noise and distortion must be quantified.

For this purpose, in C37.118, three kind of test are required:

- a modulation test is required to simulate the behaviour of the measurement system in presence of power system oscillations. In fact, these phenomena appear as a modulation of the AC power signal. This test is split in two session, one phase modulation test and one magnitude modulation test
- a ramp change frequency test determines how closely the tested PMU tracks the input during a constant rate of change of frequency.
- a step change in amplitude or phase for asses the measurement performance in occurrence of a fault or a switch operation.

During the last test, the PMU is not expected to correctly measure the input because the estimation time windows are too long to produce short transient. Therefore, the output is evaluated in terms of response time, delay time and overshoot.

The response time (fig. 1.13) is evaluated as the length of time from when the measurement estimate leaves the specified TVE, FE or RFE limit at the old state level until it enters and stays within the specified TVE, FE or RFE limit at the new state. This gives a good measure of how quickly the measurement will react to the step change. This value assume particular importance for protection applications.

Delay time evaluates how closely the measurement time stamp corresponds to the actual step change. The requirement of 25% of the reporting time interval ensures that the measured step appears close enough to the actual time of step change occurrence .

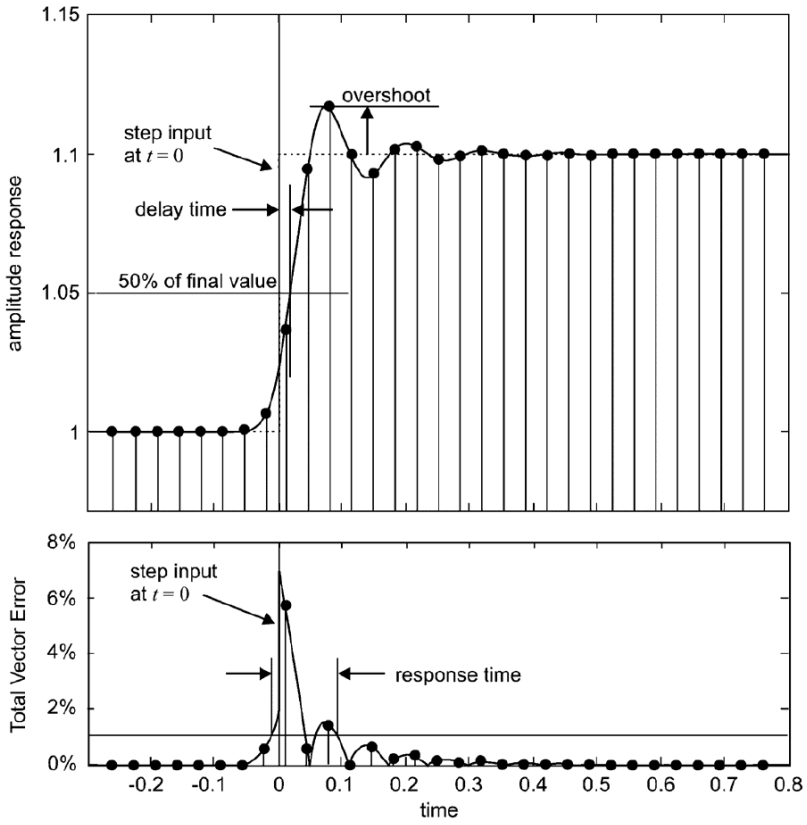

Figure 1.13: Example of a step change measurement with all the indices for this test. Step at t=0.

1.5 Algorithms for synchrophasor estimation

The implementation of Phasor Measurement Units has brought about a revolution in power system measurement technology. In the last decade, the interest of the international scientific community towards these device has increased steadily and technological progresses have made possible to reach high accuracy levels together with high reporting rates, encouraging even more to think of this measurement system as the obvious mean for implementing WAMS. As previously stated, a phasor measurement unit is basically a device to compute time synchronized phasor representations of input signals. At this time, in the Standard a suggested

or favourite method to estimate a phasor is not included, not only because the performances of each algorithm are different but also because, for encouraging PMU's diffusion and improve their performance, manufacturers have to be free to adopt the most suited solution for their applications. To perform this task there are many different algorithms proposed in literature. Nevertheless, they can be divided in two categories: algorithms relying on a steady state phasor model and algorithms based on an intrinsically dynamic phasor model[24].

Steady state algorithms are based on the classic definition of the phasor shown in 1.2 on page 7 and they are based on the computation of the Discrete Fourier Transform of the input signal. Indeed, given a sinusoidal signal $x(t)$ with frequency kf_0 expressed as follow by its Fourier Series expansion:

$$\begin{aligned} x(t) &= a_k \cos(2\pi k f_0 t) + b_k \sin(2\pi k f_0 t) \\ &= \{\sqrt{{a_k}^2 + {b_k}^2}\} \cos(2\pi k f_0 t + \phi) \qquad \text{where} \qquad \phi = \arctan(-\frac{b_k}{a_k}) \end{aligned} \tag{1.12}$$

its phasorial representaion is:

$$\bar{X}_k = \left[\sqrt{\frac{\{{a_k}^2 + {b_k}^2\}}{2}}\right] e^{j\phi} \tag{1.13}$$

Using the relationship of the Fourier series coefficients with the Discrete Fourier Transform(DFT), the phasor representation for every k^{th} harmonic component of a signal is given by

$$\bar{X}_k = \frac{1}{\sqrt{2}} \frac{2}{N} \sum_{n=0}^{N-1} x(n\Delta T) e^{-\frac{j2\pi kn}{N}} \tag{1.14}$$

where N is the number of samples acquired during the observation interval. Considering $x(n\Delta T) = x_n$ and $\theta = \frac{2\pi}{N}$ where θ is the sampling angle measured in terms of period of the fundamental frequency component, it is possible to write:

$$\bar{X}_k = \frac{\sqrt{2}}{N} \sum_{n=0}^{N-1} x_n \left[\cos(n\theta k) - j \sin(n\theta k)\right] = X_{kc} - jX_{ks} \tag{1.15}$$

In case of electric power systems, it's well known that the fundamental frequency is 50 or 60 Hz. Therefore, the main interest is in estimating the fundamental harmonic of the signals. Supposing that its harmonic order is $k = 1$, the signal phasorial components are respectively:

$$\begin{aligned} X_{1c} = X_c &= \frac{\sqrt{2}}{N} \sum_{n=-N/2}^{N/2-1} x_n \cos(n\theta) = \frac{\sqrt{2}}{N} \sum_{n=-N/2}^{N/2-1} X_m \cos(n\theta + \phi) \cos(n\theta) \\ &= \frac{\sqrt{2}}{N} X_m \sum_{n=-N/2}^{N/2-1} \left[\cos(\phi) \cos^2(n\theta) - \frac{1}{2} \sin(\phi) \sin(2n\theta)\right] = \frac{X_m}{\sqrt{2}} \cos(\phi) \end{aligned} \tag{1.16}$$

$$
\begin{aligned}
X_{1s} = X_s &= \frac{\sqrt{2}}{N} \sum_{n=-N/2}^{N/2-1} x_n \sin(n\theta) = \frac{\sqrt{2}}{N} \sum_{n=-N/2}^{N/2-1} X_m \cos(n\theta + \phi) \sin(n\theta) \\
&= \frac{\sqrt{2}}{N} X_m \sum_{n=-N/2}^{N/2-1} \left[\frac{1}{2} \cos(\phi) \sin(2n\theta) - \sin(\phi) \sin^2(n\theta) \right] = \frac{X_m}{\sqrt{2}} \sin(\phi)
\end{aligned}
\tag{1.17}
$$

It is worth to mention that to obtain equations 1.16 and 1.17 it has been noted that the summation of the $sin(2n\theta)$ term over one period is identically equal to zero, and that the average of the $cos^2(n\theta)$ term over a period is equal to $1/2$. Moreover, the summation indexes have been shifted due to synchrophasor definition given in C37.118, in fact, it is specified that each synchrophasor is representative of the time instant placed at the center of the observation interval. Traditional Fourier analysis is usually burdensome in terms of computational time: a DFT based on an N-sample window requires N complex multiplications and (N-1) complex additions for each coefficient. To overcome this inconvenient that may cause critical problem, Fast Fourier Transform and recursive algorithms can be used[4].

The DFT-based algorithm works correctly when, in stationary conditions, the observation window perfectly matches an integer number of cycle durations of the periodic signal $x(t)$. Thus, N is usually chosen as a multiple of $N_0 = 1/(f_0 T_s)$, which is the number of samples in one cycle at nominal frequency and selecting a sampling frequency $f_s = 1/T_s$. When this condition is not met, particularly under off-nominal frequency conditions, good results can be achieved by weighting the samples with a specific window, such as Hamming or Hanning windows [25].

In an ideal case, the power system should work in a sinusoidal steady state, characterized by a nominal frequency of either 50 or 60 Hz. In the reality, however, voltage and current signals differ from these ideal conditions, in terms of both variable fundamental frequency and distorted waveform. As for the system frequency, the system usually operates in a narrow band around the nominal frequency, but it is possible to encounter particular occasions where the real frequency of the system is far from the nominal value (up to $+4\%$ and -6%). When these critical events occur, the capability of correctly measuring the synchrophasors with a DFT-based algorithm rapidly deteriorates. However, retrieving a reliable estimation of electrical quantities is fundamental for those PMU application that are sensible to high dynamic phenomena, such as protection and control systems.

There are algorithms that, while keeping the simple steady state model, try to compensate these errors, like the interpolated DFT algorithm cited in [26], but their computational burden of course increases.

Dynamic phasors

An important step towards the solution of problems in assessing dynamic electric system phasorial quantities has been taken thanks to the innovative introduction of the so called dynamic phasor [27].

As previously said, static phasors are picture of an electrical system for a given time instant. Anyway, during a N-long observation interval, the system can be

affected to a multitude of phenomena, some of them characterized by fast dynamic behaviours. Taking this into account the traditional definition for a phasor can be expanded. A generic electric system signal $x(t)$ can be better modeled by a signal of the form:

$$x(t) = a(t)\cos(2\pi f_0 t + \phi(t)) \tag{1.18}$$

This model can be rewritten in terms of complex exponential functions as:

$$\begin{aligned} x(t) &= \frac{1}{2}(p(t)e^{j2\pi f_0 t} + \bar{p}(t)e^{-j2\pi f_0 t}) \\ &= \mathrm{Re}\left\{p(t)e^{j2\pi f_0 t}\right\} \end{aligned} \tag{1.19}$$

where $p(t) = a(t)e^{j\phi(t)}$ is the complex envelope of the signal $x(t)$ and it is called *dynamic phasor*.

The continuous time phasor definition 1.19 can be translated in the following discrete time formulation:

$$p(kT_s) = a(nT_s)e^{j\phi(nT_s)} \qquad \text{with} \qquad n = 0, 1... \tag{1.20}$$

Definition 1.19 is well suited to follow the non-sinusoidal conditions because it highlights the time-changing behavior of phasor amplitude $a(t)$ and phase $\phi(t)$. The signal $x(t)$ acts like a passband signal centered at frequency f_0 (figure 1.14) in the frequency domain: all the frequency components inside the band are considered meaningful, whereas the components outside the band are considered as disturbances.

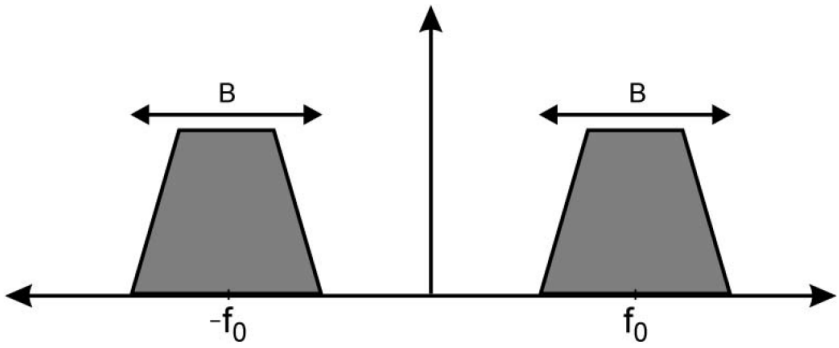

Figure 1.14: Qualitative behaviour of dynamic phasor model in the frequency domain

Dynamic phasor definition of 1.19 applies for every window of lenght T in which the signal is observed. If $p(t)$ function is expanded by means of its Taylor series, a finite differences equation can be written to evaluate the phasor. Limiting the expansion to the second-order signal $p(t)$ is expressed by:

$$p^{[2]}(t) = p_o + p_1 t + p_2 t^2 \qquad \text{for} \qquad -\frac{T_0}{2} \leq t \leq \frac{T_0}{2} \tag{1.21}$$

where p_0 is the static phasor corresponding to the instant t at the center of the considered interval and, (p_1,p_2) are respectively its first and second order derivatives

assessed in t. Supposing N samples of the signal are acquired, through equation 1.21 on the preceding page N linear equation are written. N must be an odd number in order that the instant at the center of the interval is always included in the window.

Therefore, considering what it has been just said:

$$x^{[2]} = \underline{\underline{B}}\ \bar{p}^{[2]} \tag{1.22}$$

where the elements of the column vectors of the matrix $\underline{\underline{B}}$ are of the form $n^2 e^{jn\omega_0}$, $ne^{jn\omega_0}$,$e^{jn\omega_0}$and their complex conjugates. In addition, it can be noted that the traditional phasor estimation algorithm comes from a subsystem of 1.22, in which only the two central column vectors of $\underline{\underline{B}}$ are taken into account.

The error between the input signal x and its approximated nth-order Taylor polynomial is defined as:

$$\xi = x - \underline{\underline{B}}p \tag{1.23}$$

Hence, minimizing the error function the best estimates of p can be obtained[27].

1.6 Applications and Deployment

Phasor Measurement Units, which measure voltage and current synchronized phasors, along with frequency and rate of change of frequency, are the emerging measurement devices for power network monitoring. Due to the wide range of possible applications, many pilot projects have been developed in recent years and hundreds of PMUs have been installed, in particular by Transmission System Operators. The largest of these projects is the Western Interconnection Synchrophasor Program (WISP), with 584 PMUs deployed. The WISP shares real-time operational data with 97 participants over a dedicated, highly secure, wide-area data network spanning the Western Interconnection. WISP synchrophasor data is enabling better visualization tools for dispatchers and operators in transmission owners' and grid operator control rooms [28].

Today, according to U.S Department of Energy, the installation cost for a PMU is ranging between 40k and 180k U.S. dollars [29]. Hence, it is straightforward that the first step towards a Wide-area monitoring system is to place PMUs in optimal locations in order to reduce their number. PMU placement aimed at system monitoring is usually developed for full system observability, however, in literature omnifarious algorithms can be found and they may differ in their final goal and design criteria. According to the consensus, the minimum number of PMUs to be installed in a system equals 1/3 of the total number of buses present in the system.

Now more than ever, the rapidly changing scenario of distribution networks, characterized by an increasing presence of distributed generation and storage systems asking for increased measurement accuracy, faster reporting rates and higher communication capabilities, makes PMUs a major perspective also for such grids. In this context, synchrophasors should be integrated with traditional monitoring systems, such as SCADA, which use traditional measurement devices, without absolute phase-angle information, and operate at lower reporting rates.

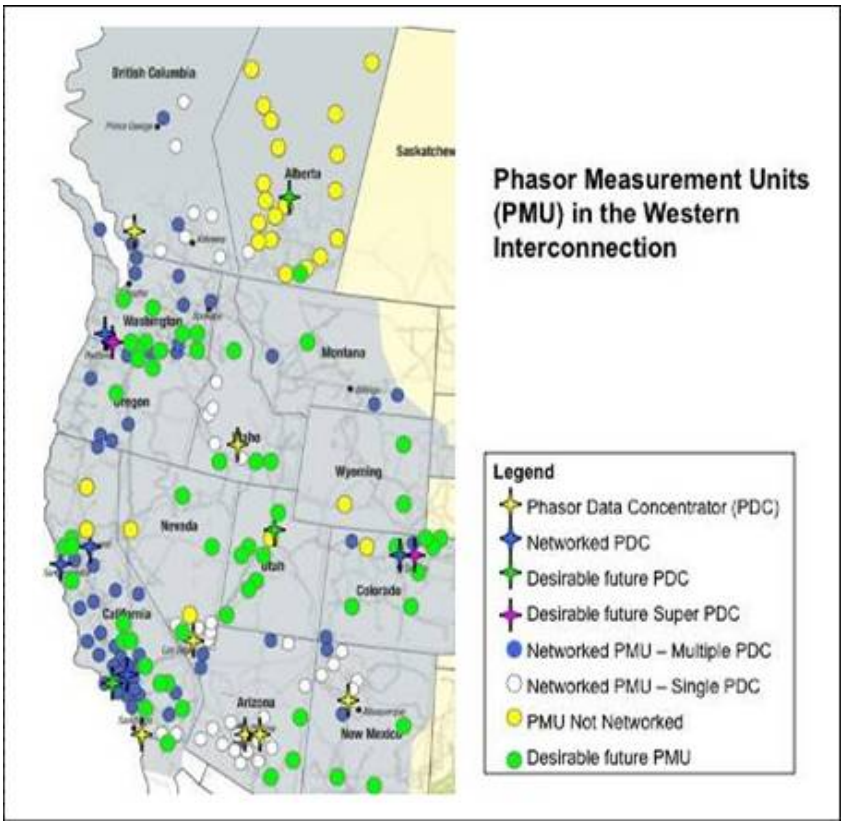

Figure 1.15: PMU deployment for WISP project

However, the direct use of currently available Phasor Measurement Units in the distribution grids should be cautious. Indeed, the performance offered by current PMUs, although normally suitable for applications in transmission grids, can be in some cases insufficient for the distribution systems, for the following reasons:

- lower length and extension of the lines leads to lower amplitude and phase differences between the electric quantities in the different nodes, hence, higher accuracy for PMUs should be required to correctly measure these differences;
- the faster dynamics that are expected in smart grids, caused by possible intermittent behavior of generators, loads and storage devices, may require time responsiveness beyond the limits indicated in the standard;
- the higher distortion that is usually present in distribution grids may lead to a need for re-defining compliance limits with harmonic and interharmonic interferences, again beyond the current standard;
- lack of human supervision requires higher trustworthiness of the information coming from PMUs, so it can be used in automatic control and protection processes [30].

The number of PMU manufacturers has constantly increased in the last years, from the few pioneer companies of the 1990s to tens of producers now. The reasons behind such a push towards this technology is found in the different and interesting

applications in which a synchrophasor measurement can be used. Nowadays, there are three main fields for PMUs application: state estimation, power system protection and power system control.

State Estimation

Prior to synchronized phasor measurements, the state could not be measured directly but only inferred from the unsynchronized power flow measurements. This fact and the process of getting large numbers of measurements into the control center forced early state estimators to make compromises that today have an influence on how phasor measurements are integrated into existing state estimation algorithms. Among these assumptions, the most significant is that the system did not change during the scan. While scans have become quicker, the introduction of phasor measurements forces to question the validity of the static assumption. The direct integration of a few synchronized phasor measurements into an existing nonlinear estimator is straightforward but results in an estimator that has most of the limitations of the original conventional estimator.

If an estimate could be formed with only PMU data, not only the static assumption can be removed, but also, considering that voltage and current measurements are linear functions of the system state, the estimation problem becomes a simple linear weighted least squares problem which requires no iterations. Given PMU data can be reported at rates as high as 60 frames per second, a truly dynamic estimate would be available. To sum up, if complete observability of the system is achieved, a picture of the actual system for a given time instant can be acquired.

Issues that must be addressed include the need for redundancy to eliminate bad data and determination of how many PMUs are required. Recognizing that a PMU in a substation would have access to line currents in addition to the bus voltage reduces the number of PMUs needed. Measuring line currents can extend the voltage measurements to buses where no PMU is installed.

An interesting subproblem is the issue of sequentially adding PMUs to a system. With limited annual investments it would be desirable to add a limited number of PMUs until a final goal was achieved. Initially there will not be enough PMUs to have a linear estimator. The attempt is to place the PMUs so that at each stage the selection satisfies some design criteria. One criterion is the degree of unobservability of the system [31].

Power System Protection

Synchronized phasor measurements offer solutions to a number of complex protection problems. In general, phasor measurements are particularly effective in improving protection functions, which have relatively slow response times. For such protection functions, the latency of communicating information from remote sites is not a significant issue.

Protection systems that could take advantage from remote phasor measurements information could include control of backup protection of distance relays, protection functions concerned with angular voltage stability of networks and voting schemes where dependability and security could be reassessed based upon the stress of the

system:

1. backup zones of distance relays are prone to tripping due to load superposition during power system disturbances. Wide-area measurements offer a possibility for restraining the remote back-up relays in the event that the load swing is being interpreted by the relay as a fault.

2. it is well-known that a group of generators going out of step with the rest of the power system is often a precursor of a complete system collapse. To prevent such occurrence, out-of-step relays are designed to perform this detection and also to take appropriate tripping and blocking decisions. However, in their traditional configuration, these relays are found to be unsatisfactory in highly interconnected power networks because they fail to determine correctly whether or not an evolving electromechanical swing is stable or unstable. Wide-area measurements of positive sequence voltages provide a direct path to determining stability using real-time data.

3. It should be recognized that relays can be affected by two failure modes. They can trip when they should not trip (a false trip) or they can fail to trip when hey should trip. These two failures modes, that constitute two different types of reliability, are identified by protection engineers as "security" and "dependability". The existing protection systems, being designed with high redundancy and with multiple zones of protection, are biased toward dependability. The result is a system that virtually always clears the fault but as a consequence permits larger numbers of false trips. An attractive and interesting field of research can be to mold the security—dependability balance in response to changing system conditions exploiting real-time data provided by Phasor Measurement Units.[32]

Power System Control

Before the introduction of real-time phasor measurements power system control was essentially local. The introduction of synchrophasors offers the possibility of control systems based on measurement value of remote quantities. The phasor data will be time tagged so that control could be based on the actual state of the system a short time in the past. An issue that must be addressed regards the latency of the measure, anyway most of the controlled process are characterized by frequencies in the range of $[0.2; 2]$Hz [33].

In the future, remote control techniques can be used to coordinate a number of local controllers of different types. For example, a collection of power system stabilizers, dc lines, and FACTS devices could be coordinated to provide damping for a collection of interarea modes with a variation of the technique used for PSSs alone [34].

Chapter 2

Grid-Connected converters

2.1 Grid integration of renewable resources

Throughout the first chapter it has been clarified the significance of the terminology "smart grid" and the innovation that this new concept of network would bring about to the whole electric power system. In particular, it has been highlighted how it represents a promising evolution that would allow a massive introduction of renewable resources as electric power supplies, speeding, therefore, the transition of the planet towards a green sustainability.

Nowadays, technological developments have furnished many and diverse types of alternative resources, some of which are still under study and not ready for being employed in wide scale. Examples of such developments can be fuel cells technology, which produces electrical energy through a chemical reaction between hydrogen and oxygen, as well as biomass fuels and even the emerging marine hydrokinetic technology, based on the collection of kinetic energy produced by sea waves. Without any doubt, the most rising and advanced technologies are in the aeolian and the solar energy fields. The increasing success of these renewable energies is noticeable considering also the recent energy market trend. In figure 2.1 on the following page an economic comparison for the years 2010 and 2014 between the main renewable resources is reported. On the y-axis of the chart the levelized cost of electricity(LCOE) is indicated. The LCOE is an economic assessment of the average total cost to build and operate a power-generating asset over its lifetime divided by the total energy output of the asset over that lifetime. It is interesting to highlight that in 2014 the LCOE has fallen as low as USD 0.08/kWh and USD 0.05/kWh respectively for utility-scale solar and wind projects.

Nevertheless, it must be clear that, being these two energy sources very different as concerning harvesting and conversion process, wind turbine(WT) systems and photovoltaic(PV) systems are generally thought to be installed in two distinct contexts. For large scale applications, such as for industrial scale power production, wind turbines are the most obvious solution. Unlike the early large turbines, modern turbines are virtually silent and the largest systems can generate in the region of 6 megawatts of power, enough to power over 6,000 homes. Large scale WTs are efficient and effective, and can be installed in a variety of locations, including far out to sea, where the wind generally blows hard and steady.

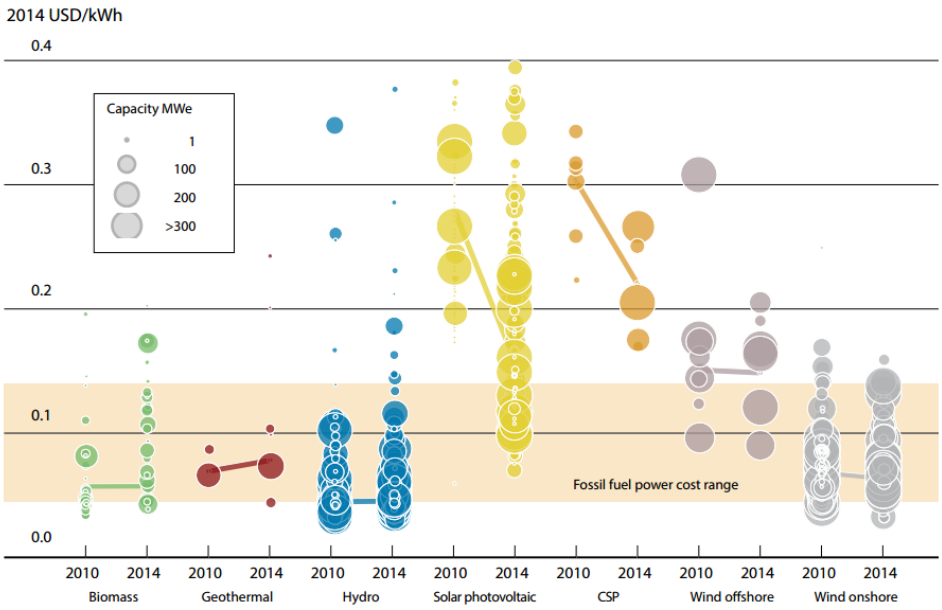

Figure 2.1: Size of the diameter of the circle represents the size of the project. The centre of each circle is the value for the cost of each project on the Y axis[35].

Although WTs are capable of producing electricity 24 hours a day and their cost, considering an equal net generation, is generally lower than a PV panel, there are some applications where is still preferable to exploit solar energy. As a matter of fact, among the features of PV panels the longer lifespan, quantifiable in a 20-years long lifetime, and the little maintenance required when comparing with WTs are the most advantageous. Moreover PV panels are less location sensitive, indeed, whereas most people can implement a small solar array in most locations and achieve success, the same cannot be said about turbines. Considering these features is straightforward that PV panels are more suitable in urban environments than aeolian energy systems.

It is difficult to utilize electricity for the injection of power into a grid or a load directly from renewable energy sources, hence the system needs power electronics converters as an interface between the two. Depending on the considered load or grid, the power electronic section is composed typically by one or two stages and may have a DC/AC conversion unit. In fact, there may be some stand-alone systems that are totally powered by direct current where an inverter is not needed but that is usually not the case. In typical applications(household or business), appliances require alternating current to operate. This makes the inverter an essential component for the system in order to take advantage of renewable power supplies.

While renewable energy systems are capable of powering houses and small businesses without any connection to the electrical grid, many people prefer the advantages that grid-connection offers. A grid-connected system allows to power an estate with renewable energy during those periods when the sun is shining or the wind is blowing. Any excess electricity produced may be fed back into the grid. When renewable resources are unavailable, electricity from the grid supplies all the needs, eliminating the expense of electricity storage devices like batteries.

In addition, electric utilities in most states allow net metering, an arrangement that allows the electricity meter to "turn back" when the power generated by grid-connected resources is fed back into the grid. If the use of electricity is more than what the system feeds into the grid during a given month, the amount of money due to the power provider is only the difference between what has been used and what has been produced[36].

The advantages deriving from a solid utilization of WT and PV systems are evident even though, as it has been previously mentioned, renewable energy resources cannot be connected to the grid without a certain fundamental shrewdness. Electricity grids must have standard condition of supply to ensure that end-use equipment and infrastructure can operate safely and effectively. These conditions are usually referred to as power quality requirements, and they commonly relate to voltage and frequency regulation, power factor correction and harmonics injection. In all distribution networks, to maintain these power quality requirements, some challenges arise from the technical characteristics, end-user operation of electrical loads and the network lines. Power quality at different points of the distribution network at any time is affected by the aggregate impacts of loads and network equipments in highly complex ways. Renewable sources connected to the distribution network can significantly influence these aggregated impacts. It is for this reason that power electronics section and its management are the pivot characteristics of a renewable energy system(RES). Power electronic technology should be of high efficiency and exceeding reliability, it should be able to transfer the renewable energies to the grid and also able to exhibit advanced ancillary functions such as harmonic compensation and grid support with reactive power injection. A demonstrative

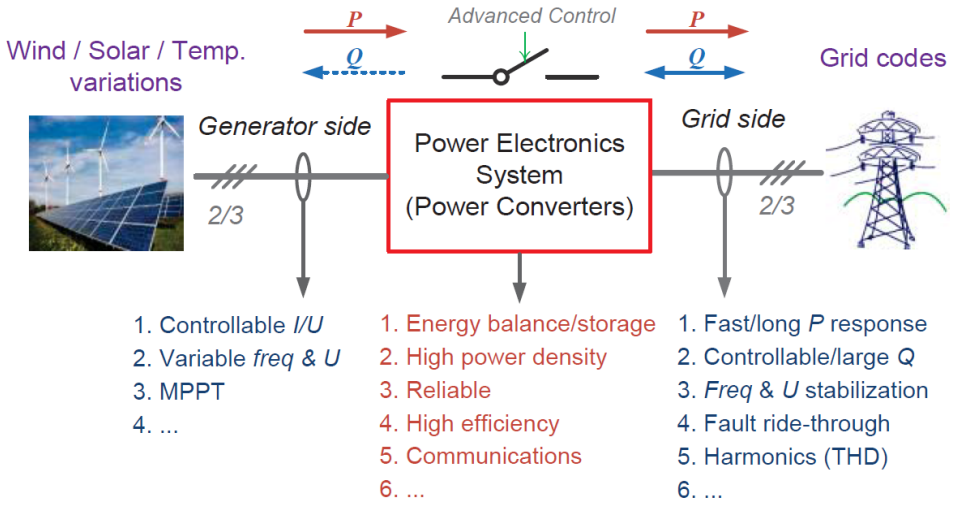

Figure 2.2: Demands for renewable energy systems when integrated into the power grid [37].

and simplified architecture of up-to-date RES based power generation systems is shown in figure 2.2, where the power electronics unit is the key component. The most common requirement of a RES is to transfer the renewable energy to the grid, according to its inherent characteristics. Other specific demands can be summarized as ride-through operation, reliable and secure power supply, efficient and effective protection and system monitoring and communication.

In light of what it has been discussed it is useful and interesting to deepen the discussion on the power electronics section of renewable energy systems, particularly paying attention on wind and solar power. For the sake of this work the configurations of grid-connected systems will be described, focusing on power electronics main characteristics[38].

2.1.1 Wind turbine systems

Wind turbines are those power conversion systems that exploit the air flow through the blades of turbines to mechanically power electric generators. Although the wind kinetic energy increases with the cube of the wind speed, a wind turbine is able to extract only a portion of the available energy and, therefore, the optimization of the extraction process is paramount.

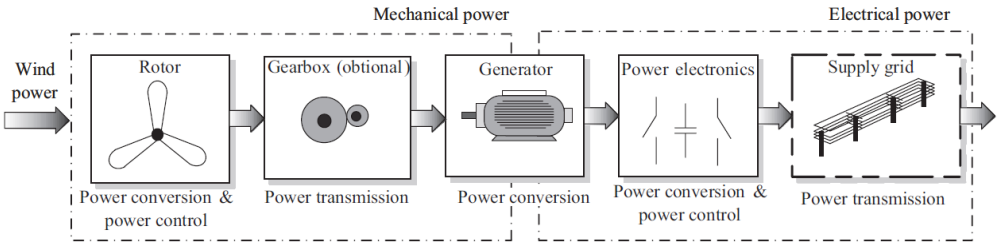

Figure 2.3: Basic power conversion wind turbine system

The basic power configuration of a wind turbine system is made of two parts: a mechanical part, that makes the kinetic energy of the wind available to a rotating shaft and an electrical one, where the electrical energy is converted into a suitable form for the electric grid. The connection between the two subsystems is made by means of an electric generator, which transforms the mechanical energy into electrical energy. Hence, there are three stages used to optimize the extraction of energy from the wind: one mechanical, one electromechanical and another one electrical. The structure of the electromechanical stage can vary depending on the type of machine used and on its structure. In particular, as of now, generators for wind turbine applications are commercialized in two main typologies: induction generator and synchronous generator. The induction generator has dominated the wind turbine market in its early stages. It has several advantages, such as robustness and mechanical simplicity, but the need of a reactive magnetising current is one of its major drawbacks. The rotor of an induction generator can be designed as a so-called short-circuit rotor (squirrel-cage rotor) or as a wound rotor. Wind turbines based on a squirrel-cage rotor are typically equipped with a soft-starter mechanism and an installation for reactive power compensation, as this kind of generator consume reactive power. Conversely, because of advantages such as full speed controllability and an independent excitation, the synchronous generator is dominating the actual market. The magnetic field in the synchronous generator can be created by using permanent magnets or with a conventional field winding. If the synchronous generator has a suitable number of poles it can be used for direct-drive applications without any gearbox.

Lastly, the third stage of the conversion system, the electrical one, adapts the waveforms of the grid currents. Power electronics converters may be present in the second and/or third stage. The main idea beneath the use of power converters in such application is to approximate as much as possible the functioning of WT systems to the operation of a standard power plant. This implies stabilization of active power injections into the grid and the management of reactive power exchanges to make WT systems capable of participating to the voltage regulation [39].

Since the wind power plants and the wind energy market have increased in size, optimizing turbine and power plant design for specific site conditions has become a common practice. As a matter of fact, geographic and temporal variations in wind speed, site topography, interactions among different wind turbines and their integration into the larger electricity system can impact the design of turbines and plants. A main distinction there is between offshore WTs, installed far out to sea, and onshore WTs. The primary motivation to develop offshore wind energy is to provide access to additional wind resources in areas where onshore wind energy development is constrained by limited technical potential and/or by planning and siting conflicts with other land uses. Other motivations for developing offshore wind energy include an higher average wind speed, the ability to use even larger wind turbines due to avoidance of certain land-based transportation constraints and the potential to gain additional economies of scale. These factors, combined with a significant offshore wind resource potential, have created considerable interest in offshore wind energy technology in Europe and, increasingly, in other regions, despite the typically higher costs with respect to onshore wind energy.

At the present, onshore wind plants are often 5 to 200 MW in size, though smaller and larger plants do exist. Offshore wind power plants involve 200 to 600 MW projects and employ turbines that are typically larger than onshore, with nameplate capacity ratings of 2 to 5 MW [40].

Mode of operation of WT systems constitutes another important design choice. In fact, it is possible to distinguish between fixed-speed and variable-speed wind turbines. Fixed-speed wind turbines started to spread in the early 1990s and are usually equipped with induction generators. A fixed working speed implies that regardless of the wind speed, the rotor speed is determined by the frequency of the supply grid, the gear ratio and the generator design. Being designed to achieve maximum efficiency at one particular speed, in order to increase power production, in some cases the generator has two winding sets: one is used at low wind speeds (typically 8 poles) and the other at medium and high wind speeds (4–6 poles). Although simple and robust, fixed-speed WTs present several problems for instance an uncontrollable reactive power consumption, mechanical stress and limited power quality control. For such inconveniences, during the past few years the variable-speed wind turbine has become the dominant type among the installed systems. Contrary to a fixed-speed one, a variable-speed system keeps the generator torque fairly constant and the variations in wind are absorbed by changes in the generator speed. The electrical system of a variable-speed WT is more complicated than that of a fixed-speed WT. Indeed, it is typically equipped with an induction or synchronous generator and connected to the grid through a power converter. The doubly fed induction generator(DFIG) represents the first solution allowing partial

control on the grid electrical quantities. In this configuration the rotor windings of an induction machine are fed by a back-to-back converter with a reduced rated power (usually 30% of the overall system power), while the stator windings are connected directly to the grid. Thus, the converter, decoupling mechanical and electrical systems and varying the electrical rotor frequency, makes variable-speed operation possible even if in a quite limited range ([-30;+30]%) [41].

The use of a full-power back-to-back converter, though more expensive, leads to a generator completely decoupled from the grid. As a consequence, this system has a full speed controllability as well as a complete rolling capacity, being able to actively contribute to the limitation of the effects of grid faults and to the restoration of the normal grid operation. The generator can be an asynchronous generator, an electrically excited synchronous generator (WRSG), or a permanent magnet synchronous generator (PMSG). In case a multi-pole generator is used the gearbox could be not necessary. Therefore, it may be an ideal solution if the WT has to be installed in extreme environmental conditions where the maintenance can be difficult like in offshore installations or at very low temperature. At the present, it is a trend to use a PMSG in the full-rated power converter wind turbine since this type of generator offers high efficiency, gearless configuration, self-excitation, low maintenance cost and weight and higher power density [42].

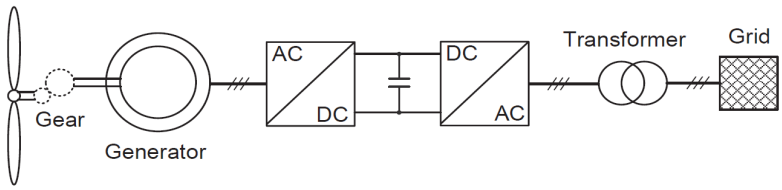

Figure 2.4: Full-power converters

To conclude, the main benefits of variable-speed wind turbines are an increased energy capture, improved power quality due to power control capability and reduced mechanical stress on the wind turbine. The disadvantages are losses in power electronics, the use of more components and the increased cost of equipment because of the power electronics. The introduction of variable-speed wind-turbine increases the number of applicable generator types and also introduces several degrees of freedom in their combination with different power converter type [43].

2.1.2 Photovoltaic systems

As previously said, besides the aeolian energy, the sun represents the most promising renewable source of power at the present. A photovoltaic system, that converts the solar energy into electricity, is composed in its basic structure by two elements: a photovoltaic module and a power conversion unit. The typical PV module is made up of around 36 or 72 photovoltaic cells connected in series and encapsulated in a structure made usually of aluminum and polyvinyl-fluoride (PVF). A PV cell is an electrical device that produces electrical power when exposed to sunlight and connected to a suitable load. Conversely to wind turbines, a PV module has not rotating parts and this makes it able to survive longer in time up to more than 25 years.

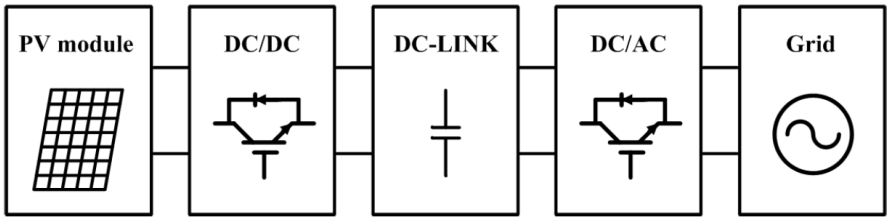

Figure 2.5: Schematic structure of a PV system

The current-voltage and power-voltage characteristic curves of a PV cell vary a lot depending mainly on the cell temperature and the incident solar radiation. Therefore, due to daily and monthly varying conditions, a Maximum Power Point Tracking (MPPT) is required to extract the maximum power from the module and to optimize the efficiency. The power conversion unit is always present independently on the type of PV system considered(stand-alone or grid-connected). In grid-connected PV power systems the PV inverter is the key element. The main function is to convert the DC power generated by PV panels into grid-synchronized AC power. Additional elements include a grid connection filter, a grid monitor or interaction unit and a low-frequency transformer (which is optional depending on local regulations, converter topology, rated power and the modulation used to control it). Another option is an intermediate DC/DC power stage between the PV modules and the grid-tied inverter.

Several categorisations of converter topologies can be done with respect to the number of stages, location of DC links, use of transformers, and types of grid interface. Anyhow, before discussing PV converter topologies, three designs of inverter families are defined: central inverters, module-integrated inverters, and string inverters (see fig. 2.6 on the next page).

In a common central inverter layout the PV modules are divided into series connections called strings. The strings are arranged in parallel and interfaced to the grid through a single inverter, in order to reach a high power rating. A blocking diode in series to each string is necessary to prevent them from acting as load when partial shading or mismatch occurs. In addition, when connecting several modules in series, bypass diodes are connected in reverse bias between positive and negative output terminals of a solar cell. The bypass diode has no effect on the output but it is needed to provide an alternative path for currents coming from well-exposed panels and thereby avoiding the overheating of shaded modules. Ideally there would be one bypass diode for each solar cell, but this can be rather expensive so generally one diode is used per small group of series cells. As it provides a simple-structure and efficient converter, central inverter configuration is employed in large-scale PV plants with a rated power higher than tens of kW. To increase the power rating, some manufacturers commercialize two central inverters connected through a 12-pulse transformer, with a rating up to 1.6 MW. Because the whole array of strings is connected to a single inverter, this configuration can only provide a single MPPT operation, leading to the lowest MPPT efficiency among all configurations. Other major drawbacks are the need for high-voltage DC cables between PV panels and inverter, power losses due to module mismatches, losses in the string diodes and a low overall reliability due to the presence of a single inverter.

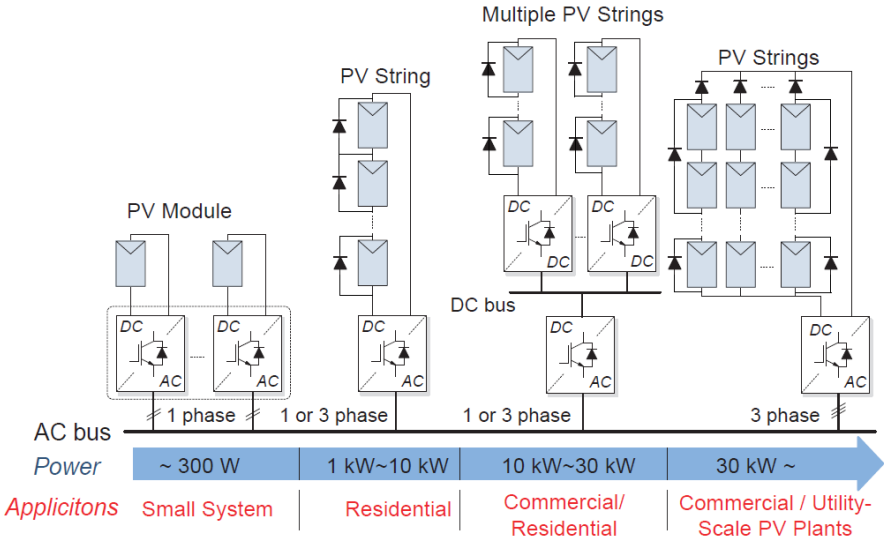

Figure 2.6: Grid-connected PV systems

The string inverter is a reduced version of the centralized inverter where single strings of PV modules are interfaced to separate inverters, connected in parallel to the grid. They can be subdivided into single-stage and two-stage conversion topologies, depending on the addition (or not) of a DC/DC stage. When the voltage of the string is sufficiently high there is no need for a DC/DC boost converter or a transformer and thus the efficiency of the system can be improved. The presence (or not) of transformer has led to a further classification of string inverter as with or without galvanic insulation. Other than with line frequency transformers, insulation can be introduced within the DC/DC stage with a high-frequency transformer. Compared to central inverters, the string inverter can achieve MPPT separately, leading to a better total energy yield, and eliminates the power losses caused by the string diodes. Furthermore, they are characterized by a lower price due to the ease of mass production. However, there are still mismatches in the PV panels connected in series. The string inverter is very popular for small to medium scale PV systems, particularly for residential rooftop PV plants.

The module-integrated inverter is just attached to the back of each PV module. This solution, also known as AC-module or microinverter because of the small size and low power rating, uses a dedicated grid-connected inverter for each PV module of the system. Because of the low voltage rating of PV modules, AC-module inverters are only found with an additional DC/DC stage for voltage boosting, usually also with an high frequency transformer to provide galvanic isolation. Due to the presence of the additional DC/DC stage and high frequency isolation, this is the configuration with the lowest power converter efficiency. However, this disadvantage is fairly compensated by the highest MPPT accuracy and by the lowest mismatch losses thanks to the dedicated converter. This configuration is useful for places with lots of partial shading, complex roof structures, small systems (50–300 W) or combinations of different roof orientations. Furthermore, the modular structure simplifies the modification of the whole system because of its plug-and-play nature. However, despite those listed advantages, the price per watt is still higher compared with the other architectures.

Another PV technology is an intermediate and more flexible solution between the string inverter and the module inverter, being a multi-string inverter. The strings are divided into smaller pieces (fewer modules in series) and connected through independent DC/DC converters to the DC/AC inverter. It combines the advantages of both string and module inverters by having many DC/DC converters with separate MPPTs. Since it is possible to control each PV string individually, this guarantees an high overall efficiency of power extraction. Another function that is accomplished by the DC/DC stage is to boost the voltage of the smaller strings. The additional DC/DC stages are also a cost-effective solution compared to having several string inverters. Since they reduce partial shading and mismatching, they are suitable not only for rooftop PV systems but also for medium and large-scale plants [37],[39],[44],[45].

2.1.3 Role of converters in renewable energy systems

In the previous paragraphs solar and aeolian energy have been introduced as the most important renewable energy system of the actual market. Also, the importance and the convenience of a grid-connected plant have been discussed, referring in particular to the advantages that a well-integrated system would give to those consumers that invest on renewable energies. Of course, from the above description great differences in the managements of those power sources arise, not because there is an unequal technological advancement between wind turbine and photovoltaic systems, despite one technology is younger than the other one, but rather because they have different intrinsic characteristics and diverse connection interfaces. Nevertheless, although the needed conversion stages are generally very different, some similarities do exist between these RESs as regards the power electronic section. In this part of the chapter the system structure for both photovoltaic and wind turbine plants is deepened, concentrating the focus on the power electronics stages and highlighting differences and similarities.

The power electronic section of renewable energy sources plays a fundamental role in a smooth and effective transition of the power system from a fossil-fuel based to a sustainable energy production. Using highly efficient power electronics in power generation, power transmission, distribution and end-user applications, together with advanced control solutions, can pave the way for renewable energies.

As far as RESs are concerned, a wide-scale adoption of power electronics technology makes those environmentally dependent energies more controllable, but increasingly intricate. Enabled by intelligent control strategies, the power electronics technology can fulfill the conversion requirements as well as provide ancillary service for the system operators.

Figure 2.7 on the following page summarises the possible grid connection configurations for wind turbine systems. Among the most common structures of generators that can be employed, namely DFIG, WRSG/PMSG or induction generator(IG), only the DFIG-based solution usually involves the use of a reduced power converter. Nevertheless, due to the development of the electrical machine manufacturing industry and the reduction of solid-state devices' cost of the last years, nowadays systems composed by DFIGs with reduced power converters are experiencing a

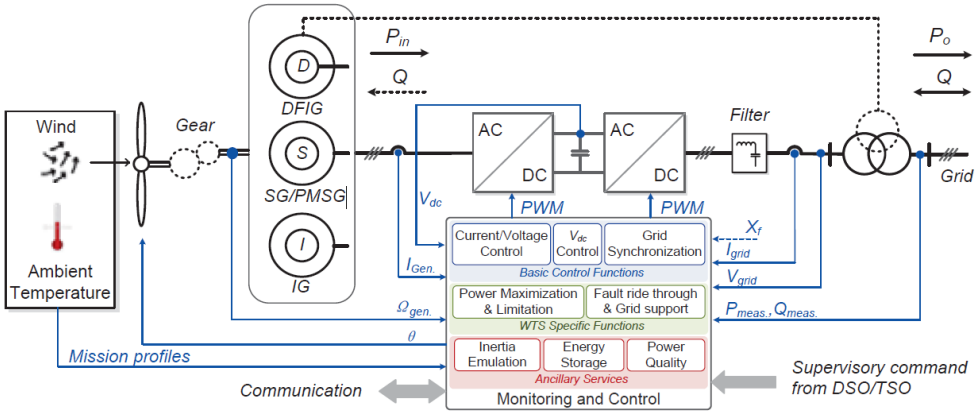

Figure 2.7: General control function blocks for wind turbine systems

continuous reduction in installation demands. The actual trend, indeed, is to install WTs with PMSGs that offer not only less mechanical stress and higher efficiency but also a full speed controllability thanks to complete grid decoupling provided by the converters. The most commonly adopted full power three-phase converter is the two-level voltage source converter (2L-VSC) in a back-to-back configuration. From a control system standpoint, the implementation of a back-to-back solution allows the best exploitation of the aeolian energy. The full decoupling of the wind turbine from the electrical grid is realised by means of a DC link. Because of the presence of a DC bus, the control of the grid electrical quantities is carried out exclusively by the grid-side converter. In fact, it has to deal with the current and/or voltage control, the grid synchronization and also the DC bus voltage control. Vice versa, the generator-side converter manages all those functions related to the optimization of the energy extraction, such as speed and machine current control. The use of a 2L-VSC solution, that is shown in figure 2.8, has several technical advantages such as the relatively simple structure and the reduced number of components, which contributes to a robust and reliable performance. However, one of the most common problem of this architecture is that only two output voltage stages can be commanded. This, in turn, produces relatively high $\mathrm{d}v/\mathrm{d}t$ stresses to generators and transformers.

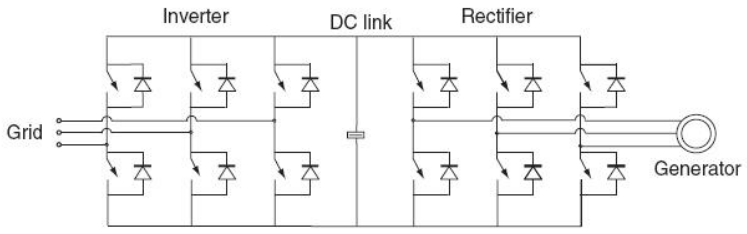

Figure 2.8: Three-phase back-to-back converter for wind turbines

As the voltage range and power of the wind turbine increase, the need of utilize other power converters comes out. In order to achieve an efficient and reliable management of higher power, two possibilities are given: the exploitation of high-power converters topologies or the use of several medium-power converters

connected as series or parallel cells. The most commercialized high-power converter

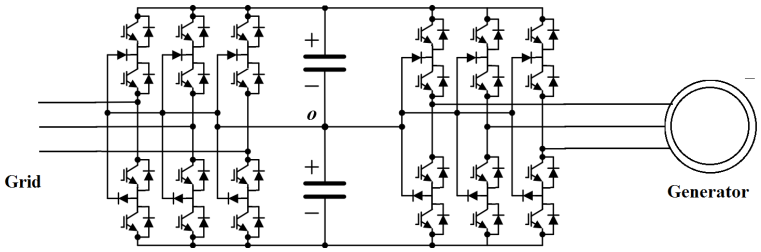

Figure 2.9: Three-phase back-to-back converter for wind turbines

is the three-level neutral-point diode clamped(3L-NPC) topology, shown in figure 2.9. The main benefits of the 3L-NPC are a double output voltage amplitude, using the same voltage rating switching devices, and the ability of providing three output voltage stages that, in turn, leads to a better voltage harmonic content and a reduced dv/dt stress. Anyhow, being the loss distribution among the switching devices of the same arm different, this converter must be oversized in terms of power capacity during the design process[46].

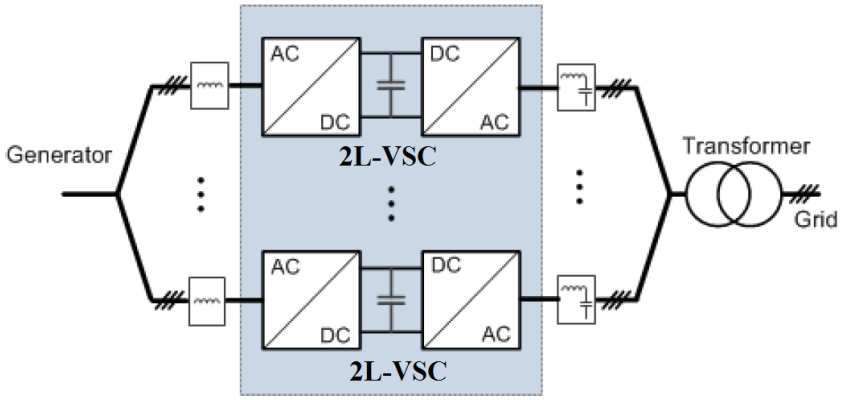

Figure 2.10: Multicell converter with paralleled 2L-VSC converter cells with multi-winding generator

Another option to increase the overall power of the system is to use more power converter cells in parallel or in series. Among the possible multi-cell configurations, in the last years the solution proposed by Gamesa has gained popularity. This topology, shown in figure 2.10, has several 2L-VSC converters paralleled both on the generator and grid sides. The parallel connection of the power cells on the grid side is a typical feature of multi-cell converters since it allows interleaving operation. The greatest advantage is the cancellation of side-band harmonics obtained by properly shifting the PWM signals. However, to an increase of power-handling capability corresponds a decrease of reliability. Indeed, to ensure the correct operation of a device composed by several modules a certain level of redundancy must be reached, but this means also that the number of possible failures increases [42],[47].

A block diagram, similar to the one presented for wind turbines, is reported for solar energy systems in figure 2.11 on the next page. When comparing this

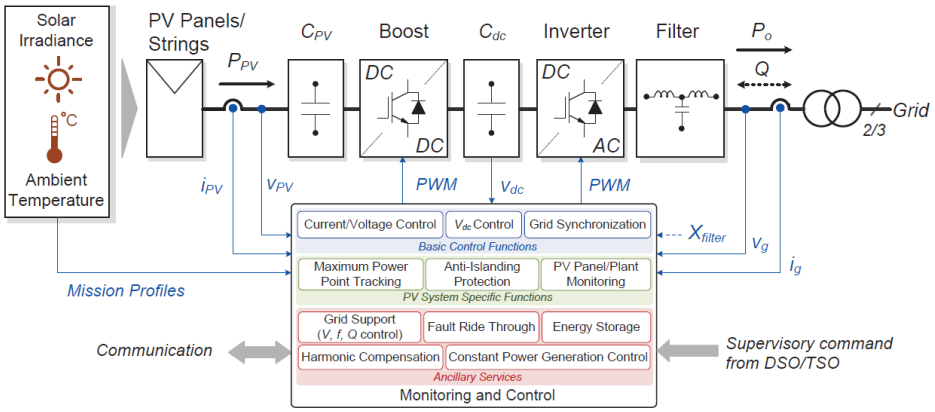

Figure 2.11: General control function blocks for photovoltaic systems

schematic with the one in figure 2.7 on page 42 it is noticeable that the two interface systems for the considered renewable resources present strong similarities. The most evident characteristic regards the presence in both applications of a two-stage power conversion system, made in this case of a DC/DC boost converter and a DC/AC inverter. Although in low power PV applications the implementation of a DC/DC stage is avoided for cost and efficiency reasons, lately, the so called module integrated converters(MIC) are becoming, as time goes on, more popular. Generally, an MIC is a high-efficiency step-up DC/DC converter integrated usually on the back of the PV panel. The MIC operates with autonomous control for tracking the maximum power point locally and is provided with galvanic insulation. Currently to improve power density and efficiency of MICs the resonant power conversion is the most popular approach. Indeed, resonant power converters take advantage and exploit the presence of the parasitic elements of the circuits. So the maximum possible utilization of those parasitic elements together with wide-bandgap semiconductors are leading research trends nowadays. As in wind turbines, also in PV systems the presence of the double conversion stage allows a full decoupling between the energy source and the electrical network, thus facilitating and simplifying considerably the control system. The grid-side converter functions are completely analogous to those described in case of WTs, namely grid synchronization, DC bus control and grid current/voltage control, instead, the DC/DC stage implements MPPT algorithms in order to collect the maximum available power at every operating point since the characteristic of the PV modules are influenced by the solar radiation and the temperature as mentioned earlier. The combined presence of the boost converter and the inverter allows, similarly to the aeolian dual case, the provision of ancillary services for the grid such as the reactive power control, anti-islanding protection algorithms or grid current harmonic compensation. Although PV panels, typically employed in low/medium power applications, are gaining popularity also in high rated power systems, the main difference between photovoltaic and aeolian systems remains, as of today, the rated power of the installed plants. For this reason the majority of power electronics converter for PV systems on the market are single-phase. The driving forces during the design process of PV inverters, besides legal regulations, are the performance requirements. Due to the high cost of solar energy, efficiency is probably the most influential. It can be affirmed that

the PV inverter efficiency for state-of-the-art brand products stands around 98%. Other requirements are the installation cost, the minimization of leakage currents and the power density, especially for domestic and commercial applications. As far as the leakage current is concerning, it appears because of the high-frequency harmonics caused by the modulation of the power converter and because of the high stray capacitance(10 nF/kW) between the PV cells and the grounded metallic frame of each module. Galvanic isolation can help to interrupt the leakage path and to have a safer structure, but the use of a transformer lowers the efficiency and has additional costs.

The simplest solution among single-phase PV inverters is the full bridge inverter. This topology includes in its basic configuration a grid-side low frequency transformer that guarantees galvanic isolation and voltage elevation. Despite its simplicity this configuration possesses important advantages like the large range of input voltages and the simplicity of its control: this converter can be controlled either with bipolar, unipolar or hybrid modulation since, due to isolation, the common-mode voltage cannot generate a leakage current. As mentioned before, the attempt to increase the overall efficiency of the system has led to the development of configurations without the transformer. A very popular transformerless solution is the H5 converter. This converter topology, with respect to the H-bridge, adds an additional switching devices S_5 in the positive bus of the DC link to give to the stray currents another path during the command of zero voltage vector. In particular, switch S_1 is always ON during the positive half of the reference voltage and S_3 is always ON during the negative one. Switches S_2, S_4 and S_5 are switched at high frequencies. During the zero voltage vector the switch S_5 is turned OFF and the current find its path through S_1 or S_3 (red line in fig. 2.12) depending on the considered half-cycle, thus bypassing the stray capacitance.

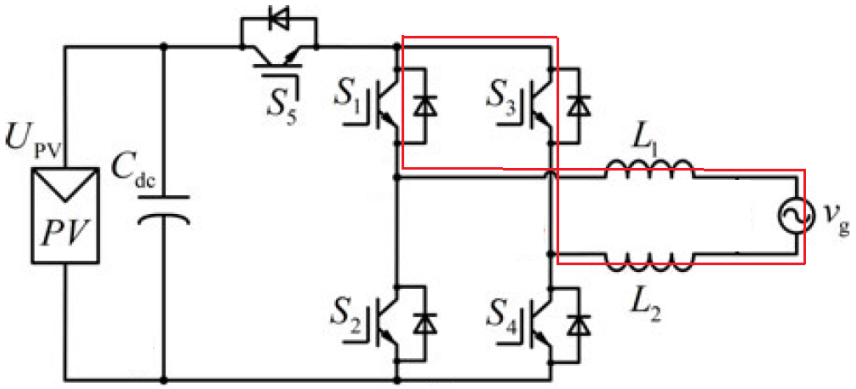

Figure 2.12: H5 inverter by SMA

Therefore, this stratagem prevents the reactive power exchange between the inductances and the DC-link capacitor, increasing the efficiency, and isolates also the PV module from the grid, eliminating the high-frequency content of common-mode voltage [44]. Another transformerless topology derived from the full bridge is the High Efficiency and Reliable Inverter Concept(HERIC) patented by Sunways (see fig. 2.13). While the PV bypass in the H5 converter is placed on the DC side, in the HERIC converter, in order to achieve the same function, two extra switches

are added on an additional branch placed in parallel with the load, before the output filter. In this case, during the positive half-cycle of grid voltage, switch S_6 is turned ON and it is used during the free-wheeling period of S_1 and S_4. Adversely, during the negative half-cycle of grid voltage, switch S_5 is turned ON and it is used during the free-wheeling period of S_2 and S_3. In the free-wheeling modes, the inductor current of HERIC topology is flowing through two switches. Therefore, although the H5 topology features less power devices than the HERIC topology, its conduction losses are higher [48].

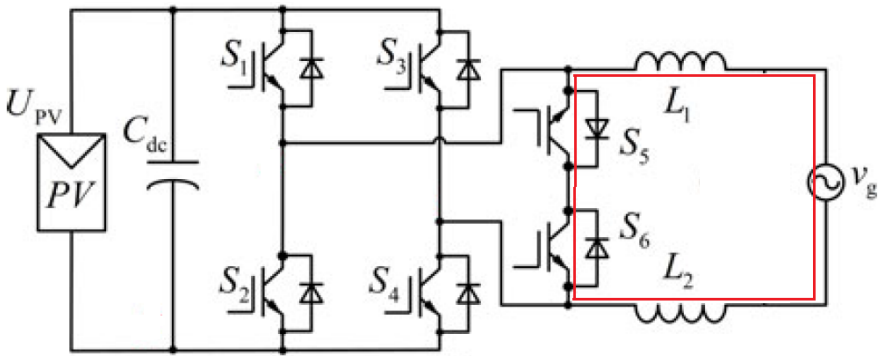

Figure 2.13: HERIC inverter by Sunways

To conclude, it is worth to mention that other transformerless high efficiency topology are research objects. The most adopted practice in PV inverters is the two-stage power conversion that allow a wide range of input DC voltage. However, the multiple-stage power conversion system lower the efficiency and reliability of the PV system. To overcome these problems in 2003 the quasi-Z-source inverter(qZSI), a novel family of single-stage buck-boost inverters, was proposed. It is a combination of the two-port passive quasi-impedance network with a 2L-VSC (see fig. 2.14). The distinctive characteristic of the qZSI is that it can boost the input voltage by using an extra switching state:the shoot-through state. The shoot-through state is the simultaneous conduction of both switches of the same phase leg of the inverter. This operation is forbidden for the traditional VSC because it would cause the short circuit of the DC-link capacitors. Instead, here the shoot-through state is used to boost the magnetic energy stored in the inductors without short-circuiting the capacitors. This increase in inductive energy provides the boost of the voltage across the inverter during the traditional operating states. In addition, the properties of the qZSI allow the connection of energy storage devices, such as batteries, in parallel with one of the capacitors of the quasi-Z-source network. The charge and discharge of the batteries can be controlled by means of duty cycle variations during the shoot-through state. This simple energy storage system doesn't require any additional circuit and can help to cover the peak power demands. It is worth to notice that, in case of higher power applications, the two-level qZSI could be easily extended to the multilevel topology [49].

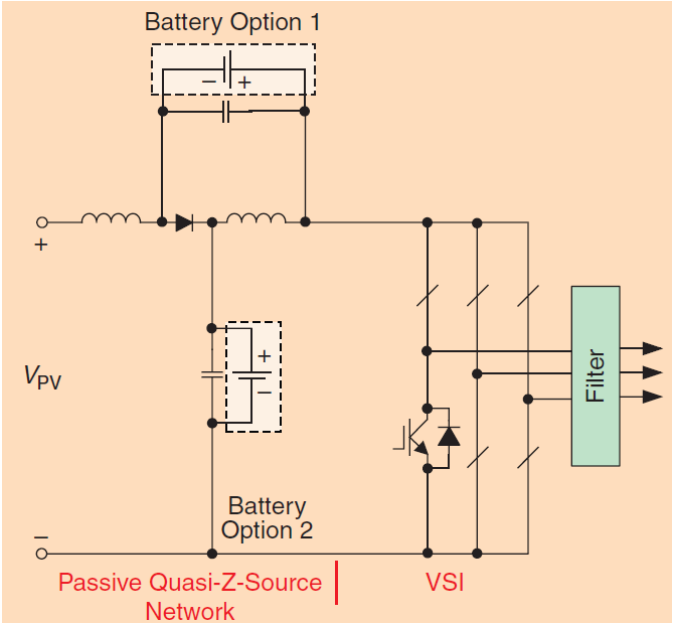

Figure 2.14: qZSI inverter with optional battery for PV power generation

2.2 Grid-tied converter control

The previous section has discussed the grid integration of renewable resources into the electrical network. Initially, being the most important RESs of the actual scenario, solar and wind energy systems in their overall composition have been described. The characteristic of each production plant as well as the most adopted configurations have been analysed in terms of efficiency and conveniences, providing an in-depth description of the power conversion stages and major state-of-the-art converter topologies. As outlined before, the fluctuation and unpredictable features of wind and solar energies are non-preferred for grid operation. To facilitate the integration of renewable resources and to guarantee a stable operation, distribution/transmission system operators have issued and continue to develop strict requirements for the behavior of RESs, known as grid codes. Basically, the grid codes are always trying to make the RESs to act as conventional power plants from the electrical utility point of view. That means they should not be a passive power source that simply injects the available power, but also behave like an active generation unit. This has forced power converters manufacturers to find innovative solutions and to design multi-function control systems to perform all the required tasks. In fact, only through a proper control of the power electronics section of renewable systems their grid integration can be accomplished without worsening network stability and power quality. As previously mentioned, the different functions of a converter control system can be divided in basic control functions, namely grid current/voltage control, DC voltage control and grid synchronization, RES specific functions, such as MPPT, anti-islanding protection or energy storage, and ancillary functions like reactive power support, fault ride-through or harmonic current compensation. Given their importance for the general system behaviour, hereinafter the basic control functions are further investigated.

Even though the varieties of renewable energy systems are distinguished in their

grid connection in single- or three-phase and single- or double-stage structures, in this section a single stage system will be considered. In addition, the analysis will be carried out supposing a three-phase balanced structure since, by a control standpoint, three-phase systems are analogous to single-phase systems and the control techniques applied to the first can be extended also to the second if proper techniques are applied in the control design.

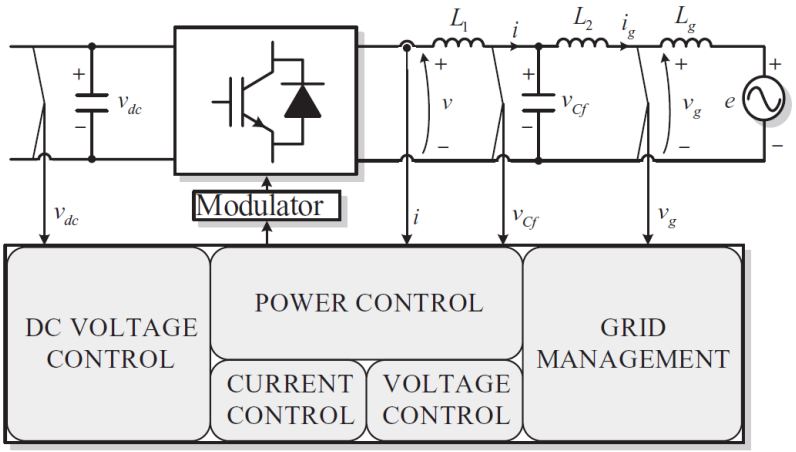

Figure 2.15: Overall scheme of the LCL filter grid converter control

Figure 2.15 sums all the basic control functions of a grid-connected power converter and shows the typical reference circuit to design the control system. In the picture can be noticed, from left to right, the DC link capacitor, to which the renewable resource is upstream connected, the DC/AC converter, the grid connection filter (in a LCL structure in the reported scheme) and finally the electrical grid, represented by an AC voltage source in series with a line inductance L_g.

The role of the grid filters in VSC-based grid converter operation is twofold. On one side the grid filter should have a dominant inductive behaviour to guarantee the proper operation of the VSC if connected to a voltage source type system such as the utility grid. On the other side, VSC-based grid converters generate PWM carrier and side-band voltage harmonics. These voltages may lead to current flowing into the grid, which can disturb other sensitive loads/equipment and increase losses if proper grid filters are not adopted. A grid filter made by a simple inductor is the simplest solution to comply with the two aforementioned requirements. However, for applications around and above several hundreds of kW the switching frequency is generally low, to limit losses. Hence to attenuate the harmonics in the current enough to meet the demands of standards and grid codes the use of a high value of input inductance could be ineffective or too expensive, as well as detrimental for the system dynamic response. The preferred solution is to implement an LCL low-pass filter which provides 60 dB per decade attenuation for the PWM carrier and side-band voltage harmonics after the resonance frequency. This implies that the resonance frequency must be chosen far enough from the switching frequency but not so much to not challenge the current control loop. With this solution, optimum results can be obtained using quite small values of inductors and capacitors.

2.2.1 Current control

One of the demands present in all standards regarding grid-tied systems is the quality of the distributed power. Power quality requirements have been mainly developed in order to preserve the quality of the grid voltage waveform in amplitude, frequency and phase. However, the quality of the current is also of concern and in this sense the grid converter, through the current controller, is the sole agent responsible for compliance with power quality standards in RES.

As previously indicated in figure 2.15, it is common practice to connect the converter to the electrical network through an LCL filter in order to mitigate the detrimental effects of higher order harmonics. However, at least during the initial part of the design process, it is common practice to neglect the influence of the C_f capacitor of the filter since it only deals with the switching ripple frequencies. In fact, at frequencies lower than half of the resonance frequency the LCL filter inverter model and the L filter inverter model are practically the same. The LCL filter-based inverter behaves as if the capacitor is not present and the frequency characteristic is equivalent to the frequency characteristic of a filter made by the sum of the inductances downstream of the converter (L_1, L_2 and L_g). Hence, considering this assumption to be valid, the reference scheme for the design process becomes the one shown in 2.16, where $L = L_1 + L_2 + L_g$ is the aggregate inductance at the inverter output.

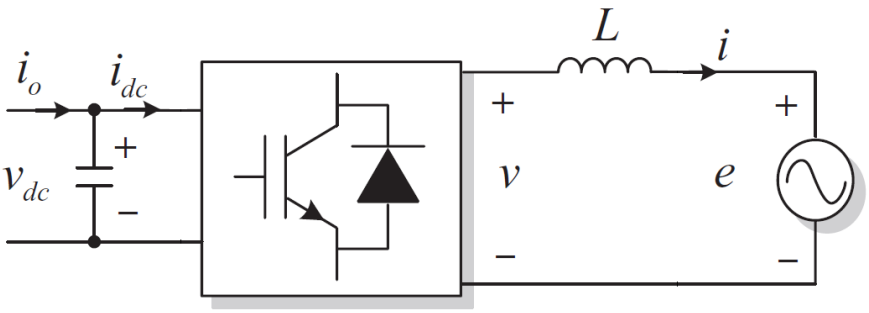

Figure 2.16: Reference scheme for DC voltage control

In this case, the dynamic equations of the system expressed in a rotating dq frame synchronous with the grid voltage vector are:

$$\frac{\mathrm{d}i_d(t)}{\mathrm{d}t} = \frac{1}{L}[-Ri_d(t) - e_d(t) + v_d(t)] + \omega i_q(t) \tag{2.1a}$$

$$\frac{\mathrm{d}i_q(t)}{\mathrm{d}t} = \frac{1}{L}[-Ri_q(t) - e_q(t) + v_q(t)] - \omega i_d(t) \tag{2.1b}$$

The role of the current controllers is to calculate the desired components of the commanded voltage vector ($v_d(t)$ and $v_q(t)$). Afterwards, a modulator selects the converter switching states and their time of application.

The most common control techniques used when current control has to be performed are traditionally three: the proportional-integral control(PI), the proportional-resonant control(PR) and the deadbeat predictive control.

PI controller

One of the most adopted control system is the well-proven PI controller. This type of control is easy to design and to implement and the related literature is wide. Figure 2.17 shows the block diagram of the current loop with a PI controller: $G_{PI}(s)$ is the controller, $G_d(s)$ is the delay due to elaboration of the computation device and to the PWM, quantifiable as 1.5/2 times the sampling period(T_s), and $G_f(s)$ is the transfer function of the filter.

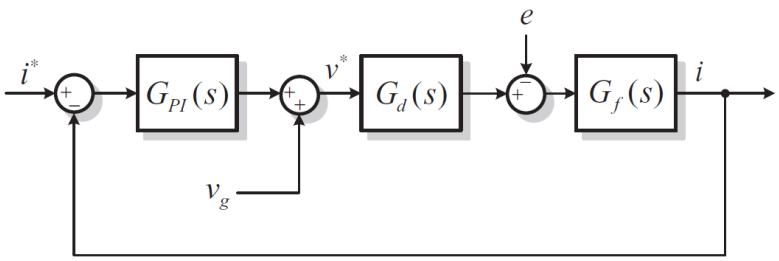

Figure 2.17: PI current control

The equation describing the PI controller in the Laplace domain is:

$$G_{PI}(s) = k_P + \frac{k_I}{s} \tag{2.2}$$

where k_P is called proportional constant and k_I is the integral constant. In sinusoidal systems the PI controller usually presents as major drawback the inability to eliminate the steady-state errors. This is due to the poor performance of the integral action when the disturbance is a periodic signal. However, to overcome this important drawback, the PI control can be implemented in a rotating dq frame synchronized with the electrical frequency of the system. Indeed, in this case the reference current is no more periodic but becomes a constant value. The PI controller implemented in the dq frame is traditionally considered to be a good solution for regulating sinusoidal currents in balanced three-phase systems. However is not good at correcting unbalanced disturbance currents unless the positive and negative sequence currents are dealt with separately. This, of course would require additional computational power and more complex control system. It is worth to notice that, in single-phase systems, the use of a rotating frame is theoretically not possible unless a virtual system is coupled to the real frame in order to simulate a two-axis environment. One of the method to emulate a two-phase system is to add a phase delay block to shift the signal and obtain the virtual quadrature component. Once the virtual quadrature component is retrieved, the controller behaves in the same manner as in the three-phase case and the v_q component of the command voltage must be ignored for calculation of the duty cycle.

In order to obtain a good dynamic response and improve grid disturbance rejection, a grid voltage feed-forward is used. The grid voltage is feed-forwarded, after being transformed in dq components, and added to the output of the current controllers. This improves the dynamics of the controller during grid voltage fluctuations, leading to a fast response for the control system and, in addition,

facilitates the grid connection of the inverter. Also the insertion of cross-coupling terms, when a *dq* reference frame is used would improve the performance of the PI.

The PI tuning process is performed, without considering the disturbances, on the current dynamic equation. In a *dq* rotating frame both the direct and the quadrature current components have to be controlled by a PI controller. However, in a symmetrical and balanced three-phase system the dynamic equations are identical, hence the PI controllers can be designed referring to the same dynamic equation. With reference to figure 2.17 the open-loop transfer function is the product of the transfer functions of each block. Therefore, being the equation of the plant

$$G_f(s) = \frac{1}{R + sL} \tag{2.3}$$

and the first order approximation of the system time delay

$$G_d(s) = \frac{1}{1 + sT_d} \tag{2.4}$$

the open-loop transfer function is:

$$G_{OL}(s) = \frac{sk_P + k_I}{s(1 + sT_d)(R + sL)} \tag{2.5}$$

which is a third order system.

The tuning procedures for PI controllers are several and the choice of the best one depends on different factors such as level of knowledge of the process, the order of the model, the assumptions that can be made or simply the burden of the computation. For example, one of the common methods used to tune a PI controller in electromechanical systems is the pole placement technique through symmetrical optimum criterion in which the main idea is to choose the crossover frequency ω_c at the geometric mean of the two corner frequencies, in order to obtain the maximum phase margin ψ, which in turn will result in optimum damping of the controlled variable response. However, another possible way to design the controller is to reduce the open-loop function order by cancelling with the controller zeros the poles introduced by the electrical plant, namely the filter. With reference to equation 2.5, by setting the integrator gain equal to $k_I = k_P k_{PI}$ and choosing $k_{PI} = \frac{R}{L}$ the open-loop transfer function can be written as:

$$G_{OL}(s) = \frac{k_P}{LT_d} \frac{1}{(s + \frac{1}{T_d})} \tag{2.6}$$

Based on the reduced open-loop transfer function, the closed-loop transfer function is derived

$$G_{CL}(s) = \frac{G_{OL}(s)}{1 + G_{OL}(s)} = \frac{K}{s^2 + \frac{s}{T_d} + K} \tag{2.7}$$

where $K = \frac{k_P}{LT_d}$. As it can be noticed G_{CL} resembles a general second order transfer function of the form:

$$G(s) = \frac{{\omega_n}^2}{s^2 + 2\omega_n \xi s + {\omega_n}^2} \tag{2.8}$$

Therefore, being the current loop formulated as a general second order transfer function it is possible to choose the remaining two parameters according to desired closed-loop characteristics. For example, imposing the dumping ratio, it is possible to compute the proportional constant by means of the formula:

$$k_P = \frac{L}{T_d 4\xi} \tag{2.9}$$

and then, through the relation between k_P and k_{PI} previously imposed, the integral constant is obtained.

Last but not least, when dealing with PI controllers, another significant phenomenon must be taken into account. Indeed, in real control systems the actuator has a limited control power. When its limit is reached, the control action becomes ineffective. In order to avoid these undesired and damaging behaviour, the controller output is usually limited by a saturation function. If the input is either larger or less than the allowable limits, the saturation function resets the input to the maximum or minimum allowed value. This forces the control signal amplitude to respect the constraints of the practical system. Unavoidably, since the PI control algorithm assumes that the manipulated variable is unconstrained, the integral error term continues to grow without bound. The outcome of this scenario is that the response becomes overly oscillatory since the integral value is still large. This is known as integral wind-up. By using a technique called anti-windup tracking, the integral wind-up can be prevented. The principle is to compute the difference between the desired manipulated variable and the saturated version, and feed this back to the integrator within the PI controller [50].

PR control

Although they are relatively simple to implement, linear PI controllers, as discussed above, are prone to some significant drawbacks. Many variations have been proposed to improve their performance, such as the addition of multiple-state feedback and feed-forward path, but generally these variations, even though can expand the PI controller bandwidth, also push the systems towards their stability limits. For instance, a disadvantage associated with the modified PI controllers is the possibility of distorting the line current with the addition of background harmonics introduced along the feed-forward path by a distorted grid voltage. This distortion could, in turn, trigger the LC resonance when LCL filters are used at converter output. To overcome these problems without increase the computational burden and to enhance the converter tracking performance, a very appealing solution is the proportional-resonant controller.

The basic functionality of the PR controller is to introduce an infinite gain at a selected resonant frequency for eliminating steady-state error at that frequency. Hence, it is conceptually similar to an integrator whose infinite DC gain forces the DC steady-state error to zero. The resonant portion of the PR controller can be viewed as a generalised AC integrator, that is a double integrator that achieves an infinite gain at the so called resonance frequency, and almost no gain exists for other frequency components.

The transfer function of the PR controller can be derived through a frame transformation of the PI controller implemented in a synchronous frame. Indeed, through a frequency modulated process the PI controller, indicated here as $G_{DC}(s)$, can be expressed as

$$G_{AC}(s) = G_{DC}(s - j\omega) + G_{DC}(s + j\omega) \tag{2.10}$$

where G_{AC} represents the equivalent stationary frame transfer function. When a pure integrator is transformed into the equivalent AC controller in a stationary frame, the infinite gain at the resonance frequency could lead to stability problems. Therefore, it is common practice to consider a real integrator of the form

$$G_{DC}(s) = k_I\left(\frac{1}{1 + \frac{s}{\omega_c}}\right) \tag{2.11}$$

where ω_c is the controller cut-off frequency. Applying equation 2.10 the obtained PR controller transfer function is

$$G_{AC}(s) = \frac{2k_I(s\omega_c + {\omega_c}^2)}{s^2 + 2\omega_c s + ({\omega_c}^2 + \omega^2)} \simeq \frac{2k_I\omega_c s}{s^2 + 2\omega_c s + \omega^2} \tag{2.12}$$

The gain of this latter transfer function is finite, but still relatively high for enforcing a small steady-state error. Another feature of the real integrator is that its bandwidth can be widened by setting ω_c appropriately, which can be helpful for reducing sensitivity towards, for example, slight frequency variations in a typical utility grid. The current loop of the inverter with a proportional-resonant controller is depicted in figure 2.18.

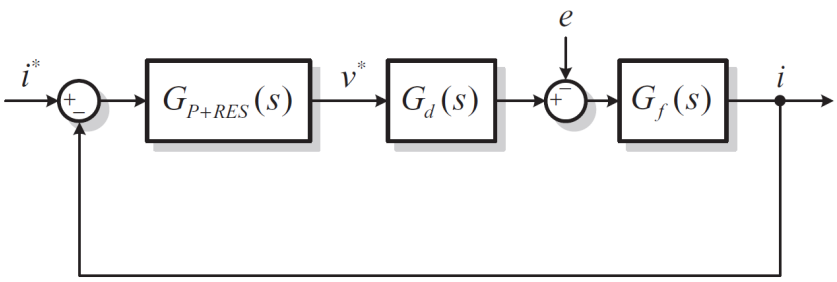

Figure 2.18: PR current control

Using a PR control the steady-state errors when tracking sinusoidal input is removed. Synchronous PI control can mitigate the tracking error, but is generally difficult to apply. Compared to a stationary PI controller, the only computational requirement imposed by the PR controller is an extra integrator for implementing a second-order system, but with a modern low-cost 16-bit fixed-point DSP, this increase in computation can generally be ignored. Besides that, using a PR controller would allow the removal of the grid voltage feed-forward path and, since it doesn't require a synchronous transformation, simplify considerably the control of single-phase systems [51].

Deadbeat control

With the increasing diffusion of digital control techniques, one of the most employed control strategies for current controllers is the deadbeat control. The deadbeat control is a discrete-time model based control scheme that belongs to the model predictive control family. The basic concept of a predictive control is to use a dynamical model of the process to forecast system behaviour and optimize this forecast to produce the best control move at the current time. In current control, this is translated into foresee the evolution of the controlled quantity, the current, and, on the basis of this prediction, choose the state of the converter or the produced average voltage. In principle, the deadbeat control strategy is nothing but a particular application case of discrete time dynamic state feedback and direct pole allocation, and, as such, its formulation for a VSC model can be obtained applying standard digital control theory.

Referring for the sake of simplicity to an equivalent single-phase model of the system, the average inverter model can be described by the set of following equations:

$$\begin{cases} \dot{x} = Ax + Bu \\ y = Cx + Du \end{cases} \tag{2.13}$$

where $x = i$ is the state current vector, $u = [v, e]$ is the vector composed by the inverter output voltage and the grid voltage, $y = i$ is the output variable and the matrices are defined as:

$$A = [-R/L], \quad B = [1/L, -1/L], \quad C = [1], \quad D = [0, 0] \tag{2.14}$$

It is possible to derive a zero-order hold discrete time equivalent of the continuous time system as

$$\begin{cases} x(k+1) = \Phi x(k) + \Gamma u(k) \\ y(k) = Cx(k) + Du(k) \end{cases} \tag{2.15}$$

where by definition $\Phi = e^{AT_s}$ and $\Gamma = (\Phi - I)A^{-1}B$. In most of the application, the system model can be simplified considering the resistance R to be negligible. If this assumption is valid the previous matrices become

$$\Phi = [1], \qquad \Gamma = [T_s/L, -T_s/L] \tag{2.16}$$

Given 2.15, it is possible to derive the predictive controller as a particular case of state feedback and pole placement. In order to show that, it is convenient to rewrite the state equations explicitly. The following result is obtained:

$$\begin{cases} i(k+1) = i(k) + \frac{T_s}{L} v(k) - \frac{T_s}{L} e(k) \\ y(k) = i(k) \end{cases} \tag{2.17}$$

In equations 2.17 it is interesting to notice how the grid voltage can be considered an external disturbance, whose compensation can be obtained by adding a suitable signal, ideally the e signal itself, to the control input v. However a perfect

compensation of this signal is practically unachievable because of the delay due to the calculations.

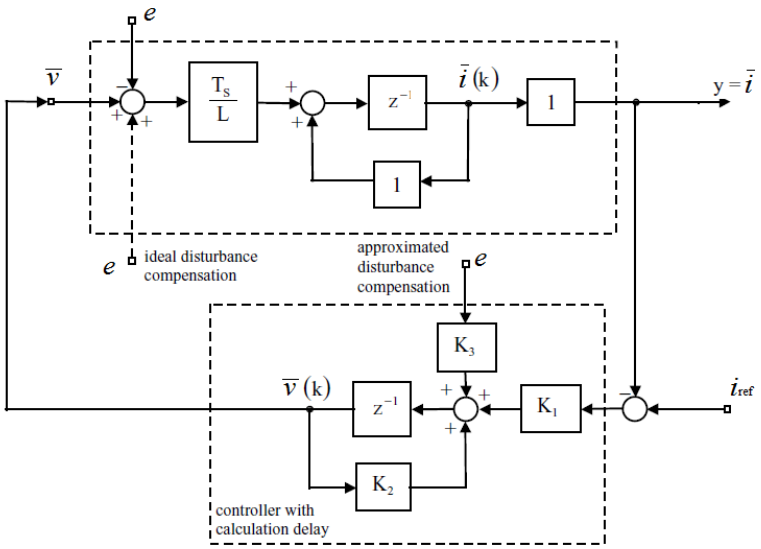

Figure 2.19: Deadbeat controller block diagram

Figure 2.19 shows the overall block diagram derived from the previous equations with the addition of the deadbeat controller. Referring to the picture, the equation describing the controller is

$$v(k+1) = K_1 v(k) + K_2[i_{ref}(k) - i(k)] \tag{2.18}$$

By adding the controller, of course the considered dynamic system increases its order. The new augmented system is described by the following equations:

$$\begin{cases} i(k+1) = i(k) + \frac{T_s}{L} v(k) - \frac{T_s}{L} e(k) \\ v(k+1) = K_1 v(k) + K_2[i_{ref}(k) - i(k)] + K_3 e(k) \\ y(k) = [1, 0] \begin{bmatrix} i(k) \\ v(k) \end{bmatrix} \end{cases} \tag{2.19}$$

where the approximated compensation of the disturbance, governed by gain K_3, has been considered. The new state matrices of the system are as follow:

$$\Phi = \begin{bmatrix} 1 & \frac{T_s}{L} \\ -K_1 & K_2 \end{bmatrix}, \qquad \Gamma = \begin{bmatrix} -\frac{T_s}{L} & 0 \\ K_3 & K_1 \end{bmatrix}, \qquad C = [1, 0], \qquad D = [0, 0] \tag{2.20}$$

In order to obtain a deadbeat controller, the eigenvalues of the state matrix Φ, that identify the position of the system poles, have to be zero. Therefore, in order to get this goal the constant K_1 and K_2 have to be set to

$$K_1 = L/T_s, \qquad K_2 = -1 \tag{2.21}$$

It is possible to demonstrate that the allocation of poles in the origin of the complex plane makes the closed loop system behaviour very peculiar, sharing no similarity with any continuous time system's one. That is because the position of poles in the origin of the complex plane in the discrete time domain corresponds in the continuous time domain to minus infinity, which is of course not physically realizable. In the discrete time domain instead, the allocation in the origin is perfectly doable and the step response of the closed-loop system becomes equal to a combination of pure delays, which is the typical deadbeat closed-loop behaviour.

Lastly, in order to complete the design, also the last constant, responsible of the compensation of the e term, must be chosen. To accomplish this, the transfer function in the Z-domain between the current i and the signal e is computed.

$$\frac{I(z)}{E(z)} = C(zI - A^{-1}) \begin{bmatrix} -\frac{T_s}{L} \\ K_3 \end{bmatrix} = \frac{1}{z^2} \frac{T_s}{L}(-z - 1 + K_3) \tag{2.22}$$

As it can be seen, there is no value of K_3 that can guarantee a zero transfer function from disturbance to output. This is due to the fact that the compensation term of the controller equation is one step delayed with respect to the control output and, as such, is only approximated. Under these conditions, the best is to minimize the transfer function 2.22. It is easy to verify that the choice $K_3 = 2$ achieves this minimization.

Having determined the controller parameters K_1, K_2, and K_3, it is now possible to explicitly write the control equation, which turns out to be

$$v(k+1) = -v(k) + \frac{L}{T_s}[i_{ref}(k) - i(k)] + 2e(k) \tag{2.23}$$

The derivation presented here refers to the basic predictive controller implementation, where the phase voltage e is assumed to be measured. If the use of an output voltage estimator is considered, additional care must be taken. The estimation equation can be directly obtained from the state variable i update equation but this would increase the order of the system. As a general rule, this makes the deadbeat properties and stability of the controlled system more sensitive to model and parameter mismatches, reducing its robustness.

The predictive controller derivation assumes that the model of the converter and its load is valid. Although this is a generally solid assumption, in certain conditions the model validity can be questioned. There can be at least two different reasons for this to happen, namely model mismatches and parameter uncertainties. Model mismatch can occur when, for example, circuit components are not properly modeled or are wrongly neglected that is what happens in some cases with the resistance R of the converter output filter. The effect of model mismatches is normally very serious: since the control equation is based on a given system model, any deviation of the physical system from the model makes the controller interaction with the physical system unpredictable in its effects. As regards parameters uncertainties, they are typically determined by construction tolerances or parameter value drifts, such as those due to varying physical or environmental operating conditions.

Considering the controller design process, several parameters contribute to the choice of the coefficients, hence each of them can be a potential source of mismatch.

For example, one of the common source of uncertainties is the filter inductance L. To perform the analysis of the impact of an inductance mismatch, the eigenvalues of the state matrix have to be computed. Therefore, indicating with ΔL the error on the inductance value it is possible to write

$$\Phi = \begin{bmatrix} 1 & \frac{T_s}{L} \\ -\frac{L+\Delta L}{T_s} & -1 \end{bmatrix} \tag{2.24}$$

Thus, the eigenvalues of the system are given by

$$\lambda_{1,2} = \sqrt{\frac{\Delta L}{L}} \tag{2.25}$$

As it can be noticed, the position of the poles depends only by the relative error on the inductance value. Therefore, unless the error is above 100% the stability of the system is always ensured. Anyway, the system dynamic performances are easily worsened and the typical deadbeat behaviour can be lost. It is worth to notice that the position of the poles in this case does not depend on the sampling frequency. The aforementioned week points of the deadbeat controller seem to undermine its overall applicability. However, the use of a disturbance observer relieves these problems, making the controller more robust with respect to parameter mismatches and controller delays.

It has been demonstrated that the deadbeat is the fastest current controller allowing nulling of the error after two sampling periods. During transient conditions typical of distributed power generation systems such as sudden variation of the power produced by the source or voltage sag due to grid faults, the deadbeat controller can be proven to have superior performances in limiting the peak current. Nevertheless, to directly measure the grid voltage, the predictive controller requires the sensing and analog to digital conversion not only of the regulated variable but also of the voltage. Moreover, contrarily to PI controller, the set-point for the average inverter computed through the deadbeat equation must be correctly scaled down so as to fit it to the digital pulse width modulator. The fitting is normally accomplished normalizing the output of the controller to the inverter voltage gain[52]. Thanks to the easiness of its implementation and its good performance the deadbeat control has been employed during the experimental part of this work.

2.2.2 DC bus control

When single-stage inverters are employed as grid interface for renewable energy systems, the DC bus voltage, that is the voltage at the capacitor terminal on the DC side, is directly dependant on the voltage produced by the renewable source. Thus, when the produced power increases or decreases, the DC bus voltage may be subjected to voltage overshoot or undershoot that would compromise the quality of the injected power as well as the performance of the control system. Therefore, from the point of view of the DC voltage control, power changes result in voltage variations that should be compensated by charge or discharge processes. To better understand the behaviour of the DC link voltage let's consider it by an energetic point of view.

When a capacitor C is charged at a voltage v_{dc}, the amount of energy stored in it is equal to:

$$U = \frac{v_{dc}^2 C}{2} \tag{2.26}$$

Supposing that the capacity C is constant, differentiating the energy with respect to the voltage the following expression is found:

$$d(U) = v_{dc} C d(v_{dc}) \tag{2.27}$$

Therefore, a finite variation of the DC link voltage produce an energy variation equal to:

$$\Delta U = v_{dc} C \Delta(v_{dc}) \tag{2.28}$$

In addition, also imbalances between the power produced by the renewable source and the power injected into the grid may occur. Those power imbalances, considering that they are composed mainly by a second harmonic power mismatch, can be expressed as follow:

$$p_{in} - p_{out} = \frac{\Delta p_{pk-pk}}{2} \sin(2 \cdot 2\pi f t) \tag{2.29}$$

where f is the electrical frequency of the system(50 or 60 Hz) and the peak-to-peak value of the power oscillation is considered. The amount of energy associated with this instantaneous oscillation is:

$$\Delta U = \int_0^{T/2} [p_{in} - p_{out}] \mathrm{d}t = \int_0^{T/2} \frac{\Delta p_{pk-pk}}{2} \sin(4\pi f t) \mathrm{d}t = \frac{\Delta p_{pk-pk}}{4\pi f} \tag{2.30}$$

where $T = 1/2f$.

Hence, by substituting equation 2.30 in 2.28 the DC voltage ripple can be expressed as:

$$\Delta v_{dc} = \frac{\Delta p_{pk-pk}}{4\pi f C v_{dc}} \tag{2.31}$$

Equation 2.31 demonstrates that the decrease or increase of the DC voltage level is obtained by injecting more or less power into the grid with respect to that produced by the source. It is well known that the power injected by the inverter into the grid depends on the product between voltages and currents at the point of common coupling. Hence, to achieve the DC voltage control, the most common strategy consists in a direct control of the output AC current.

The control of the DC voltage through the AC current can result in the identification of two loops, an outer DC voltage loop and an inner current loop. During the voltage control design process it is common practice to consider the two loops to be decoupled, and hence the actual grid current equal to its reference value. This can be justified by the fact that the main goal of the inner current loop is to achieve short settling times and fast dynamic response, on the other hand, the outer loop main goals are optimum regulation and stability, allowing a slower dynamic for the DC voltage.

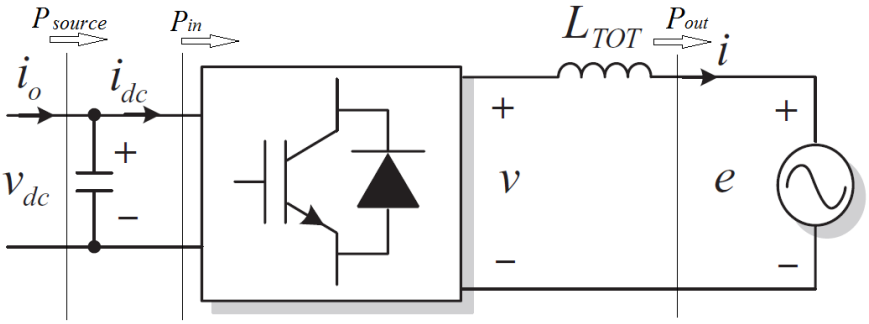

Figure 2.20: Reference scheme for DC voltage control

The most common strategy to control the DC voltage is to utilize a proportional-integral controller. In order to derive a proper tuning procedure is important to analyse the DC link dynamic equation. Referring to the scheme in figure 2.20 and considering the instantaneous input–output power balance for the grid converter in a synchronous rotating dq frame under a no-loss condition, the following equation holds:

$$p_{out} = \frac{3}{2}\{e_d i_d + e_q i_q\} = -v_{dc} C \frac{\mathrm{d}v_{dc}}{\mathrm{d}t} + v_{dc} i_0 = p_{in} \tag{2.32}$$

A small signal linearization of the previous equation leads to:

$$\frac{3}{2}\{[E_d+\hat{e_d}][I_d+\hat{i_d}]+[E_q+\hat{e_q}][I_q+\hat{i_q}]\} = -[V_{dc}+\hat{v_{dc}}]C\frac{\mathrm{d}[V_{dc}+\hat{v_{dc}}]}{\mathrm{d}t}+[V_{dc}+\hat{v_{dc}}][I_0+\hat{i_0}] \tag{2.33}$$

If the synchronous rotating frame dq is voltage oriented, that means the d axis is aligned on the grid voltage vector, the injected active power is independent on the quadrature component of the current. Hence, if the purpose is to control the DC voltage v_{dc} through the grid current, the transfer function $\hat{v_{dc}}/\hat{i_d}$ has to be found. Thus the other perturbations have to be considered null and the second order terms are neglected, resulting in:

$$\frac{3}{2}\{E_d I_d + E_d \hat{i_d} + E_q I_q\} = -V_{dc} C \frac{\mathrm{d}\hat{v_{dc}}}{\mathrm{d}t} + \hat{v_{dc}} I_0 + V_{dc} I_0 \tag{2.34}$$

Considering that in a steady-state condition the power balance is

$$\frac{3}{2}\{E_d I_d + E_q I_q\} = V_{dc} I_0 \tag{2.35}$$

Equation 2.34 can be further simplified resulting in:

$$\frac{3}{2} E_d \hat{i_d} = -V_{dc} C \frac{\mathrm{d}\hat{v_{dc}}}{\mathrm{d}t} + \hat{v_{dc}} I_0 \tag{2.36}$$

To allow the inverter to control the current, the voltage at the DC bus cannot be higher than the line-to-line voltage. However it is usually not much lower in order to limit the switching losses. Thus, indicating with $R_0 = \frac{V_{dc}}{I_0}$ and approximating $V_{dc} \simeq \sqrt{3} E_d$, the transfer function between the DC voltage and the direct component of the current in the Laplace domain is:

$$\frac{\hat{v_{dc}}}{\hat{i_d}} = \frac{\sqrt{3}}{2}\frac{R_0}{1 - sR_0C} \tag{2.37}$$

This dynamic equation is used to tune the PI controller. Usually, if enough information about the plant and the intrinsic delay of the system are known PI controller can be tuned exploiting pole placement or pole zero cancellation techniques. As it can be noticed the plant transfer function has a pole in the right side of the **S** plane and this may lead to instability. However, as the capacity C tends to infinity the pole tends to zero and makes the system always stable again. Moreover, the equivalent resistance R_0 seen by the grid converter at its DC terminal depends on the kind of upstream converter to which it is connected. In fact, when an MPPT algorithm that maximize the power extraction is implemented, the required additional DC/DC converter works in constant power mode. This imply that the V_{dc}-I_0 characteristic can be approximated during transient operations to a straight line with negative slope. In this case the small-signal linearization leads to consider the upstream system as a negative resistance. Therefore, the DC link fed by a constant power source has positive effects for the stability because the plant pole will be in the left side of the **S** plane.

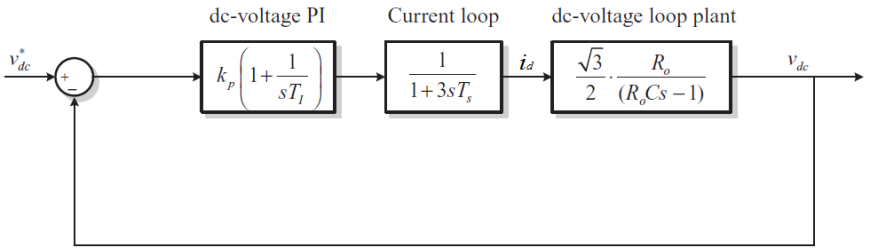

Figure 2.21: DC voltage control block diagram

In conclusion, supposing that the current control loop is designed with the technical optimum and hence can be described by a first order time delay equal to three times the sampling period(T_s), the overall system block diagram is the one shown in figure 2.21. In the diagram theoretically also perturbations of grid voltage and DC current, that affect the DC bus voltage, should be included but they are usually filtered by a correctly chosen DC capacitance.

However, since the proposed DC voltage control loop has been designed considering a linearization of the dynamic equations works well when the variable are not far from their working point, hence it must be used with particular careful. Another way to control the DC bus voltage without involving linearization processes is by an energetic point of view.

Indeed, considering the expression of the energy stored in the capacitor as

$$U = \frac{1}{2}CV_{DC}{}^2 \tag{2.38}$$

with reference to figure 2.20, neglecting the losses of the converter, the following power balance holds:

$$\frac{\mathrm{d}U}{\mathrm{d}t} = P_{source} - P_{out} \tag{2.39}$$

Equation 2.39 shows that the transfer function between the capacitor energy and the output power is a pure integrator and hence, the squared DC bus voltage can be controlled by means of a linear control function that guarantees the same stability for every working point. Generally a PI regulator is used that is fed by the energy error $\Delta U = \frac{1}{2}C{V_{DC\_ref}}^2 - \frac{1}{2}C{V_{DC}}^2$ and provides the active power reference as output.

2.2.3 Grid synchronization

It should be clear now that the primary function of a grid-connected converter is to make the energy produced by renewable resources suitable for its insertion into the power network. This means that the injected current must be, generally, a sinusoidal three-phase current at the the grid frequency. In addition, a proper detection of voltage disturbances is particularly important for grid-connected power converter since they might be harmful for its control system, which can lose controllability on the power signals under such distorted operating conditions, or for the power converter itself. In the light of this, one of the most important aspects to consider in the control of power converters connected to electrical grids is the proper synchronization with the utility network. This function, also called grid synchronization, is an adaptive process by means of which an internal reference signal generated by the control algorithm of a grid-connected power converter is brought into line with a particular grid variable. Such a variable is in most of the cases the grid voltage and, therefore, grid synchronization lies in the accurate detection of amplitude and phase-angle of its fundamental component.

The most adopted synchronization method is the phase-locked loop (PLL). A PLL is a closed-loop system in which an internal oscillator is tuned to the oscillatory dynamics imposed by the grid. In other words, by means of a feedback loop, the internal oscillator is controlled to keep the time of the grid voltage signal.

The basic structure of a phase-locked loop is shown in figure 2.22. It consists of three fundamental blocks namely the phase detector (PD), the loop filter (LF) and the voltage-controlled oscillator (VOC). The PD generates an output signal proportional to the phase difference between the input signal v and the signal v' generated by the internal oscillator of the PLL. The LF is typically a PI controller with a filtering action to attenuate the high frequency components from the PD output. The voltage-controlled oscillator generates at its output an AC signal whose frequency is shifted with respect to a given central frequency ω_c as a function of the input voltage provided by the loop filter.

To better understand its working principle let's consider the case in which the input signal is a sinusoidal single-phase signal of the type $v = \sin(\omega t + \phi)$ and the internal oscillator generates a cosinusoidal function described by the equation

$$v' = \cos(\theta') = \cos(\omega' t + \phi') \tag{2.40}$$

In its simplest structure, the phase detector is made of a simple multiplier with gain k_{PD}, as shown in figure 2.22. In this case, the error ε_{pd} at the output of the

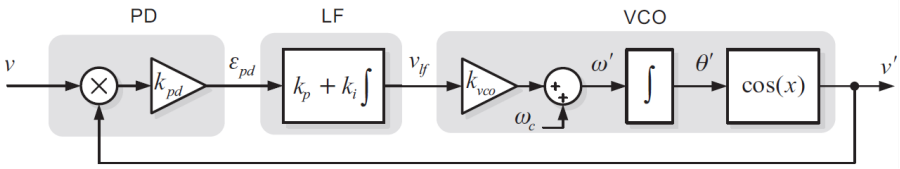

Figure 2.22: Phase-locked loop structure

PD is indicated by:

$$\varepsilon_{pd} = V k_{PD} \sin(\omega t + \phi) \cos(\omega' t + \phi') \tag{2.41}$$

where V is the sinusoidal input signal peak value. Using the goniometric relations, the error can be reformulated as follow

$$\varepsilon_{pd} = \frac{V k_{PD}}{2} \{\sin[(\omega - \omega')t + (\phi - \phi')] + \sin[(\omega + \omega')t + (\phi + \phi')]\} \tag{2.42}$$

If the loop filter is well tuned the high frequency component of the error is cancelled. Therefore the error reduces to

$$\varepsilon_{pd} = \frac{V k_{PD}}{2} \sin[(\omega - \omega')t + (\phi - \phi')] \tag{2.43}$$

In addition, if it is assumed that the VOC is already locked on the input signal, that is $\omega \simeq \omega'$, the error at the phase detector output is described by

$$\varepsilon_{pd} = \frac{V k_{PD}}{2} \sin(\phi - \phi') \tag{2.44}$$

From the previous equation can be observed that the multiplier phase detector produces non-linear phase detection because of the sinusoidal function. However, when the phase error is very small, that is when $\phi \simeq \phi'$, the output of the multiplier PD can be linearized in the vicinity of such an operating point. Therefore, once the PLL is locked, the relevant term of the phase error signal is given by

$$\varepsilon_{pd} = \frac{V k_{PD}}{2} \sin(\phi - \phi') \simeq \frac{V k_{PD}}{2} (\phi - \phi') = \frac{V k_{PD}}{2} (\theta - \theta') \tag{2.45}$$

As it can be noticed by equation 2.45, the phase detector, when the PLL is locked, can be considered a simple zero order block with gain k_{PD}. As far as the VOC is concerned. the generated cosinusoidal signal has frequency

$$\omega' = \omega_c + \Delta\omega = \omega_c + k_{VCO} v_{lf} \tag{2.46}$$

where $\Delta\omega$ is the signal at the loop filter output multiplied by the gain of the voltage-controlled oscillator and ω_c is the VOC centre frequency that is usually provided to the PLL as an external parameter, dependent on detected frequency range. The phase of the signal produced by the oscillator is computed through integration of the angular frequency. Therefore, a small signal variation of the phase θ' is given by

$$\tilde{\theta}' = \int \tilde{\omega}' \mathrm{d}t = \int \tilde{v_{lf}} k_{VCO} \mathrm{d}t \tag{2.47}$$

The previous equation can be easily transformed in the Laplace domain using small signal analysis

$$\mathscr{L}\{\varepsilon_{pd}(t)\} = \frac{V k_{PD}}{2}[(\Theta(s) - \Theta'(s)] \tag{2.48}$$

$$\mathscr{L}\{\tilde{\theta}'(t)\} = \frac{k_{VCO}}{s} V_{lf}(s) \tag{2.49}$$

Hence, the system block diagram related to the described PLL structure is the one of figure 2.23

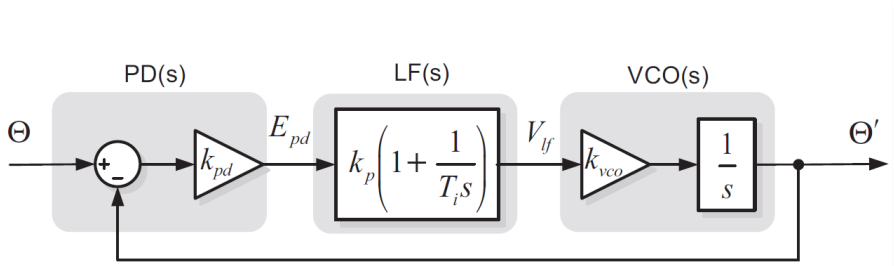

Figure 2.23: Block diagram of basic PLL in Laplace domain

The closed loop transfer function of such a system is a second order system and as such it presents a filtering characteristic in the detection of the phase-angle which is an interesting feature for attenuating the detection error caused by possible noise and high-order harmonics.

Nevertheless, this basic PLL structure ensures its designed performance under the assumption that the frequency of the signal to be locked is much higher than the bandwidth of the PLL. Indeed, when this assumption is not valid, the high frequency term of the phase error signal provided by the multiplier PD can not be neglected when the dominant dynamic response of the PLL is studied. This is the reason why this simple PLL architecture is usually not employed in grid-connected applications in which the grid frequency is very close to the cut-off frequency of the PLL and the high frequency oscillations in the phase-angle error signal are only twice the input frequency.

To overcome this problem, instead of a simple PD multiplier the so called quadrature signal generator (QSG) is adopted in grid-connected applications. The ideal QSG is a function capable of extracting from a generic distorted signal a clean set of in-quadrature signals without introducing any delay at any frequency. The typical structure of a PLL with an ideal QSG is shown in figure 2.24

According to this structure, the phase-angle error at the phase detector output is expressed by

$$\begin{aligned} \varepsilon_{pd} &= V \sin(\omega t + \phi)\cos(\omega' t + \phi') - V \cos(\omega t + \phi)\sin(\omega' t + \phi') \\ &= V \sin[(\omega - \omega')t + (\phi - \phi')] = V \sin(\theta - \theta') \end{aligned} \tag{2.50}$$

According to this equation, when the PLL is well synchronized the in-quadrature phase detector does not generate any steady-state oscillatory term, which allows

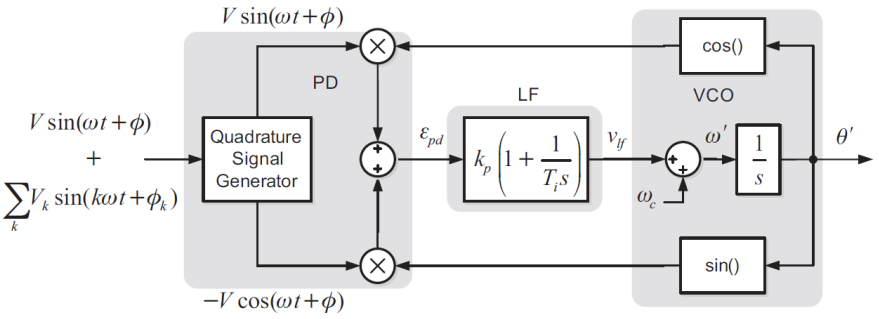

Figure 2.24: Block diagram of a PLL with quadrature signal generator

the PLL bandwidth to increase, making possible the PLL design for grid-connected applications. There are several method to implement a QSG in single-phase applications, probably the simplest one is to delay the input signal by a constant value $\pi/2$. However, if the signal is distorted, also all the other harmonics are delayed of the same amount and the resulting signal will not maintain the same harmonic content as before. To overcome this problem other methods have been studied, for example the Hilbert transformation.

The implementation of a quadrature signal generator in three-phase application might seem a complex task if the same procedure of the analysed for the single-phase case is just applied to the three phase voltages. However, it is well known that three-phase control systems are usually implemented through Park transformation, a coordinates change that basically decouples the voltages of the three-phase system in three orthogonal axes($dq0$). If the Park transform equation are considered, it can be noticed that equation in 2.50 is a part of the Park transform. Hence, taking this into account, the previous diagram can be modified into figure 2.25. Therefore, supposing that the d and q voltage components in three-phase systems are correctly computed, the quadrature signal generator is not really needed. In fact, the PI controller of the three-phase PLL receives the voltage v_q as input and will force it to be zero. In this sense, the quadrature voltage component can be considered as the phase error since it is proportional to the difference $(\theta - \theta')$.

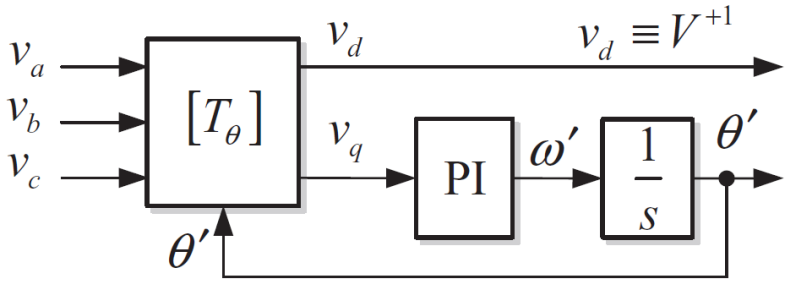

Figure 2.25

Nevertheless, grid synchronization in three-phase systems is not a trivial transposition of the procedures used in single-phase case. Indeed, even though the

three-phase grid is often supposed to be balanced and symmetric, there are some circumstances, such as the occurrence of a fault, in which those proprieties are lost. However, even during these circumstances, it is paramount that the converter is still able to correctly execute its control functions, above all when RESs help reducing fault consequences and contribute to grid restoration after the fault. For these reasons, grid synchronization of three-phase grid-connected converters is carried out through the computation of the magnitude and phase angle of the positive- and negative sequence voltage components and, in particular, the correct detection of the positive-sequence component at the fundamental frequency of the three-phase grid voltage can be considered as the main task of the synchronization system. Therefore, comparing with single-phase systems, it is not sufficient to increase the PLL bandwidth to correctly synchronize the converter but it is required to implement compensation algorithms to reduce the effects of mutual coupling terms between positive and negative voltage components. To accomplish this task, it is common practice to adopt a three-phase synchronous PLL based on using two synchronous reference frames, rotating with positive and negative synchronous speeds, respectively. The usage of this double synchronous reference frame allows decoupling of the effect of the negative-sequence voltage component on the dq signals detected by the synchronous reference frame rotating with positive angular speed, and vice versa, which makes possible accurate grid synchronization even under unbalanced grid faults.

Chapter 3

Auxiliary Services in RES

The first prototypes of renewable energy resources have been implemented and connected to the electric power system in the early 1980s. Since then, penetration level of renewables into power systems has been increasing rapidly, year by year, all around the world. At the beginning of this process, the power system, managed and protected according to traditional power flows concepts, did not undergo to any sort of change since generation from RESs was a little percentage of the whole generated power and it could be absorbed by the existent infrastructure. In the 21st century, technological developments, together with an increasing sensitivity of the world population towards green sustainability and earth care, have encouraged a rapid diffusion of solar and wind power systems, so fast that only in year 2014 40GW of solar power and 51GW of wind power have been added to the world generation. This trend is doomed to continue even faster in the next years as different countries have fixed precise objectives in this direction. In particular, as far as the European Union is concerning, during the European Council reunion in 2009, the 2020 climate & energy package has been approved. The so called "20-20-20" package sets as targets to be reached before 2020 a 20% curtailment of greenhouse gas emissions (from 1990 levels), an increase up to 20% of EU energy production from renewables and a 20% improvement in energy efficiency. The direct consequence of this shift of paradigm is an increase of solar and wind power exploitation and, by consequence, of the share of distributed power sources that, despite their huge potential and convenience, are intermittent and may be detrimental for the system [53].

The majority of the existent electric power systems are, at the present, vertically integrated utilities. An electric utility is characterized as vertically integrated when the generated electric power flows only in one direction, from the power plants to transmission network, then to distribution network and finally to the consumers, and power generation, transmission, and distribution sectors are owned and operated by one body. As such, a massive introduction of renewable power sources and integration of dispersed generating units in the actual power systems must always be cautious. Without opportune countermeasures and adaptations, as the injected power of grid-connected RES increases, the power quality and overall system's reliability decline.

The decline of power quality can be quantified in terms of voltage level variations, frequency fluctuations and harmonic content in the waveforms. Voltage rise effect is one of the issues that would appear as a result of increasing renewables inter-

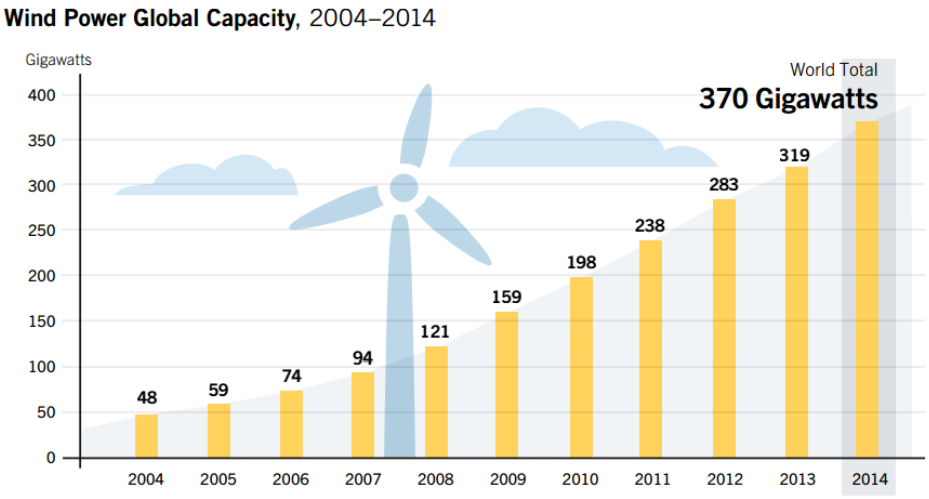

Figure 3.1: Wind Power Global Capacity trend from 2004 to 2014

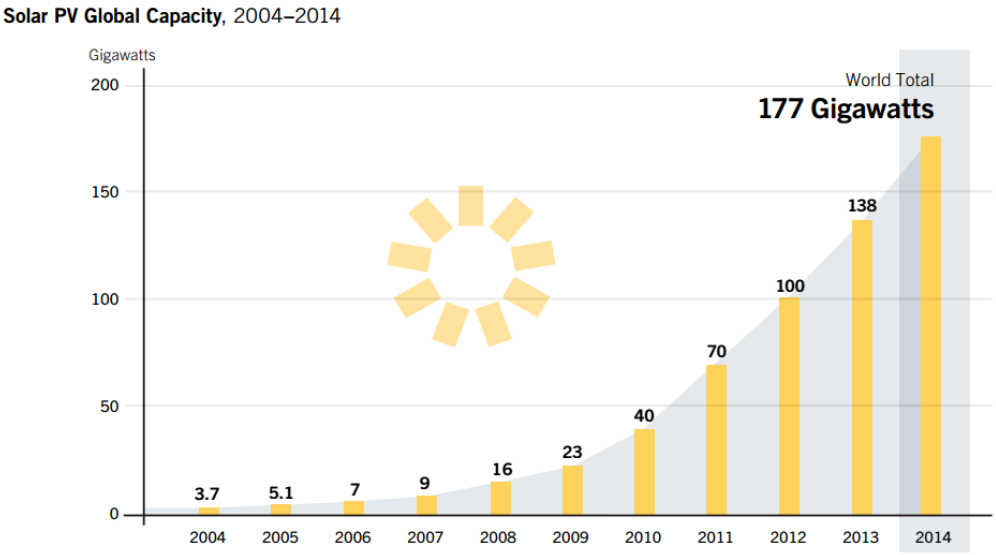

Figure 3.2: Solar Power Global Capacity trend from 2004 to 2014

connection when periods of low power demand occur. Some RESs, such as small PV systems, are usually intended to operate near unity power factor to optimize energy use. Therefore these systems, by injecting only active power into the utility side of the grid, may change the rate of reactive power flow in the network, and the nearby buses may experience under/overvoltage problems. Moreover, unlike customary non-renewable resources, in case of wind and solar energy systems, the output power is affected by fluctuations caused by minute-to-minute variations in wind speed or solar irradiance. The severity of such phenomenon depends on weather conditions, installation, geographical condition and topology of the system. Power fluctuations may increase overloading or underloading and unacceptable voltage fluctuations such as the voltage flicker, that can produce annoying and objectionable changes in light output. These voltage variations may also be caused by switching operations in the RES installation, usually start or stop operations of

equipment. Frequency fluctuation is one of the most important factors influencing power quality. Any imbalance between power production and power consumption can result in frequency fluctuation. Small RESs cause negligible frequency fluctuations compared with large production plant. However, at increased penetration levels, distributed generating units can increase the severity of this problem. At last, harmonic distortion which is known as a critical power quality can occur because of the power electronics converters used in renewable systems. Harmonic distortion can increase the risk of parallel and series resonances, overheating in capacitor banks and transformers and false operation of protective devices.

Also reliability is affected by green energy resources introduction into the power system. When these sources are interconnected at the utility distribution level, the bidirectional power flow may cause some operating conflicts that could affect the system's reliability. In fact, the utility breakers and reclosers are set to see certain distance down the radial feeder, referred to as the reach of the device. The device reach is determined by minimum fault current that the device would detect. The minimum fault current could be degraded with the presence of grid-connected RESs which inject power into the grid [54].

In order to limit the disrupting effects of a massive DG presence in the network is therefore necessary to evolve and improve the actual power system architecture (smart grids have been indicated as a solution in the previous chapters). Nevertheless, before undertaking such a difficult change that would require new infrastructures and elevated costs an optimization of the power system performance is surely a more feasible and cost effective way to encourage the adoption of distributed energy resources. This is the reason why transmission and distribution system operators, have issued a set of rules and regulations for the grid connection of renewable resources. Those norms, exploiting the widespread use of power electronic converters in distribution systems, are addressed to enhance the participation of distributed generating units to the management of the electrical grid through the provision of the so called ancillary services [55].

3.1 Auxiliary services

Traditionally, ancillary services in the electricity supply sector are defined as services provided by grid operators in addition to the transmission and distribution of electrical energy and aimed to support the transmission of power, maintain reliable operation and ensure the required level of power quality and safety. Since the development of interconnected power systems, ancillary services have been a necessity of any electrical system and they are used by every independent system operator to maintain the system frequency within certain limits, control the system voltage profile, ensure the stability of the system, preventing overloads and restoring the system, or portions of it, after an outage.

The classification of ancillary services varies from one system to another depending on market structure and technical requirements and even some similar services have different names in different countries. According to the directive 888 issued by the Federal Energy Regulatory Commission(FERC) in United States there are 12 different functions classified as ancillary services some of which are mandatory

and, as such, must be sold by the transmission operators and purchased by the consumers. These are:

1. Regulation: minute-to-minute management of generation or load to keep generation-load balance within the control area.

2. Load Following: this service refers to load-generation balance towards end of a scheduling period.

3. Energy Imbalance: management of generation to meet the hour-to-hour variations in load.

4. Spinning Operating Reserve: unloaded generating capacity that is synchronized to the grid and fully available for several minutes to correct for generation-load imbalances.

5. Supplemental Operating Reserve: generating capacity and plug-in load to match generation-load demand. However, unlike spinning reserves, supplemental reserve is not required to respond immediately.

6. Backup Supply: supply guarantee to ensure the ability of providing power to consumers in case of unavailability.

7. System Control: control area operator functions that schedule and control generation and transactions in real time to maintain generation-load balance.

8. Dynamic Scheduling: control system able to transfer some or all of generator's output or a customer's load from one control area to another.

9. Voltage Control Support: the injection or absorption of reactive power from generators or capacitors to maintain system voltages within required ranges.

10. Real Power Transmission Losses: compensation of the difference between the energy supplied to the network by the generator and the energy at the consumer's disposal.

11. Network Stability Services from Generation Sources: maintenance and use of special equipment to maintain secure transmission system.

12. Black Start Capability: the ability of generation unit to proceed from a shut-down condition to an operating condition without assistance from the grid [56].

However, despite the proposed classification is considered thorough and complete, it does not provide a clear understanding about the benefits and the advantages that those ancillary services bring to the power system. Therefore hereinafter the four main ancillary services that an independent system operator can deliver are described.

3.1.1 Frequency regulation

Frequency regulation is the control of the system frequency by maintaining a balance between generation and load on a real-time basis within a control area. Imbalances between load and generation may arise due to different causes such as uncertainties in demand forecasting, generators' inability to follow up load changes and generation or load trips. The symptoms of an imbalance between load and power generation is a variation of system frequency and bus voltages. This is much like what happens to a car on cruise control if you start going up a hill: if the hill is not too steep you can maintain speed, once you reach the limits of the torque supplied by the engine, the car and engine slow down. If the combined output of all the generators cannot supply enough power then the frequency will drop for the entire grid.

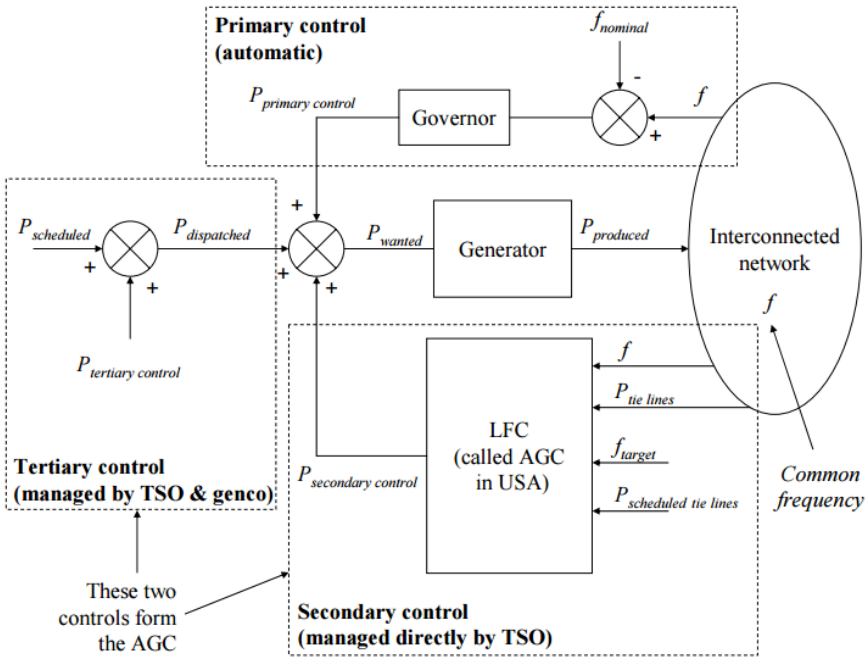

Figure 3.3: Simplified block diagram for frequency regulation

Frequency deviations, if large enough, may lead to serious consequences such as total system collapse. If the system frequency drops drastically due to a sudden mismatch between generation and load, the under-frequency protection relays isolate the generating units to avoid damage. This disconnection further increases the drop in frequency. This unbalance and series of events may cause disconnection of tie-lines and affect the stability of neighboring control areas.

To avoid this sort of contingencies, when a load-generation imbalance occurs the frequency drift triggers an instantaneous response in the system generation, for example, if the frequency decreases the generation of active power increases. This is commonly known as the primary regulation. Primary control provides an immediate automatic action to a sudden change of frequency and it is performed by the speed governors of the generating units. Primary regulation must respond to changes within few seconds.

Once primary control has accomplished its control action, the system will stabilize at a frequency that is slightly lower or higher than its nominal value. However, this produces unscheduled power flows on the tie-lines and lead to undesirable accumulation of area control error (ACE). To recover the nominal frequency, the output of selected generators is adjusted by an automatic generation control (AGC) or, in some cases, through a manual adjustment. This control action is referred to as secondary regulation and its transients are in the order of minutes. Moreover, in order to guarantee and adequate reserve of secondary control at the right time, a further control action, known as tertiary control, takes place. Tertiary control is an economic dispatch that is used to drive the system as economically as possible and to restore security levels if necessary. This would include actions such as adjustments to scheduled interchange and deployment of additional generation resources. Tertiary control is usually performed every 5 minutes.

The benefits of frequency control include avoided costs of loss of industrial production, community disruption and inconvenience, equipment damage and market distortion. Many of these benefits are very difficult to assess because of the large number of people involved. Above all, frequency control is necessary to maintain power system security and, therefore, it has a commercial value[57].

3.1.2 Voltage regulation

System voltage control is used to keep voltage levels within prescribed limits at various points in the transmission grid and to compensate for the reactive requirements of the network. Keeping transmission level voltages at nominal value or within a tight range, usually within $\pm$ 5% of the nominal voltage, ensures proper voltages at the distribution levels. Since the voltage on a bus is strongly coupled with the supply of reactive power, the voltage control is also called reactive power support service. Injection and absorption of reactive power is also required to maintain system stability, in particular to protect against contingencies that could lead to voltage collapse. Voltage is controlled throughout the transmission system through the application and operation of ratio-changing devices, like tap-changers and voltage regulators, and reactive power-control devices. It is convenient to control the bus voltages by providing for reactive power locally, rather than making it to travel through the transmission system. In fact, the power transmission capability of a line is limited by technological as well as economical constraints. Most devices like lines, transformers or breakers are load limited by current rather than by real power. If they are carrying significant reactive power and reactive current, they have less capacity available to transport real power. Moreover, dispatching reactive power using far generating unit would reduce generation capacity and would increase real power losses. Therefore, to maximize the amount of real power that can be transferred across the network, reactive power flows must be minimized. The equipment used to provide or absorb reactive power can be categorized as dynamic, mainly generating units, or static referring primarily to power electronics devices called Flexible AC Transmission System (FACTS) devices [58]. Various sources of reactive power support have different characteristics in terms of dynamics and speed of response, ability of voltage changes and costs. As an example, synchronous generator and synchronous condensers are dynamic equipments. The synchronous

generators are very fast reactive support devices. Usually, a synchronous generator is mandated to absorb or produce reactive power within certain limits, given by its maximum current and its real power production. Synchronous condensers are synchronous machines that are designed exclusively to provide reactive power. They have the response speed and controllability advantages of synchronous generators without the need to construct the rest of the power plant. However, compared to the static devices for the provision of reactive power support, they require more maintenance.

The cheapest way to inject or draw reactive power is through passive elements like capacitors and inductors that accomplish this task without significant real power losses. Capacitor banks are composed of individual capacitors, parallel or series connected to obtain the desired capacitor-bank voltage and capacity rating. They can be switched on or off but offer no variable control. Finally, the newest technology for reactive power support consists in power electronics devices such as Static VAR Compensators(SVC) and Static Synchronous Compensator(STATCOM). An SVC combines the advantages of fast switching capability with conventional passive elements for reactive support(inductors and capacitors) to provide a continuous range of control from the absorption to the injection of reactive power. Consequently, the controls can be designed to provide very fast and effective reactive support and voltage control. However, because SVCs use capacitors, they suffer from the degradation in reactive capability as voltage drops. The STATCOM is a solid-state shunt device that generates or absorbs reactive power. As regarding the response speed, the control capabilities and the use of power electronics the STATCOM shows similar performance as the SVC. However, the basic difference is that the STATCOM uses power electronics to synthesize the reactive power output, without employing capacitors and inductors. The STATCOM ensures very quick and efficient reactive power support by virtue of its solid-state nature. STATCOM capacity does not suffer from degraded voltage as seriously as SVCs and capacitors do [59].

3.1.3 Reserves

The reserve services are designed to be activated when a large power deficit occurs due to a contingent situation such as outages of generators and tie-lines. Depending upon the minimum time in which the generation should start providing corrective action, the reserve services are classified into following two categories: spinning reserve services and supplemental reserve services.

The spinning reserve is the potential generating capacity which can be activated on decision of the system operator and which is provided by devices which are synchronized to the network and capable to affect the active power. The spinning reserves must start responding quickly to the frequency change, generally must be available within 10s and should be sustainable for further 20s. These reserves are available in the form of generators that generate at a level lower than the maximum rated capacity. In power systems with large penetration of wind power, spinning reserve is particularly important for the forecast error of wind power that greatly increases the uncertainty of system.

Consequently to its definition spinning reserve are often included in those devices capable of providing frequency control. However, usually the primary control reserve,

which is not controlled by the TSO, has to be excluded from the spinning reserve. In addition, if a consumer agrees to be disconnected or to reduce its load under request of the system operator, can be considered as a spinning reserve (this is often the case of pump loads).

Supplemental reserve is an off-line service that in some special cases can be brought online to the grid quickly to meet additional contingencies. Supplemental or standing reserve units do not need to start responding immediately and actually they are considered as backups for the first ones. The supplemental reserve services are provided by the generators that have fast start-ups such as gas or oil fired generators or hydro generators. This response must be fully available within 30s of the incidence and must be sustainable for further 30 minutes. The supplemental reserve then helps to bring the system frequency closer to nominal value[60].

3.1.4 Black start capability

Even if rare, blackouts are events that occasionally do occur. In order to limit the economical and social consequences, it is paramount for the system operator to recover from the power system collapse as fast as possible. Black start is a process of re-establishing the operation of a power station without relying on external energy sources after a complete or partial outage. During power system recover, black start generation availability is fundamental for stabilizing the system, establishing the transmission path, and picking up load.

Following a failure of the power system, power stations use their own generators to provide the required power. For example, small diesel generators can provide enough power to start larger generators, which in turn can be employed to start the main power station generators. However, there are cases where generators require auxiliary power of up to 10% of their generating capacity for their auxiliary services. Hence, it is not economical to provide such a large standby capacity at each station, so black start power is provided over the transmission network from other stations or from the grid. According to the start-up power requirement[61], generating units can be separated into two main categories: black start generators and non-black start generators, such as steam turbine units, which require cranking power from outside. Typical black start generators are hydroelectric generating units, needing low initial power to open the intake gates, diesel generators, which require only a battery power and gas turbines that can be started remotely with the help of local battery power. However, not all generating plants are suitable for black start service, for instance wind turbines equipped with induction generators that are incapable of providing power to a de-energized network.

However, restoration of the system after a major outage is not a random process, but needs a methodical sequential approach. Available black start generating units must provide cranking power to non-black start generating units in such a way that the overall available generation capability is maximized. Given limited black start resources and different system constraints on different generating units, the maximum available generation can be determined by finding the optimal start-up sequence of all generating units in the system .

Therefore, it is not straightforward that installing additional black start generators would be helpful to the restoration process of a system, in fact also the generator

start-up sequence, the best transmission path and the load pick up sequence would change. This explains why power systems need to evaluate the strategy of both placement and size of new black start generators very carefully before introducing any alteration [62].

3.1.5 Other services

A part from the main ancillary services described above, there are some others which definition and applications strongly depends on the considered context. Among these, there are a few that are worth to mention since are usually associated with grid-tied inverters additional functions namely inertia response, anti-islanding detection and harmonic compensation.

Inertia response

Unlike frequency regulation, which regulate the grid frequency, and therefore balances electricity generation and consumption, inertia response (IR) stabilizes the oscillation of the grid frequency. Traditional power plants, thanks to the employment of big electrical machines, inherently possess the inertia required to damp the grid frequency vibration. The idea of electrical frequency inertia is exactly what we see in mechanical world: inertia of a body measured by its mass m. By implementing an ability to slowly respond to change we can attenuate the oscillation. The bigger the inertia magnitude m, the higher is the ability to absorb oscillations. In power electronics converters for RESs, various methods have been used to emulate the inertia response. One way for stabilizing the swing in grid frequency is to implement an integrator that emulates a virtual frequency inertia with a custom magnitude m. Choosing inertia magnitude is, hence, a trade-off between dynamic response and ability to absorb oscillation.

While a simple IR emulator is a good and intuitive way to stabilize grid frequency, there are some situations and requirements in real world where the simple IR is not enough performing. Some improvements with the purpose of increase power electronic converters performance consists in implementing the virtual IR by controlling the amount of active power P injected into the grid in such a way that the frequency oscillation is reduced. In power generation systems, grid frequency reflects the balance between generation and consumption of active power. So if frequency is lower than the nominal frequency, the injected active power is reduced to counterbalance the frequency oscillation. Besides, the IR may be combined with a frequency recovery function, which makes sure that activation of the IR function does not subsequently lead to over frequency events. If the total frequency at the point of interconnection is above a certain threshold, the soft recovery function is activated and power output is adjusted according to a specified droop curve. In another embodiment of the invention, the IR function is only activated when the error in grid frequency is above a specified threshold. So most of the time when grid frequency is within a specified range of the nominal frequency, the IR function is disabled. The thresholds for activating and deactivating the IR function are different. This hysteresis in the operation of IR function is needed to keep the overall system more stable. Although synthetic inertia is not yet required,

many countries have strongly recommended its use and it is possible that will become a grid requirement in the near future.

Anti-islanding detection

Small-scale energy sources can supply substantial levels of power, enough to satisfy an individual building's needs and still feed excess power back to the grid. With this type of distributed generation of power, however, loss of power in the grid can create a hazardous situation when a solar array or wind turbine, for example, continues to supply power. Islanding refers to the condition of a DG generator that continues to feed the circuit with power, even after power from the electric utility grid has been cut off. Islanding can pose a dangerous threat to utility workers, who may not realize that a circuit is still powered while attempting to work on the line and also can complicate the process of restoring grid power. Anti-islanding protection provides mechanisms designed to prevent occurrence of these power islands by breaking the connection between the energy source and the grid when a blackout occurs.

Determining when the grid has lost power can be a significant challenge in many circumstances. On casual inspection of a typical grid-tied energy system, the loss of power from the grid would seem to be quickly evident. In some cases, however, the local load can present characteristics that result in only very small changes in active and reactive power when the grid loses power. As a result, an inverter would not be able to detect the difference and so would continue supplying power to the unpowered grid, resulting in an islanding condition. The set of conditions under which an inverter cannot detect loss of power in the grid is called a non-detection zone (NDZ). The goal of effective anti-islanding methods is to reduce or ideally eliminate NDZs, using some form of feedback from the grid. Conventional approaches for reducing NDZ typically rely on so-called passive methods, where the inverter measures grid voltage or frequency. When the measured characteristic falls below threshold values, the inverter determines that an islanding condition exists and either shuts itself down entirely or disconnects from the grid while continuing to power the local load.

Anti-islanding protection is so important that specific capabilities and specifications for anti-islanding are required in many countries with a developed power grid system.

Harmonic compensation

The increasing utilization of electronic devices household and business applications is a growing concern for utility companies due to harmonic distortions. The harmonic problem could be further complicated by the harmonic resonance introduced by other system components, such as the power factor correction capacitors. Besides the degrading power quality, the harmonic current flow is also a concern for the telecommunication industry as this may interfere with the adjacent telephone lines.

The power quality can be improved by the use of filters which reduce the harmonic content of the characteristic waveforms of the system. Other than passive

filters, which use the passive components such as inductors and capacitors, also active filters can be employed. Active filters are those power electronics devices controlled in order to inject a compensating current for the harmonics detected at the point of common coupling. The active filters are more advantageous than the passive filters because they can eliminate all types of harmonics in the system whereas passive filters compensate specific order harmonics. The example for the active filter is the inverter, in which the controlled switching of the inverter compensates the harmonics in the specified system. Achieving the acceptable level of power quality can be obtained through a cooperative effort among the power users and equipment manufacturers. This will result in a near sinusoidal waveform on the circuit, which will allow all connected load equipment to operate properly. Thanks to the increasing penetration of renewable energy and to their power electronics grid interface, it is possible to mitigate the total harmonic distortion by controlling the inverters properly and implementing active filter functions.

3.2 Grid Requirements

To ensure consumers participation in ancillary services in the medium and low voltage grid, several regulators around the world have come up with newly developed grid standards requesting the RESs to have essentially similar operating capabilities as conventional plants. The technical terms of grid codes are divided into static and dynamic requirements. The static part of each code consists of issues related to continuous operation of generating units; the dynamic part of the codes considers issues regarding the operation of distributed generating(DG) unit during fault sequences and disturbances in the grid.

3.2.1 Static requirements

Static requirements are specified at the point of common coupling(PCC) of the power source. Voltage and reactive power control, power factor requirements, frequency requirements, and power quality are some of the common issues which are addressed.

Among the main factors influencing voltage regulation in a power system there are the short-circuit capacity, the impedance of the network, tap-changing operations of on-load tap changer transformer and the reactive power flow, which can be shaped by generating units. In general, there are three common reactive power control modes, namely fixed reactive power, fixed power factor and voltage set-point control. In fixed reactive power mode the reactive power flow at certain set point, specified by the regulator, is maintained. In fixed power factor mode, commonly adopted for small-scale generators connected to LV grid, the ratio between active and reactive power is kept constant. Lastly, voltage set-point control mode consist in injecting the necessary reactive power at PCC to regulate the voltage magnitude. The reactive power generation capability of the renewable power sources at PCC is usually defined by power factor regulation. The requirements request to operate within the range specified by capacitive and inductive power factor. Some grid codes consider the variation in voltage level instead of fixing power factor requirements at

PCC.

Other than voltage magnitude, also the system frequency must respect certain boundaries. Mechanical failures of generators, quick load changes, or loss of line in the transmission system are some of the reasons behind load-generation mismatches that often result in transient fluctuations of system frequency. In the presence of a large share of RESs this load-generation mismatch issue happens during light load or unpredictable changes of environmental conditions. In general, the regulators request the generators' primary frequency control to maintain the continuous frequency operating range at PCC, that for the italian power system corresponds to a range of $[47,5-51]Hz$. When RESs are entirely decoupled by the electrical grid because of the presence of full rated power converters, their active power injection is not affected by frequency variations. It is for this reason that some regulators require wind plants and large PV farms to be equipped with an inertia emulation system to support system frequency following a major frequency event.

Since the power system needs to run in a stable state and be able to deliver power to consumers at an acceptable quality, apart from voltage and frequency limits, the static grid requirements provide also power quality standards. Harmonics and flicker at PCC are two major power quality disturbances, which need to be taken care of while dispatching power through RESs. Sources, which contributes in harmonics injection in renewables include dynamic reactive power compensation equipments, power electronics and the electric grid itself, being the impedance a function of loading level and switching state in the grid. Voltage distortion limits are usually given in the [1.5-5]% range for the total harmonic distortion (THD) and [1-3]% range for any individual harmonic.

Flicker is a concern only for distribution networks in areas of the system where fault currents are very low, in other words where the system is weak. The perception of short-term flicker (PST) is measured as a weighted average of the flicker contribution over ten minutes, whereas perception of long-term flicker (PLT) is measured over two hours. The recommended values of PST and PLT at planning levels are always given.

In the italian power system, grid codes for interconnection of distributed resources in medium voltage and low voltage grids are given, respectively, by the norms CEI 0-16 and CEI 0-21. Considering low voltage distribution grids, the italian norm states that all the generating units interfaced by grid-connected converters with a rated power above 3kW must participate to voltage control through reactive power supply. In particular, referring to figure 3.4, two characteristic curves are defined by the distribution system operator(DSO). The first curve regulate the reactive power support by means of a function $cos\phi = f(P/P_n)$ whereas the second one defines a fixed power factor $cos\phi$. Both of them are identified by the so called power lock-in value, which is the P/P_n value that triggers the reactive power control. Beyond this value, that is 50% or 5% depending on the considered curve, the converter must measure the voltage at PCC. If the voltage is higher than $1.05V_n$ the generating unit stops working at unity power factor and move its operating point according to the characteristic curve, supplying reactive power to the grid.

In addition, norm CEI-0-21 states that, if the power plant has a rated power higher than 6 kW, it must also follow a reactive power control logic based on characteristic curves $Q = f(V)$ where V is the voltage at the PCC. This kind of

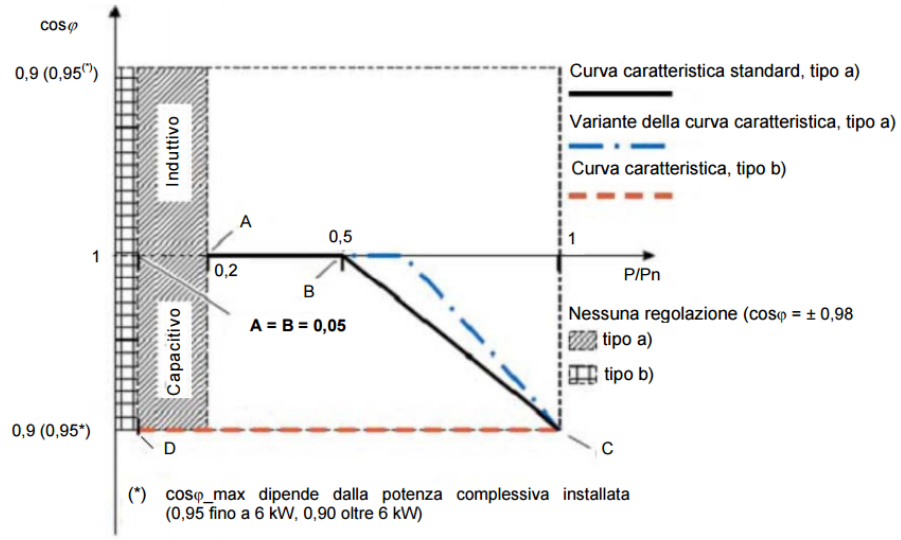

Figure 3.4: Characteristic curves $cos\phi = f(P)$ defined on three points A, B and C [63]

regulation is such that the generating unit may operate in working points outside the triangular capability curve ($cos\phi < 0.9$). With reference to figure 3.5 $-Q_{min}$ and $+Q_{max}$ are the maximum and minimum reactive power values defined by the rectangular capability curve but in any case they cannot have a magnitude lower than 48.43% of P_n. When a regulator prescribes a characteristic curve, any operating point indicated must be reached within ten seconds.

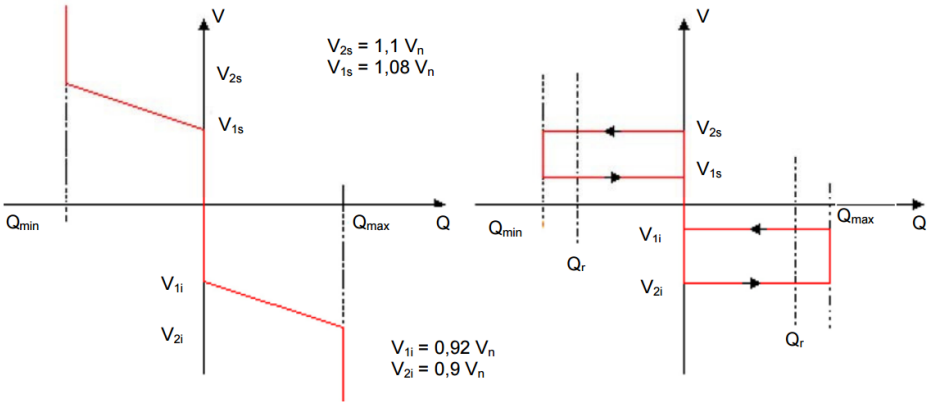

Figure 3.5: Standard characteristic curves Q=f(V) [63]

Norm CEI 0-21 provides also active power limitation curves to make distributed generating unit contribute to frequency regulation. In the frequency range comprised between 47.5 Hz and 50.3 Hz grid-connected generating units must produce the maximum available active power. During system frequency transients, active power injection must be regulated according to the curve in figure 3.6. When the threshold of 50.3 Hz is reached, all the production plants interfaced through power converters must reduce their active power injection in function of the frequency deviation, according to the defined droop of the system. Active power reduction must be

linear and must be accomplished within an interval of time about equal to one second. If subsequently to the control action the frequency decreases, the active power produced by the generating units will be kept constant to the minimum value reached during the frequency transient until the system frequency remains inside the range of 50 ± 0.1Hz continuously for 300 seconds.

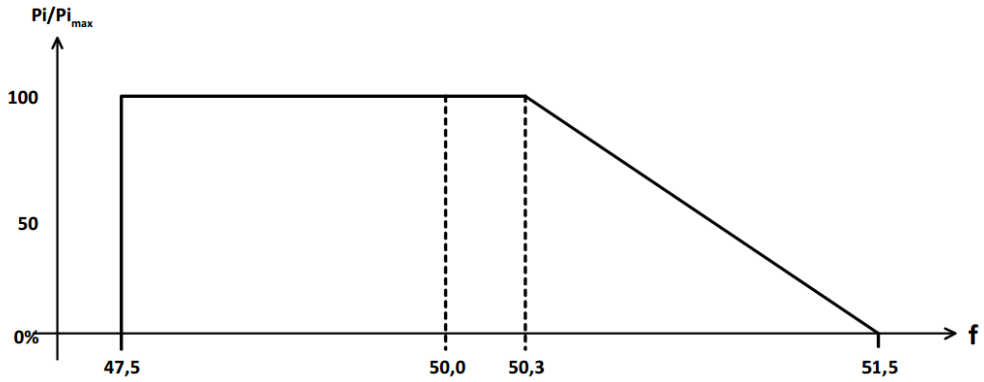

Figure 3.6: Active power limiting ramp for over frequency occurrences

3.2.2 Dynamic requirements

Reliability is greatly affected by system disturbances such as asymmetrical and symmetrical faults on transmission system. After the occurrence of such disturbances, it is expected that transition to the acceptable, new steady state is stable and fast. In this sense, dynamic requirements are mainly oriented to help the attainment of the new operating point, thus improving the overall reliability of the system.

Along with control and protection units, generation units play a significant role in providing satisfactory dynamic performance during and after disturbances. When a fault occurs in an electric network, the feeder voltage level drops until the protection devices trip and isolate the faulty region from the rest of the network. Depending on the location and the type of the fault, RESs experience different types of voltage sags at PCC and, by consequence, the protection devices may disconnect them from the grid. When renewable energy constitutes a large share of the total generation the disconnection of RESs is not acceptable since not only this would lead to a shut-down of healthy portions of the grid but may also cause a worsening of the fault condition. Thus, modern grid codes demand large RESs to continue their uninterrupted operation according to given voltage–time profiles under different fault conditions. Connection to the grid must always be maintained within the boundaries provided by the voltage-time profiles. Sometimes, due to switching off of large loads, energization of capacitor banks or faults, voltage level at the PCC experience an increase instead of a decrease. In order to ride through also such a condition, voltage-time requirements have been recently added in several grid codes. As well as specifications for undervoltage are identified as low voltage ride-through (LVRT), overvoltage requirements are known as high voltage ride-through (HVRT).

Another dynamic requirement that in some cases is requested concerns reactive

current supply at PCC to support the PCC voltage during voltage sags. Voltage support during short-circuits helps to contrast the voltage drops dues to HV grid faults. Indeed, the lower is the short-circuit power of the network, the more dangerous is the downstream propagation of faults in HV lines. For this reason, grid codes demand that generating unit remains connected to the grid during faults to provide an inductive reactive current proportional to the voltage drop. This service can be required for almost all the type of faults on the HV and MV lines but the single-phase to ground in MV grids.

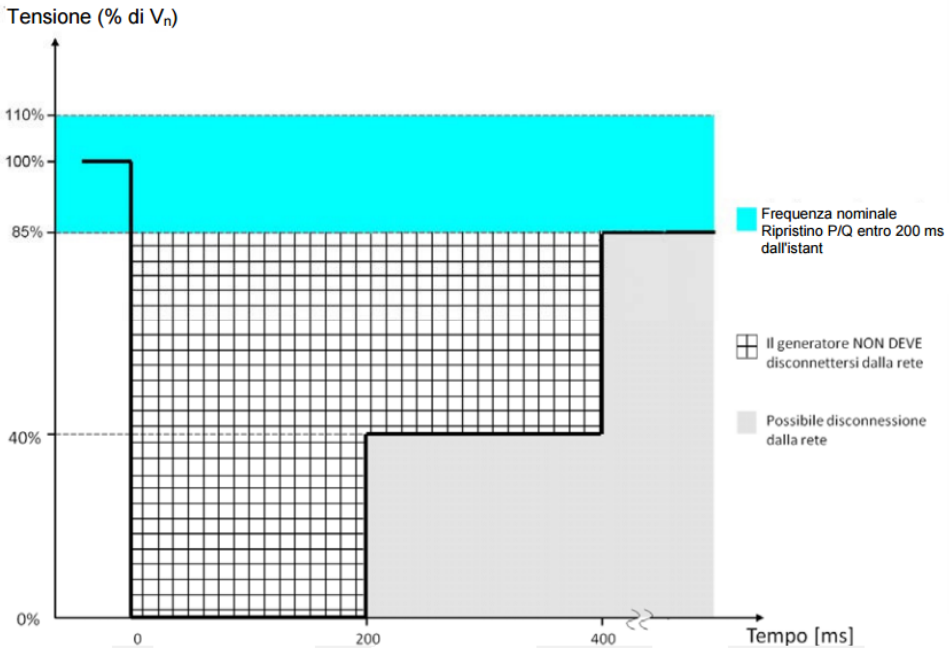

Figure 3.7: LVRT requirements in italian power system

In figure 3.7 the voltage-time curve provided in CEI 0-21 for low voltage grid is reported. The requirement applies to production plants with rated power above 3 kW. In the dashed area the generating unit must not disconnect from the power system, however, it is allowed to temporarily interrupt the active and reactive power injection. In the grey area the generator can be disconnected from the grid, even if for the best of the network is better not, whereas in the turquoise zone, corresponding to +10% and -15% of the rated voltage, the generating unit must re-establish active and reactive power injections as they were before the contingency within 200 ms [63].

A similar voltage-time profile is also provided in CEI 0-16 for high and medium voltage power systems (see fig. 3.8 on the following page). In this case, however, it is possible to notice also HVRT requirements in the same graph as LVRT requirements. As far as HVRT is concerning, the generation unit must remain connected in the dashed area, between the overvoltage and undervoltage limits. Instead, when the overvoltage is detected for an amount of time so that the limit is crossed, the generation unit can be disconnected. It is worth to notice that the behaviour suggested by the curve must be ensured for overvoltages regarding one or more phases [64].

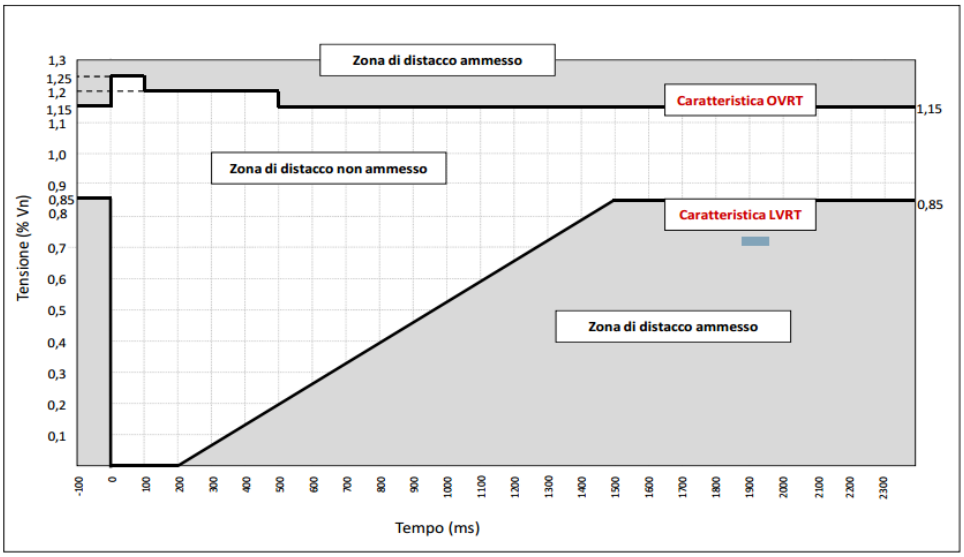

Figure 3.8: V-t voltage profile for static generating units

3.3 Converter control for ancillary services

The first priority of the RES control is to extract as much energy as possible from the renewable energies in normal operation. Besides, as it has been shown in the previous sections, because of the introduction of many specific grid requirements, which have as main purpose a reliable and efficient power generation, these resources are nowadays required to implement multifunctional control systems to provide ancillary services. The most common auxiliary services provided by grid-connected converters for renewable resources are reactive power injection, current harmonic compensation and anti-islanding detection. Theoretically the renewable resource can contribute also to frequency regulation through active power control, nevertheless, in case of renewable energy systems connected to low voltage grid, the rated power of power electronics interface is not sufficient to influence frequency regulation through active power injection, hence this function is usually not implemented.

3.3.1 Voltage grid support

In wind plants and photovoltaic parks, among ancillary services, voltage control is gaining popularity thanks to its importance to improve grid efficiency, safety and reliability in a distributed manner. The main goals of reactive power control is to regulate, or at least support, the system voltage level and to enhance the system stability during faults. Considering power converters for renewable resources connected to low and medium voltage grids, the available reactive power to be exploited for these purposes depends on the instant-by-instant production of active power. Indeed, being these systems sized in terms of their maximum apparent power S_{max}, the reactive power deliverable to the grid is equal to

$$Q_{max}(t) = \sqrt{S_{max}^2 - P^2(t)} \tag{3.1}$$

If the inverter's sizing S_{max} matches exactly the rated active power generation

there is no capacity for reactive power left when $P_{act}(t) = P_{rated}$. By consequence, if the network requires a reactive injection higher than what is available, the injection of reactive power may become disadvantageous for the system's owner because it would imply a power generation reduction. A certain oversizing of the inverter leads to a certain secured reactive power control capacity but also to increased costs.

Reactive power injection is controlled indirectly through current control. Indeed, considering the expression of the power in a *dq* frame synchronous with the grid voltage and supposing small variations of the voltage under balanced conditions, reactive power injection can be considered dependant exclusively on reactive current injection at the PCC. Hence, the reactive power control consists in identify the opportune amount of power to be injected. Different methods can be implemented to control the power injections, including open- or closed-loop approaches as well as direct power controls. The most common way to implement a reactive power control system and to comply with grid requirements is the droop control. The basic idea of such control system is to reproduce the characteristic of the synchronous generators connected to a turbine regulated through a speed governor, which are controlled such that the frequency decreases as the fed active power increases and the voltage amplitude decreases as the fed reactive power increases. This principle

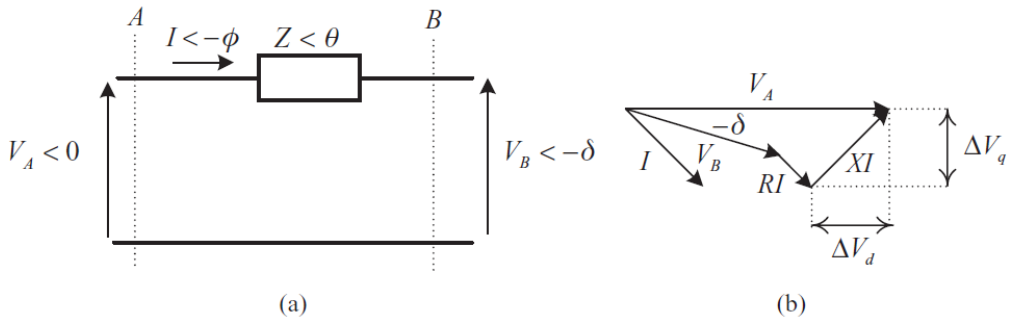

Figure 3.9: Power flow through a line and its relative phasor diagram

can be explained by looking at the power transfer between two sections of the line connecting a converter to the grid. This can be derived using a short-line model and complex phasors. The analysis below is valid for both single-phase and balanced three-phase systems. Referring to figure 3.9, the active and reactive power flowing into the line at section A are

$$P_A = \frac{V_A^2}{Z}\cos(\theta) - \frac{V_A V_B}{Z}\cos(\theta + \delta) \tag{3.2}$$

$$Q_A = \frac{V_A^2}{Z}\sin(\theta) - \frac{V_A V_B}{Z}\sin(\theta + \delta) \tag{3.3}$$

where δ is the power angle and θ is the power factor angle at section A. As $Z\cos(\theta) = R$ and $Z\sin(\theta) = X$ equations 3.2 and 3.3 are rewritten as

$$P_A = \frac{V_A}{R^2 + X^2}[R(V_A - V_B\cos(\delta)) + XV_B\sin(\delta)] \tag{3.4}$$

$$Q_A = \frac{V_A}{R^2 + X^2}[-RV_B\sin(\delta) + X(V_A - V_B\cos(\delta))] \tag{3.5}$$

Hence

$$\Delta V_d = V_A - V_B \cos(\delta) = \frac{RP_A + XQ_A}{V_A} \tag{3.6}$$

$$\Delta V_q = V_B \sin(\delta) = \frac{XP_A - RQ_A}{V_A} \tag{3.7}$$

When the inverter is connected to the grid through a mainly inductive line, such is the case of transmission and three-phase distribution lines, R may be neglected. If also the power angle δ is small, then $\sin(\delta) \simeq \delta$ and $\cos(\delta) \simeq 1$ and it is possible to write

$$\delta \simeq \frac{XP_A}{V_A V_B} \tag{3.8}$$

$$V_A - V_B \simeq \frac{XQ_A}{V_A} \tag{3.9}$$

Equations 3.8 and 3.9 shows that for $X >> R$, small power angle δ and small voltage difference $V_A - V_B$, the power angle can be controlled by regulating P, while the inverter voltage V_A is controllable through Q. This conclusion form the basis for the well-known voltage droop regulation through reactive power:

$$V - V_0 = -k_Q(Q - Q_0) \tag{3.10}$$

where V_0 is the nominal voltage at the PCC and Q_0 is the instantaneous reactive power injection. Figure 3.10 shows the control loop to regulate the voltage at PCC using reactive power injection.

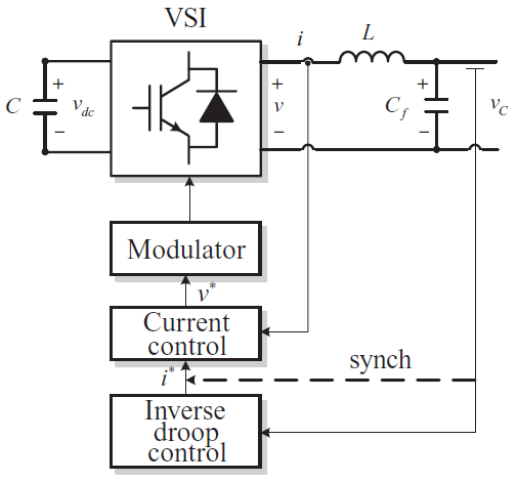

Figure 3.10: Voltage droop characteristic

However, one of the hypothesis of the voltage droop control is that the considered line must be characterized by a low R/X ratio. This implies that when the resistance of the cables cannot be neglected, the linearity between the voltage drop and the reactive power injection is no more ensured. This is the case of low voltage lines where the value of the line resistance is often higher than the line reactance. In this case the droop control can be modified to obtain satisfactory performances taking

into account both the terms of the line impedance. To take this into account a transformation matrix $\mathbf{T}$ can be applied such that new power variables are obtained:

$$\begin{bmatrix} {P_A}' \\ {Q_A}' \end{bmatrix} = \mathbf{T} \begin{bmatrix} P_A \\ Q_A \end{bmatrix} \tag{3.11}$$

where

$$\mathbf{T} = \begin{bmatrix} \sin\theta & -\cos\theta \\ \cos\theta & \sin\theta \end{bmatrix} = \begin{bmatrix} \frac{X}{Z} & -\frac{R}{Z} \\ \frac{R}{Z} & \frac{X}{Z} \end{bmatrix} \tag{3.12}$$

Applying this transformation on equations 3.6 and 3.7 results in:

$$\sin\delta \simeq \frac{Z{P_A}'}{V_A V_B} \tag{3.13}$$

$$V_A - V_B\cos\delta \simeq \frac{Z{Q_A}'}{V_A} \tag{3.14}$$

that again show that for small power angle δ and voltage difference $V_A - V_B$, the angle δ can be controlled by regulating ${P_A}'$, while the inverter voltage V_A is controllable through ${Q_A}'$ [65]. Apart from the aforementioned droop control, other reactive power control method for grid voltage support do exist. They are suitable either for low and medium voltage grids and are based either on constant value and/or first order linear equations that can be easily implemented in the inverter controllers. The simplest one is to provide a fixed amount of reactive power but this method is not so often employed since it would imply some sort of knowledge about load power and RES power production time profiles for a known facility. Another method is to use a constant power factor, so that the generated power is proportional to the active power and it is inherently enabled as long as the active power is produced. Accordingly, during the low production periods the generated reactive power will be as low as the active power by keeping the proportionality equal to

$$\cos\theta = K_1 = \frac{Q_A}{P_A} = tan\theta \tag{3.15}$$

When the real power production is low, the potential risk of grid overvoltage becomes smaller as well, since all produced real power can be consumed locally without sending excessive power to the MV network. To partially overcome the potential unnecessary reactive power that may cause an increase of grid losses, another method is to use varying power factor as a function of the produced active power making it to change linearly from a value K_1 related to low level of power production to a value K_2 related to higher levels. It is worth to notice that the main advantage of these reactive power control method consist in the absence of communication with other network equipments, simplifying notably the overall control architecture [66].

Up to now, reactive power injection from RES has been considered in continuous operating conditions only. However, injecting reactive power is helpful also during voltage sags. A voltage sag is a perturbation in the grid voltages characterized by a short-time reduction in the magnitude of one or several phases. The effects

of such disturbances are important in terms of economic losses, malfunction of devices connected to the grid and outages. As of today, majority of grid codes related to faults for distributed generating units only demand withstanding voltage sags but in the near future they could require voltage support control in transient operating conditions as well. Indeed, whenever a sag occurs far away from the distributed generating unit, low-voltage ride-through is mandatory, and a reactive current injection can avoid cascade disconnection and reduce the risk of blackouts.

Advanced control algorithms to ride through different types of voltage sags are mainly based on symmetric sequences. Among the different control algorithms to support grid voltage during voltage sags an interesting solution is proposed in [67]. In particular, to meet the voltage magnitude limits imposed by grid requirements the authors propose the injection of a combination of positive Q^+ and negative Q^- sequence reactive power to support the grid voltage. Positive sequence reactive power is related to the amplitude of the current $\frac{\pi}{2}$ radiants leading from the positive sequence voltage (i.e. the reactive current injected via positive sequence). The same applies for negative sequence reactive power, although it is shifted from the negative sequence voltage.

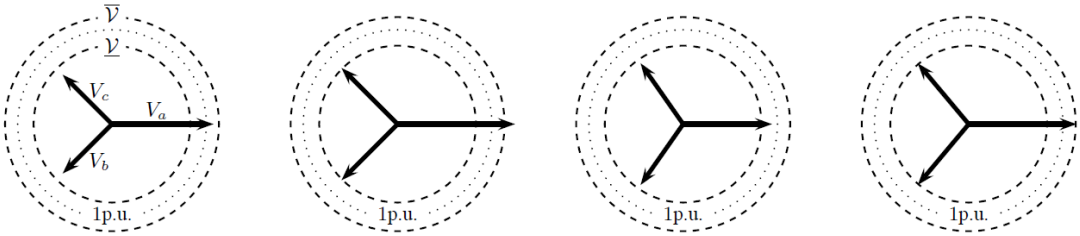

(a) PCC phase voltages without reactive power ($Q^+ = 0$, $Q^- = 0$)

(b) Positive sequence reactive power strategy ($Q^+ > 0$, $Q^- = 0$)

(c) Negative sequence reactive power strategy ($Q^+ = 0$, $Q^- > 0$)

(d) Proposed reactive power strategy ($Q^+ > 0$, $Q^- > 0$)

Figure 3.11

To understand the proposed reactive power control, figure 3.11 presents different strategies of reactive power injection during a voltage sag. The figure shows the three-phase voltages V_a, V_b and V_c, the dashed line highlights the safety limits $\overline{V}$ and $\underline{V}$ and the dotted line indicates the nominal voltage. The figure is divided in four parts describing different scenario depending on the combination of positive and negative sequence reactive power provided after the occurrence of a sag. On the left, in figure 3.11(a), the phase voltages at the PCC without voltage support are shown. If the reactive power is injected via positive sequence $Q^+ > 0$, $Q^- = 0$, then the voltage in each phase raises equally as shown in fig. 3.11(b). The phase voltages should raise until the minimum phase voltage achieves the lowest voltage limit to comply with grid codes. The problem with this strategy is that the highest phase voltage V_a suffers overvoltage. However, when the reactive power is injected via negative sequence $Q^+ = 0$, $Q^- > 0$, the phase voltages tend to be equalized as presented in fig. 3.11(c). The problem is that two phase voltages, V_b and V_c, suffer undervoltage. From these two figures, it can be concluded that some flexible combination of both positive and negative sequence reactive power can regulate the maximum phase voltage to the safety upper limit $\overline{V}$ and the minimum phase voltage to the lower one $\underline{V}$, such is the case of figure 3.11(d). It is worth mentioning that there exist more stringent targets, such as the maximization and minimization

of the voltage sequences or the regulation of the three phase voltages at the nominal pre-fault values (i.e. $V_a = V_b = V_c \simeq 1p.u.$) but they would require higher currents.

In conclusion, thanks to such control actions during grid faults, distributed energy resources can avoid disconnection and help to enhance the overall system stability.

3.3.2 Harmonic Compensation

Nowadays switching power converters are widely used in industrial, commercial, and domestic applications, including electrical drives, DC power supplies, UPS or converters for RES and storage devices. Harmonic currents injected by some of these loads are usually small and do not cause a significant distortion in distribution networks. However, when a large numbers of these devices is considered, the cumulative effect has the capability of causing dangerous harmonic distortion levels, that are further enhanced by the increasing presence of non-linear loads, such as LEDs or compact fluorescent lamps (CFLS). Harmonic distortions do not usually upset the end-user electronic equipment but they rather overload neutral conductors or transformers and cause additional losses and reduced power factor. It is therefore important for the distribution system operator to eliminate or at least mitigate the harmonic pollution at the energy delivering points.

Power quality enhancement using flexible control of grid-connected DG units is an interesting topic if the ancillary harmonic compensation capability is integrated with the DG primary power generation function through modifying control references. This idea is especially attractive considering that the available power from renewable energy resources is often lower than the power rating of DG interfacing converters due to the intermittent nature of wind and solar energy, enabling the grid-connected converter to be considered most of the time as a parallel active filter.

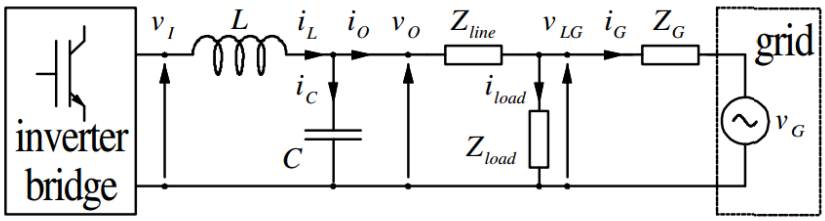

Figure 3.12: PCC connection of a DG resource in distribution line

The control strategy that must be applied in order to provide grid current harmonic compensation consists in controlling the output current of the inverter in order to cancel out the harmonics introduced by the loads. Figure 3.12 shows the typical connection of a distributed resource to the low voltage distribution grid. The impedance Z_{load} here represents the aggregated loads, generally both linear and non-linear, connected to the same bus as the DG unit and responsible for harmonic distortion. The literature proposes several control techniques to compensate for grid harmonics. They can be grouped in three categories based on the measurement

of the instantaneous power, the measurement of the current and the measurement of the voltage at the PCC.

The methods based on the instantaneous power derive the reference for the compensating current from the harmonic components of the power absorbed by the load. The main idea is that the converter should supply the load for the amount of power that is not constant so that the grid is required to provide only a constant power. Besides, even though this methods present the advantage of not requiring the identification of the harmonic currents, they also do not allow the calculation of the reference currents for the power converter. Hence, the delays introduced by the inner current loop of the controller cannot be compensated effectively by an adjustment of the reference currents, leading to a bad response of the method for high order harmonics.

When the active filtering function is performed through current measurements both open-loop and closed-loop approaches are possible depending on the measurement point. Typically, open-loop approaches refer to those methods that utilize load current measurements, as in this control strategies it is not possible to verify the actual harmonic content of the grid. For this reason, open-loop methods are employed in those situations where the compensation of load current harmonics guarantees an improvement also of grid currents. When the PCC of the inverter is in common with several non-linear loads, instead of open-loop strategy, a closed-loop approach, where the grid current is measured, is preferred. In this case, indeed, the reference current of the converter is retrieved through the current flowing into the grid and the effect of the compensation is measured with a direct feedback loop. Among this controls, an interesting distinction is made between selective methods, where the control system reduce significantly the harmonics chosen by the designer and non-selective methods. Some of these closed loop schemes are based on the direct calculation of the current reference of the converter. Although simple, these schemes require a compromise between filtering performance and system stability, particularly for compensation of higher order harmonics. Other closed loop schemes are based instead on a power balance and calculate the grid current reference by the regulation of the DC voltage link.

In general, the methods based on the measurement of the current, even if they have good overall performances, usually imply additional costs because of the required current sensors or the implementation of communication systems to receive the measurement from the system operator. In addition, if the power converter is not connected in proximity of the distribution substation, as for example towards the end of a distribution grid, the measurement of current harmonics maybe difficult or even not possible.

To overcome this sort of problems, it is possible to adopt a control strategy based on the measurement of the voltage at the PCC in order to make the converter to operate as a stand-alone filter connected to the grid. When the voltage at PCC is measured there exist two different ways to retrieve the control reference currents, both based on the consideration that, for a pure sinusoidal grid current, the voltage at the PCC would be perfectly sinusoidal, and hence any distortion of the voltage measured at the PCC is caused by harmonic currents drawn by the loads. The first one implies the computation of the grid impedance but, usually, a good knowledge of the system is critical for the effectiveness of the control and, due to the presence

of multiple sources with variable power generation, it would be particularly difficult to estimate correctly the equivalent impedance of the grid seen by the converter. The alternative way is to measure directly the harmonic content of the grid voltage. In order to attenuate the distortion of the voltage at the PCC, the power converter can be controlled as a negative resistor injecting a current that is proportional to the detected voltage harmonics but opposite in phase.

An example of harmonic compensation through PCC voltage measurement is reported in [68] and improved in [69].

The equations describing the control principle are very simple. Considering the generic voltage harmonic of order k measured at the PCC, the reference harmonic current is computed, through a proportional controller, as

$$V_k = GI_k \qquad k \neq +1 \qquad and \qquad |k| < K \tag{3.16}$$

where K is the superior limit for the harmonic compensation that takes into account the bandwidth imposed by the converter switching frequency.

Therefore, considering a Thevenin equivalent at the output of the converter for a generic harmonic k the following equation holds

$$V_k = V_{0k} + Z_k I_k \tag{3.17}$$

where the impedance $Z_k = R_k + jX_k$ is function of the harmonic order and the voltage V_{0k} is the open circuit voltage at the converter's terminals. Therefore, considering equation 3.16 the previous relation becomes

$$V_k = \frac{V_{0k}}{\sqrt{(1 + GR_k)^2 + (1 + GX_k)^2}} \tag{3.18}$$

This latter equation shows that, being $R_k \geq 0$, for high values of G the grid voltage harmonic k is reduced. The main limitation of using a proportional controller is that, being the efficacy proportional to the error, when the error approaches to zero the compensation is reduced. Moreover, high gains are needed to obtain a satisfactory compensation and, hence, this can lead to stability problems of the power converter control. If instead of a P regulator, a PI regulator is used the bandwidth of the controller can be increased and the delay introduced between measurements and actions limits the maximum values of the regulator constants, improving the stability.

Figure 3.13 shows the block diagram of the compensating algorithm. As it can be noticed, the grid voltage, represented in a synchronous reference frame, is filtered by a high-pass filter to eliminate its fundamental component, and to extract only the higher harmonic content. This allows a better performance of the PI since the regulator does not need to compensate for the voltage first harmonic. In addition, in order to reduce instability problems a rate limiter is introduced in the harmonic current references. The rate limiter is tuned to intervene only if the current reference slope is greater than the slope of the maximum harmonic to be compensated. In particular, the rate limiter slope RL_{slope} is given by:

$$RL_{slope} \geq 2\pi h f I_{h,max} \tag{3.19}$$

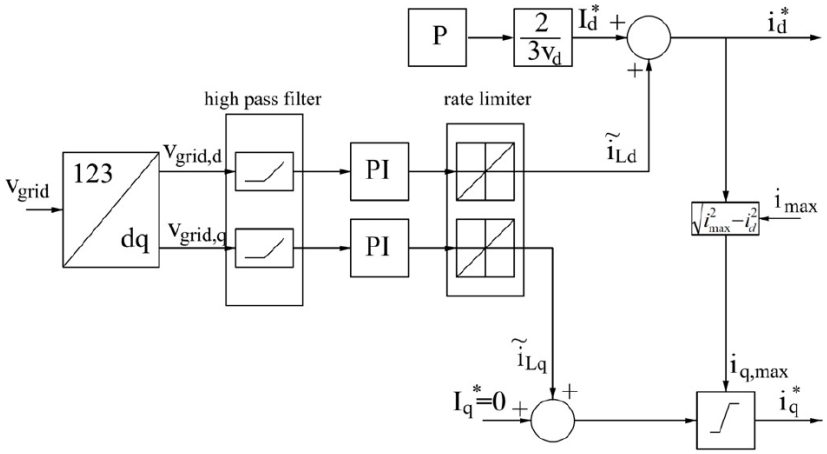

Figure 3.13: Compensating algorithm block diagram

where $I_{h,max}$ is the maximum amplitude of h^{th} harmonic of the current. The rate limiter does not affect the compensation if the derivative of the required current is inside the fixed bounds, but it avoids instability problems due to sudden changes of the load or measurement errors.

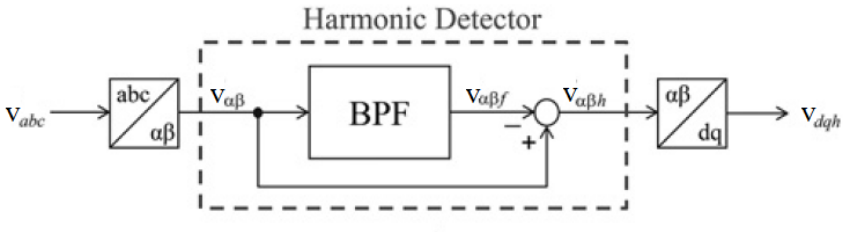

Figure 3.14: Alternative harmonic detector

An improvement for the proposed algorithm can be obtained analysing the solution proposed in [70]. When the harmonic detection is performed in a dq frame synchronous with the grid voltage, the transformation requires the knowledge of the phase-angle θ. However under disturbed conditions such as harmonic distortion and imbalance, the PLL, responsible of providing this parameter, generates a distorted phase angle which results in an incorrect generation of reference signal by the controller. Hence, to overcome this problem the harmonic detector can be implemented in a $\alpha\beta$ stationary frame by extracting the fundamental component by means of a fourth order band-pass filter and then by subtracting from the unprocessed signal the first harmonic component, as is shown in figure 3.14. Thus, even if the phase angle is distorted severely, the harmonic content can be obtained exactly. The proposed control algorithm requires only the voltage measurement at PCC and can be applied also when current harmonics are not known.

In conclusion, harmonic compensation for grid-connected distributed generating unit, such is the case of small PV systems, is a feature that can be implemented without significant additional costs and helps to enhance the overall performance of distribution networks and energy dispatching.

3.3.3 Anti-islanding Detection

Definitely the most technical challenging requirement for grid-connected distributed resources is the so-called anti-islanding. Islanding is a particular operating condition that takes place when a DG resource continues to operate with local load after a grid tripping. This situation represents a serious danger both for the system and for the people since can create safety hazard for utility line workers who assume de-energized lines during maintenance operations and can cause damages to the lines and equipment during out-of-phase closures. In order to avoid these serious consequences, safety measures called anti-islanding (AI) requirements have become very popular in grid codes and standards. It is worth to notice that high power sources, such as wind farms or large PV plants, have completely different requirements and generally benefits of communication systems to interact with the utility operator in order to allow their participation to system control. Hence, islanding detection can be considered a requirement only for low power generating units, even if, forecasting the evolution of the power system, the future scenario may consider the presence of smart micro-grids usually operated in connection to distribution grids but with the capability of automatically switching to a stand-alone operation after the occurrence of a fault. In light of this, providing anti-islanding detection function in grid-connected power converters is nowadays important to improve the overall system reliability.

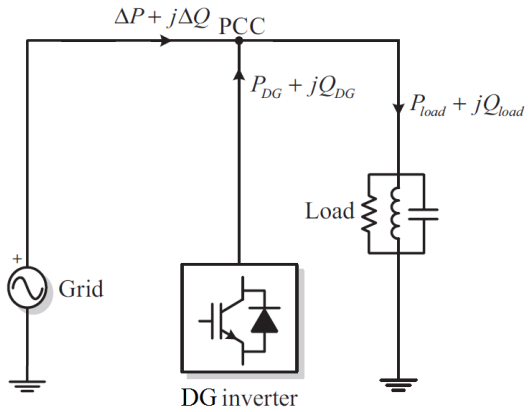

Figure 3.15: Representative scheme for converter connection in LV lines

A key concept of anti-islanding detection methods is the Non-detection Zone(NDZ) which is defined by those power mismatches (ΔP and ΔQ) at the PCC that do not allow the detection of islanding condition. For this reason, NDZ identifies the reliability of each method. For the sake of clarity let's consider the typical connection of a grid-connected converter in distribution lines shown in figure 3.15. In this case the power balance leads to

$$\begin{cases} P_{load} = P_{DG} + \Delta P \\ Q_{load} = Q_{DG} + \Delta Q \end{cases} \tag{3.20}$$

where ΔP, ΔQ are the active and reactive power output of the grid, P_{DG}, Q_{DG} are those of the converter and P_{load}, Q_{load} are the real and reactive power absorbed by the load. The behaviour of the system after the grid tripping depends on ΔP

and ΔQ at the instant before the islanding condition occurrence. In particular, after the grid fault($\Delta P, \Delta Q = 0$) the grid voltage will change proportionally to the power produced by the converter according to:

$$V' = \sqrt{\frac{P_{DG}}{P_{load}}} V \tag{3.21}$$

Reactive power instead is related to the frequency and the amplitude of the voltage through the relation

$$Q_{load}{}' = Q_{DG} = (\frac{1}{\omega' L} - \omega' C) V'^2 \tag{3.22}$$

therefore the new frequency set-point is equal to

$$\omega' = \frac{-\frac{Q_{DG}}{CV'^2} + \sqrt{(\frac{Q_{DG}}{CV'^2})^2 + \frac{4}{LC}}}{2} \tag{3.23}$$

Hence, the worst case for islanding detection is represented by the condition in which before and after the fault the reactive and active power outputs of the grid are zero, since they would not produce any change in voltage amplitude and frequency. Therefore, taking this into account, the NDZ is constituted by those power values ΔP and ΔQ that, being insufficient to influence the grid parameters, prevent the protections to recognize an islanding condition.

Anti-islanding detection algorithms for grid-connected converters are dived into passive and active methods. Passive methods are based on detection of a change of a power system parameter caused by the power mismatch after the disconnection and are characterized by non zero NDZ. A straightforward solution to implement a passive anti-islanding detection is to measure the frequency and the voltage of the system at the point of common coupling. Typically, converters are equipped with under/over voltage (OUV) and under/over frequency (OUF) protections, therefore no additional tools are required in this case. However, when the power variations are too small, the protection devices are not able to correctly detect the contingency. Moreover, the reliability of this method relies in the accuracy of the voltage and frequency measurements which can be hampered by harmonic disturbances, voltage dips and frequency variations.

Passive methods include the so called Phase Jump Detection(PJD) and Harmonic Detection(HD). PJD is based on the monitoring of the phase difference between the inverter output voltage and its output current. Before and after islanding the phase difference changes fast enough to be used as characteristic parameter. However, as nowadays fast PLL are typically implemented for robust synchronization, this phase jump can become negligible since the PLL forces the current to resynchronize with the voltage after the islanding occurrence. In addition, it is difficult to choose the correct threshold for obtaining a reliable islanding detection as phase jumps occur frequently due to system reconfigurations.

Harmonic Detection is based on the estimation of the harmonic content of the voltage at PCC. Every power electronics interface, even if well controlled to work as an ideal current source, injects some current harmonics. These harmonics, generally low, generate an amount of voltage harmonics that depends on the grid

impedance. In islanding mode, the grid impedance, usually low, is replaced by the load impedance that is generally at least one order of magnitude higher. Therefore the voltage harmonic level is amplified and can be used as parameter for islanding detection. Either the THD of the voltage or the amplitude of the most important harmonics can be used as indicator. The main advantage of this method is that it can theoretically reduce the NDZ to zero because it does not depend on the power mismatch between active and reactive powers. However, the choice of the parameters to be evaluated for islanding detection, as well as the choice of proper thresholds is a non-trivial problem. In addition, this method has to face problems related to changes of the harmonic content of the voltage due to other reasons such as plug-in/out of non-linear loads or control actions of other converters. In general, it is not easy to discriminate between the harmonic pollution created by the grid, the loads and other DG units and, therefore, not only to ensure islanding detection but also avoid false trips.

Conversely to passive detection methods, active methods are based on the generation of a grid disturbance in the PCC in order to force a change of a power system parameter that can be detected. Even though with active methods the NDZ can be significantly reduced, they can negatively affect power quality and generate instability in the grid, especially if more inverters are connected in parallel. Depending on which parameter is used different methods can be adopted.

Voltage drift methods target the grid voltage drift. As long as the grid is present, the voltage cannot be drifted, but when the grid is disconnected, the disturbance will be able to drift the voltage until it hits the OUV protection limits. Several implementations exist depending if the drift is triggered through current or reactive power injection. For instance adopting the Sandia Voltage Shift (SVS)[71] the amplitude of the voltage acts as a positive feedback to the current reference. Thus, if there is a decrease in the amplitude of voltage at the PCC, the converter reduces its current output and thus its power output. If the utility is connected, there is little or no effect on the voltage when the power is reduced. When the utility is absent and there is a reduction in voltage, there will be a further reduction in the amplitude. This additional reduction in the amplitude of voltage leads to a further reduction in the converter output current, leading to an eventual reduction in voltage that can be detected by the under voltage protections. It is possible to either increase or decrease the power output of the inverter, leading to a corresponding over voltage or under voltage protection trip. However, it is preferable to respond with a power reduction as this is less likely to damage load equipment.

Another active strategy consists in the measurement of the grid impedance. One way to accomplish this task is through Harmonic Injection(HI). HI is based on injection of non-characteristic harmonic current and extraction of the resultant voltage harmonic, which is dependent on the grid impedance at that frequency. This assumes that these frequencies are normally not present in the grid voltage so the voltage detected at this frequency will be only the voltage drop over the grid impedance. The voltage and current harmonics are estimated using an algorithm based on removing the fundamental frequency and filtering using tuned resonant filters. The non-characteristic frequencies are chosen far from the output filter resonance frequency and also in order to avoid interactions with the current controller.

A further way ti implement inverter-local detection is to trigger a frequency drift. As long as the grid is present, it is obvious that the frequency cannot be drifted, but when the grid is disconnected, the disturbance will be able to drift the frequency until it hits the OUF protection.

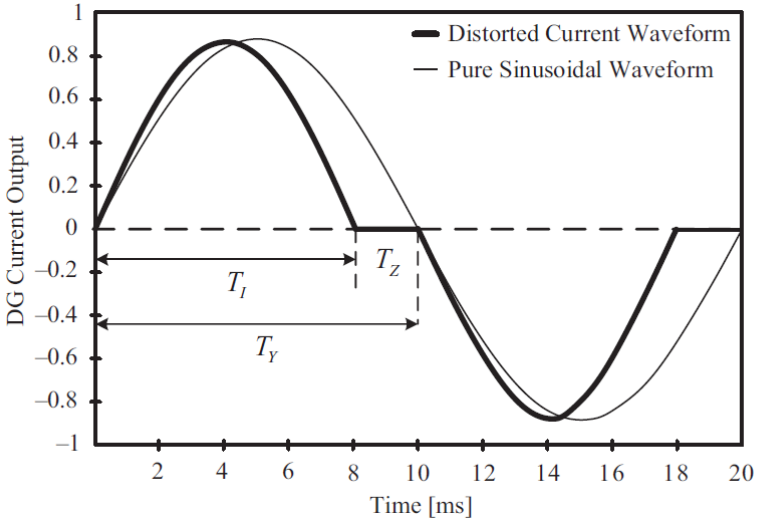

Figure 3.16: ADF current signal

A common way to implement this sort of anti-islanding detection is the active frequency drift (ADF). With reference to figure 3.16, the output current waveform is slightly distorted, presenting a zero current segment, to force the system to change its frequency. This is done by forcing the current frequency to be slightly higher than the voltage frequency in the previous cycle, (typically adding a $\Delta f = 0.5 \div 1.5Hz$) and keeping the inverter current equal to zero from the end of its negative semi-cycle to the positive zero-crossing of the voltage. Thus, the so called *chopping factor* is defined as

$$cf = \frac{2T_z}{T} = \frac{\Delta f}{\Delta f + f} \tag{3.24}$$

where T_z is the zero time of the AFD signal and T is the period of the utility voltage. Thus, there is a continuous trend to change the frequency but the grid presence will prevent this. In an island condition, the frequency will be drifted away and eventually trip the OUF protection. Typically, this method is characterized by a large NDZ, depending on the chosen Δf and on the load quality factor. Therefore a solution implementing a positive feedback for the PCC voltage frequency has been proposed in [71]. To achieve a positive feedback, the chopping factor is modified to be a function of the line frequency error:

$$cf = cf_0 + k(f - f_n) \tag{3.25}$$

where k is the so called acceleration gain and cf_0 is the chopping factor when the frequency error is null. When connected to the network, the frequency does not vary significantly and therefore the stiffness of the system ensure the nominal frequency at the PCC. During an island condition, as f increases, the frequency

error increases as well and, consequently, the chopping factor increases. Hence, the inverter acts to reinforce the frequency deviation until the frequency reaches the threshold of the OUF protection. In this way the NDZ can be reduced to zero for quality factors lower than 4.8 by choosing $cf_0 = 0.05$ and $k = 0.01$. If combined with SVS method, this anti-islanding detection strategy has very good performance, even if implies the injection of distorted currents into the grid.

To conclude, apart from the aforementioned detection strategies, some works propose the use of PLL structures to obtain an efficient anti-islanding detection algorithm. As such, the implementation proposed in [72] presents some peculiarities. As well as many other solutions, the proposed method is based on a positive feedback. However, in this case the frequency positive-feedback inherently resides in the converter system, and hence any additional techniques to generate such a positive-feedback loop is required.

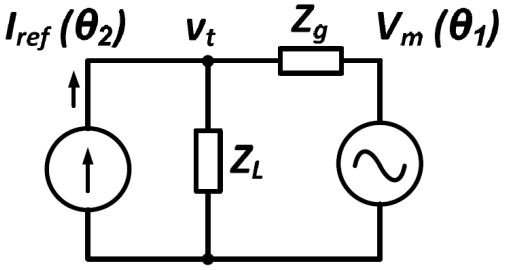

Figure 3.17: Converter equivalent model

By the point of view of the grid, the converter system basically behaves as a current source which precisely follows the current reference I_{ref}, where the phase reference θ_2 comes from the PLL. As such, the three-phase grid-interface converter system can be simplified and represented in a one-line circuit as shown in figure 3.17, where the grid-interface converter and the utility-grid are modeled as a current and voltage source, respectively. Z_g is the grid input impedance and Z_L is the local load of the converter system. The injected current flows into the system network, generating the corresponding voltage response v_t at the terminal of the converter. Based on the superposition theorem the voltage v_t can be expressed as:

$$\begin{aligned} v_t &= |\frac{Z_L}{Z_L + Z_g}|V_m e^{j(\theta_1+p_1)} + |\frac{Z_L Z_g}{Z_L + Z_g}|I_{ref} e^{j(\theta_2+p_2)} \\ &= K_1 V_m e^{j(\theta_1+p_1)} + K_2 I_{ref} e^{j(\theta_2+p_2)} \end{aligned} \tag{3.26}$$

where p_1 and p_2 are the phase-shift angle at the line frequency due to the presence of the imaginary parts in Z_g and Z_L. The PLL algorithm utilizes both θ_1 from the utility and θ_2 from the self-injected current to get synchronization with the grid. Considering these two components, it is possible to obtain a generic PLL model, as shown in figure 3.18, where $\theta_1' = \theta_1 + p_1$ and p_2 is considered as the phase-shift function in terms of the input frequency ω_2 that influences the impedances Z_g and Z_L.

The sub-model of the PLL under the stiff grid-connected condition ($Z_g \simeq 0$) and under islanded condition ($Z_g = \infty$) are shown respectively in figure 3.19 (a) and (b).

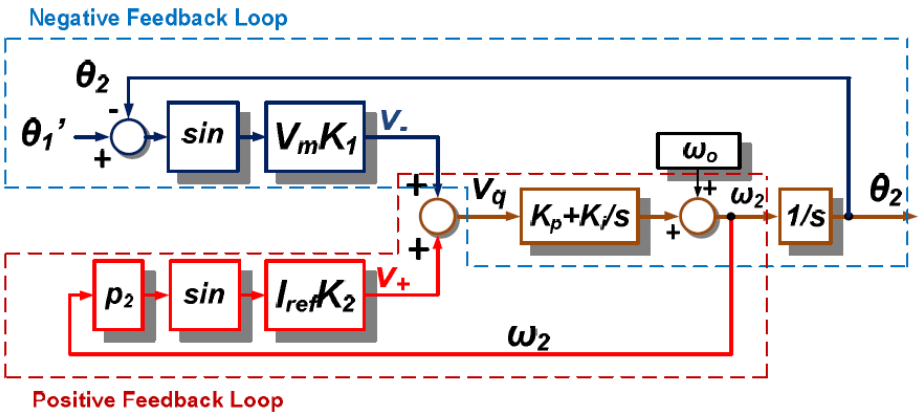

Figure 3.18: PLL block model

If is considered that Z_L is a generic parallel RCL load characterized by a resonant frequency ω_r and quality factor q it can be demonstrated that

$$p_2(\omega_2) = \arctan\left[q\left(\frac{{\omega_r}^2 - {\omega_2}^2}{\omega_r \omega_2}\right)\right] \tag{3.27}$$

The PLL model shows that the sign of p_2 determines the sign of the positive-feedback loop. When $p_2 > 0$ (inductive load), the positive-feedback loop tries to drive the frequency ω_2 up to approach ω_r; when $p2 < 0$ (capacitive load), the positive-feedback loop tries to bring the frequency ω_2 down to approach ω_r. When $p_2 = 0$ (resistive load or $\omega_r = \omega_2$), the positive-feedback loop disappears. Hence, $p_2(\omega_2)$ changes its sign at the resonant frequency, which implies that the PI in the positive feedback loop will always drive the system frequency to the resonant frequency, and the resonant frequency would be a stable equilibrium point. To

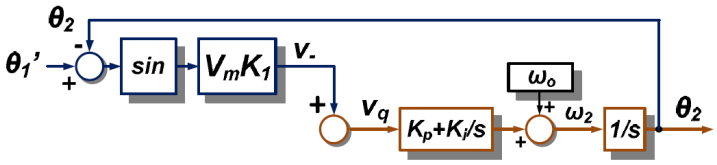

(a) PLL submodel during stiff grid connection

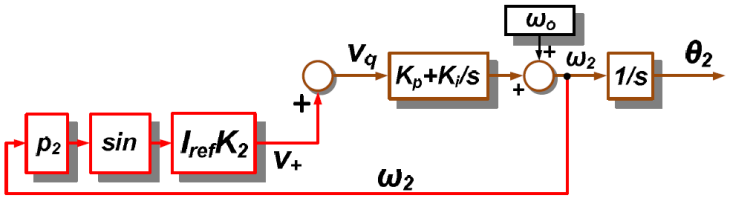

(b) PLL submodel during island condition

Figure 3.19: PLL submodels

sum up, the PLL frequency ω_2 will approach the local-load resonant frequency ω_r with a drift rate determined by integrator gain K_i in PI, p_2 and K_2. Therefore, higher PLL bandwidth leads to a higher drift rate. Due to the characteristics of

p_2, the PLL frequency will never stay at ω_r, and the drift rate will be slower when ω_2 is closer to ω_r. Moreover, the PLL frequency will not drift when the resonant frequency of the load is the same as line-frequency, or under the pure resistive load condition, therefore this represents the NDZ of this algorithm.

As it has been shown, this method only requires the change of the PLL block and no additional change on the control loops is not needed. Other advantages regard the compatibility with eventual regulation codes, such as LVRT requirements, and the injection of small perturbations in the grid to detect the island condition.

Chapter 4

Smart Controller

In the previous chapters PMUs and grid-connected converters for RES have been discussed, focusing the attention on their control systems and on the provision of ancillary services. As it has been highlighted, PMUs are the emerging measurement devices for power network monitoring and because of the range of applications that affect them, their deployment is one of the main goals in the electrical power system panorama. The trend towards an heavy installation of PMUs and their use in future smart grids is manifested by various investments and projects issued by many official institutions and governments in several countries in the world. Despite these efforts, concerning mostly transmission networks , deployment of synchrophasor measurement systems is still a challenge as far distribution grids are concerning. This is ascribable to diverse characteristics of these two networks: shorter line lengths, smaller power angles, a diminished frequency stillness and higher harmonic levels are some of the differentiating factors that make phasor measurements at the distribution grid more vulnerable to errors, and create additional challenges. Technical issues are not the only kind of problems that makes deployment of PMU systems in distribution line a challenging task, indeed, economical concerns arise due to the larger number of buses that must be monitored in a distribution line to reach observability of the system.

Considering the PMU implementation challenge by a wider point of view, the forecasted scenario implies smart distribution grids characterized by an high density of distributed generating units. As it has been shown in chapter 2, each DG unit requires a power electronics grid interface characterized at least by a DC/AC conversion stage by means of which the injected electrical quantities are controlled. Hence, grid-connected converters have almost all what is needed to implement a Phasor Measurement Unit, namely a digital signal processor (DSP) and an analog to digital converter (ADC). In fact, the converter already acquires voltages and currents at the point of common coupling and has computing capability that uses to execute the control algorithms. Therefore, in order to reduce the cost of deployment for PMU unit in distribution grid, their implementation with a grid-connected control system would be without any doubt a valuable solution. Such a device, of course, would be more expensive and technically challenging but it is possible to imagine that its overall cost can be partially relieved from the customer by means of incentives or other economical aids that divide the burden between the customer and the DSO. Before proceeding it is important to clarify that this solution seems

especially interesting for medium-small converters. For high power installations – e.g. MW level PV plants – the additional cost of a traditional PMU is only a small fraction of the plant cost; vice versa for roof top residential and industrial solution the cost of a traditional PMU may be comparable if not superior to the one of the photovoltaic installation itself. The only additional hardware required to add PMU functionalities to a grid connected converter are a time reference signal receiver and a communication media interface to transmit the computed synchrophasors. The purpose of this thesis is to design, implement and test a prototype of such "Smart controller with PMU capabality" in order to address possible issues that may arise during an higher level design of this kind of grid-connected converter controller.

This chapter is structured as follow: in the first section hardware and overall design of the controller will be described. Then in the second section the approach to the problem and the implementation of both the control algorithm and the PMU function are treated, discussing the employed software tools. Lastly, the laboratory test-bench together with the experimental results are presented to demonstrate effective validity of the prototype.

Before starting, it is worth to notice that the aim of this work is not the design of an inverter controller that exploits particular control algorithm to obtain some sort of high level performance, neither is to implement a PMU ready to be used and compliant with all the specified requirements in the standard C37.118, because the achieving of these goals would take definitely longer time. The following work have the purpose to face and address those engineering problems that it is possible to encounter when such an innovative device must be designed and implemented. Nevertheless, all the encountered challenges have been tackled at the best of the possibilities and of the knowledge available to the author, as it should always be done in this field.

4.1 Hardware and design

The hardware chosen to accomplish the proposed objective is an embedded CompactRIO controller with a real-time processor and a reconfigurable FPGA.

A field-programmable gate array (FPGA) is an integrated circuit designed to be configured by a customer or a designer after manufacturing, hence "field-programmable". FPGAs contain an array of programmable logic blocks, and a hierarchy of reconfigurable interconnects that allow the blocks to be "wired together", like many logic gates that can be inter-wired in different configurations. Logic blocks can be configured to perform complex combinational functions, or merely simple logic gates like AND and XOR. Thinking of a CPU as an application specific integrated circuit(ASIC), which basically processes code in FLASH/ROM sequentially, the differences between these two computational units are evident: an FPGA can ensure an high level of parallelization and speed contrary to CPUs, but task optimization is usually hard to achieve.

In particular the employed controller is a cRIO-9035. The major advantage of this device is the combination of two different computational units: a real-time controller made by 1.33 MHz dual core processor, 4GB of nonvolatile compactflash storage and 1 GB DDR3 memory and a Xilinx Kintex-7 70T FPGA for high-speed

control with reconfigurable I/O(Input/Output). The structure of the device is shown in figure 4.1.

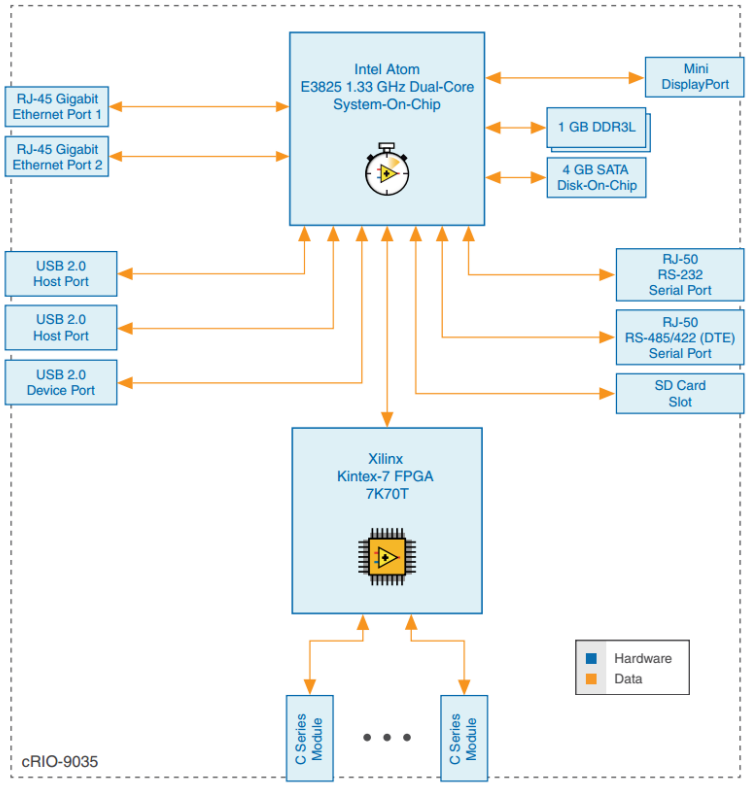

Figure 4.1: NI-9035 hardware configuration

As it can be noticed in the scheme, FPGA and CPU are provided with a bilateral communication channel that allows an extremely reliable and fast data transmission between these two units. In addition, the CPU is equipped with two Ethernet ports to stream data with other external devices such can be the case of an external server or an host computer. Moreover, cRIO-9035 controller comes with 8 slots for C-Series I/O modules, which are hot swappable I/O devices and hence can be easily substituted during operating condition. The C-Series modules employed for the realization of the prototype are five, namely two analog input modules(AI), two digital outputs(DO) and one GPS module.

All the modules are entirely managed through the FPGA, including the analog input modules that are responsible of the acquisition process. The AIs are used to acquire three-phase voltages and currents. These two modules are both characterized by a maximum input voltage in the range of $\pm$10V and they come with an antialiasing filter tuned with a cut-off frequency equal to 100kHz. However, they present some differences: NI-9201 module, employed to acquire three-phase voltages, has 8 channels and 12-bit resolution whilst NI-9215 module has 4 channels and 16-bit resolution and, for this reason, considering the different amplitude of the signals, it is used to acquire the three-phase currents.

DO modules are, instead, identical with each other: both are NI-9401 modules, they have 8 channels, can be configured as Inputs or Outputs and can generate

an output voltage at ±5V at a maximum clock frequency equal to 10MHz. Just for convenience it has been chosen to take advantage of two modules but only one would have been enough.

Lastly, the GPS module (NI-9467) has been employed to acquire the reference time signal from the satellites. For this purpose, a GPS-TMG-40 antenna has been connected to the module and positioned outdoors, in a place where the clearance towards the sky was wide enough to guarantee a steady acquisition of the signal. The acquired reference time signal is a Pulse-per-second that ensures, for this device, a synchronization accuracy in the range of ±100 ns.

The device design process has been developed mainly at the beginning of this project but it has gone through some changes and modification to face different *real world* inconveniences appeared along the way. However, the early decision of taking advantage of the differences between the FPGA and the CPU can be considered as the starting point of the design. Indeed, to exploit at its best the controller architecture, a clear division of the processes in the FPGA and in the CPU has been realized. In details, acquisition process, control algorithm and gate signal generation are implemented on the FPGA, taking also into account that I/O modules management is impossible on the CPU. On the other hand, synchrophasor computation is almost entirely carried out on the CPU, considering that the Ethernet ports, allowing data-streaming, are installed on this latter computational unit. A further reason for this task division can be found on the intrinsic architecture of the FPGA. In fact, this unit adopts fixed point representation of numbers that ensures higher computational speed but lower precision. Since the synchrophasor measurement should be compliant with the TVE values specified in the C37.118 IEEE Standard, it has been considered more appropriate to develop the measurement algorithm on the CPU in order to use double precision numbers.

4.1.1 Control design

Before stepping into the details of the adopted control algorithm, it is worth to highlight what kind of system has been considered and how it is interfaced to the network. Tipically, distributed energy resources are interfaced to the grid through a two-stage converter: a DC/DC converter in which the main functions are to stabilize the voltage at the DC bus and to maximize the power extraction from the source by means of control algorithm such as MPPT, thus providing a reference for the active power, and a DC/AC inverter that controls the active power injected into the grid by properly controlling and synchronizing the electrical quantities, and can provide auxiliary services to the network. As it has been shown in chapter 3 on page 67, there are different types of ancillary services that can be provided. Since the reactive power control can be considered the most important and also the best-regulated auxiliary service, in this project it has been decided to provide the controller with a reactive power control capability, thus enabling an hypothetical participation of the proposed system to voltage regulation. The importance of this ancillary service is further enhanced considering that, thanks to the embedded communication channels of the cRIO device, in a future smart grid application where the reactive power reference can be commanded by a remote station, the inverter can provide to the DSO a tool for improving considerably network stability.

For the goals of this thesis, the DC/DC conversion unit has been neglected. Therefore, the implementation of the DC bus voltage control, as well as MPPT control algorithm, is not taken into account. In terms of control system this would require an external loop to obtain the reference current for injecting the opportune amount of active power. The DC bus where the inverter is connected has been modeled as a constant DC source that represents either the energy source, as an example of which a photovoltaic system can be considered, and the boost converter that interface the source to the second stage of the converter.

The inverter is connected to a Low Voltage(LV) three-phase distribution network with nominal voltage level equal to $V_{RMS} = 110$ V phase-to-ground and nominal frequency $f_n = 60$ Hz; these values are typical for american LV distribution systems. The amplitude of the DC bus is chosen to be 800 V, higher enough with respect to the peak of the line-to-line AC voltage in order to allow a full controllability of the output current. Lastly, the inverter is interfaced to the network by means of a filter that has to filter out high harmonic current components. Typically RES are interfaced through LCL filter structures but to simplify the control tuning process a simple RL filter has been considered.

The grid-connected inverter control system is hence characterized by two loops: an inner current loop and an outer power loop. The block diagram of the system is shown in figure 4.2.

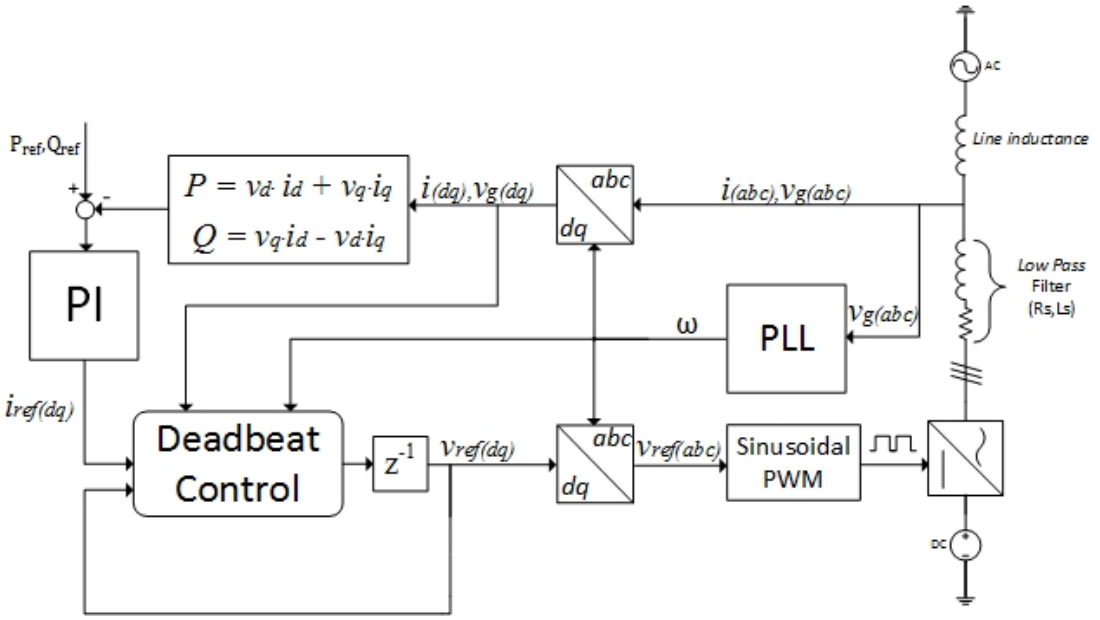

Figure 4.2: Control system block diagram

In order to have constant steady state values, the control equations have been developed using voltages and currents in a dq frame rotating at grid angular speed and using a power invariant Park transformation. The equation describing the Park transformation are the following:

$$\begin{bmatrix} V_d \\ V_q \\ V_0 \end{bmatrix} = \sqrt{\frac{2}{3}} \begin{bmatrix} \cos(\omega t) & \cos(\omega t - \frac{2\pi}{3}) & \cos(\omega t + \frac{2\pi}{3}) \\ -\sin(\omega t) & -\sin(\omega t - \frac{2\pi}{3}) & -\sin(\omega t + \frac{2\pi}{3}) \\ \frac{\sqrt{2}}{2} & \frac{\sqrt{2}}{2} & \frac{\sqrt{2}}{2} \end{bmatrix} \cdot \begin{bmatrix} V_a \\ V_b \\ V_c \end{bmatrix} \tag{4.1}$$

where $\omega = 2\pi f$ is the angular speed of the reference frame. The reference frame is obtained by means of a Phase-Locked-Loop (PLL) algorithm locked on the voltage grid. The PLL task is to maintain coherence between input (reference) signal frequency, f_1, and the respective output frequency, f_0, via phase comparison carried out by a phase detector. To achieve high speed response performances a deadbeat control has been chosen for the inner current loop. As it has been discussed in chapter 2 on page 33, this kind of control algorithm belongs to the predictive control family and, as such, it requires a system model to retrieve the control equations. If correctly designed the deadbeat ensures, theoretically, that the actual current equals its reference value after two sampling periods. In terms of dq quantities, the considered system model is described by the following equations:

$$v_d = R_s i_d + sL_s i_d + v_{gd} - \omega i_q L_s \tag{4.2a}$$
$$v_q = R_s i_q + sL_s i_q + v_{gq} + \omega i_d L_s \tag{4.2b}$$

In the previous equation R_s and L_s are the resistance and the inductance of the filter, whereas $v_g = v_{gd} + jv_{gq}$ is the space vector of the voltage at the Point of Common Coupling(PCC) and $v = v_d + jv_q$ is the voltage commanded at the inverter output. As it can be noticed by equations 4.2a and 4.2b the current control presents a coupling between direct axis and quadrature axis introduced by the derivative of the current space vector. Indeed, it is present the term $\omega i_q L_s$ on the d-axis and the term $\omega i_d L_s$ on the q-axis. In order to write the equation of the deadbeat control, equations 4.2 must be discretized. Discretization of the previous equations leads to:

$$v_d(k) = R_s i_d(k) + \frac{L_s}{T_s}\left[i_d(k+1) - i_d(k)\right] + v_{gd}(k) - \omega L_s i_q(k) \tag{4.3a}$$
$$v_q(k) = R_s i_q(k) + \frac{L_s}{T_s}\left[i_q(k+1) - i_q(k)\right] + v_{gq}(k) + \omega L_s i_d(k) \tag{4.3b}$$

Where, T_s is the control update time that has been chosen as big as $100\mu s$. Equation 4.3 represents the voltage that must me applied at the inverter output at instant k to obtain the i_d and i_q currents at the instant $k+1$. Therefore, supposing that at instant $k+1$ the current in the circuit is wanted to be equal to i_{ref} it is possible to write the equations as:

$$v_d(k) = R_s i_d(k) + \frac{L_s}{T_s}\left[i_{d_{ref}} - i_d(k)\right] + v_{gd}(k) - \omega L_s i_q(k) \tag{4.4a}$$
$$v_q(k) = R_s i_q(k) + \frac{L_s}{T_s}\left[i_{q_{ref}} - i_q(k)\right] + v_{gq}(k) + \omega L_s i_d(k) \tag{4.4b}$$

Nevertheless, the computed dq voltages are commanded at the instant next to the sampling one, therefore this control technique requires the prediction of currents $i_d(k+1)$ and $i_q(k+1)$ next to sampling instant (k). They can be computed knowing the voltage commanded at instant (k) and currents and voltages measured at the PCC:

$$i_d(k+1) = \left[1 - \frac{R_s T_s}{L_s}\right] i_d(k) + \frac{T_s}{L_s}\left[v_d(k) - v_{gd}(k)\right] + \omega T_s i_q(k) \tag{4.5a}$$

$$i_q(k+1) = \left[1 - \frac{R_s T_s}{L_s}\right] i_q(k) + \frac{T_s}{L_s}\left[v_q(k) - v_{gq}(k)\right] - \omega T_s i_d(k) \tag{4.5b}$$

The reference current at the next step is obtained by the feedback chain on active and reactive power. Theoretically, the power references can be given in open loop computing the direct and quadrature axis components of the current. However, considering the coupling between d and q axis and parameters mismatch it has been chosen to add an outer power loop control to eliminate steady state errors. The equations linking active and reactive powers to d and q currents are related to the well known *p-q theory*. According to this theory, indeed, the phase-to-neutral voltages and currents can be written as:

$$v_{dq0} = [T_{dq0}] v_{abc}, \qquad i_{dq0} = [T_{dq0}] i_{abc} \tag{4.6}$$

where $v_{dq0} = [v_d, v_q, v_0]^T$ and $i_{dq0} = [i_d, i_q, i_0]^T$. Using these variables on the $dq0$ reference frame, Akagi in [73] defined the following instantaneous powers:

$$\begin{bmatrix} p_{dq} \\ q_{dq} \\ p_0 \end{bmatrix} = [M_{dq0}] i_{dq0}, \qquad [M_{dq0}] = \begin{bmatrix} v_d & v_q & 0 \\ -v_q & v_d & 0 \\ 0 & 0 & v_0 \end{bmatrix} \tag{4.7}$$

The power p_{dq} term was defined as the instantaneous real power where th p_0 term is called "instantaneous zero-sequence power". The addition of both powers gives rise to the instantaneous active power delivered collectively by the three phases of the three-phase system, $p_{3\phi}$, i.e.

$$p_{3\phi} = p_{dq} + p_0 = v_d i_d + v_q i_q + v_0 i_0 = v_a i_a + v_b i_b + v_c i_c \tag{4.8}$$

Hence, considering a symmetrical and balanced trhee-phase system instantaneous active and reactive power can be written in terms of dq voltages and currents as follow:

$$P = v_d i_d + v_q i_q \tag{4.9a}$$

$$Q = v_d i_q - v_q i_d \tag{4.9b}$$

For the outer power loop a PI control is used. As it is shown by the equation 4.9 the relation between powers and currents is linear therefore in principle the PI can be tuned with an arbitrary bandwidth. This has been selected, both for the

active power and reactive power control, very low in order to avoid overshoots and instability of the system. In a real application active power control bandwidth should be chosen in accordance with MPPT algorithm characteristics and DC bus voltage control while the reactive power control would be chosen also taking in consideration auxiliary service requirements. To avoid instability, proper coordination with the deadbeat controller bandwidth should always be ensured. In this application it has been supposed that both active and reactive power references are commanded by a remote control station, therefore reference values are sent via Ethernet to the CPU and then streamed to the FPGA. Lastly, as regard the commanded output voltages, the gate signals generation is performed by means of a three-phase sinusoidal PWM. It is known that best performances for sinusoidal PWM are related to linear modulation. The condition to ensure this working point is to compare the triangular carrier signal with a sinusoid that doesn't exceed its peak value, in other words, keeping a modulation ratio $m_a \leq 1$. Considering a unit amplitude carrier signal, the commanded output voltage must be properly scaled and limited. Moreover, contrarily to PI controller, the set-point for the average inverter computed through the deadbeat equation must be always scaled down so as to fit it to the digital pulse width modulator. Hence, to ensure linearity of the controller and reduce current harmonics a further constraint has been added to the dq output voltages. Since the peak value of the phase voltage commanded at the inverter output $\hat{V}_{AO}$ must be equal or lower than half of the DC bus voltage $\frac{V_{DC}}{2}$, the module of the space vector is scaled by $\frac{V_{DC}}{2}$ and limited to $\sqrt{\frac{3}{2}}$. The relationship between the modulation index and the ratio of $\hat{V}_{AO}$ and $\frac{V_{DC}}{2}$ is shown in figure 4.3. It must be noticed that this constraint change depending on the considered Park transform formulation: if the amplitude invariant Park transformation was considered also a $\sqrt{\frac{2}{3}}$ factor should have been replaced by 1.

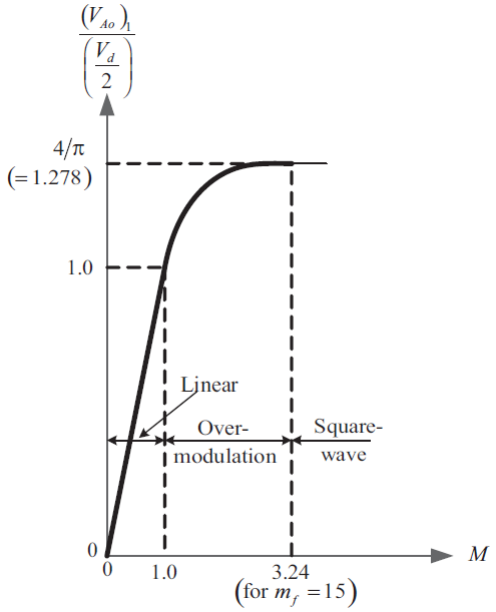

Figure 4.3: Voltage control by varying m_a

In common applications, except for particular needs, the overmodulation zone

is always avoided. It leads not only to higher harmonics in the outputs but also shatters the control system linearity. However, there are some techniques that allow to reach overmodulation zone of the inverter keeping the linearity propriety, for example third-harmonic PWM modulation.

4.1.2 PMU design

The Phasor Measurement Unit has been widely treated in chapter 1. A PMU can acquire more than a single set of three-phase quantities. The typical number of inputs is 12 that means 4 sets of three-phase signals. In this work it has been

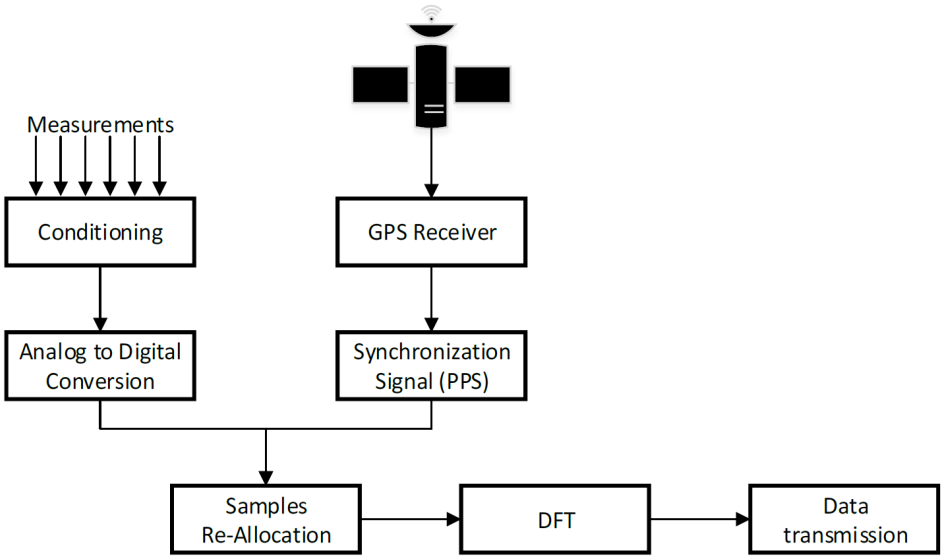

Figure 4.4: Prototype block diagram

chosen to acquire the voltages and currents at the point of common coupling of the inverter for a total of 6 analog signals. Apart from these inputs, the cRIO is acquiring a PPS signal by means of the GPS module. The sampling process is the same for the control and the PMU, therefore, the sampling frequency must comply either with the requirements of the control system and with those of the synchrophasor measurement. In general for such applications the sampling frequency is chosen very high in order to acquire an elevate number of samples per period and use them for compensation algorithms or for samples reallocation. Moreover, to ensure synchronous sampling conditions, the sampling frequency must be an integer multiple of the signal fundamental frequency. Asynchronous conditions would lead to unacceptable leakage errors that would affect the accuracy of the measurement unit.

The synchrophasor measurement requires high precision level for time synchronization. To ensure synchronization, the FPGA clock is synchronized with PPS signal provided by the GPS module. This solution allows to timestamp every acquired sample with high accuracy. The synchronization process must be also checked and verified continuously in order to include time synchronization information into the synchrophasor dataframe. Other time information included in the dataframe regards offset time with respect to coordinated universal time(UTC),

that is the difference in hours and minutes from UTC for a particular place and date, and the leap second occurrence. A leap second is a one-second adjustment that is occasionally applied to UTC in order to keep its time of day close to the mean solar time. Without such a correction, time counted by Earth's rotation drifts away from atomic time because of irregularities in the Earth's rate of rotation. Since this correction system was implemented in 1972, 26 leap seconds have been inserted, the most recent on June 30, 2015 at 23:59:60 UTC. All these information are provided by the GPS module NI-9467.

The set of collected data, composed by time information and raw samples, are then streamed to the CPU. The streaming process can be critical for two main reasons. First of all if data loss occurs the synchrophasor measurement is negatively affected, sometimes also critically depending on the chosen algorithm. Secondly, if the data streaming is not enough fast, there might be either problems with the synchrophasor reporting rate or with an excessive latency of the sent dataframe that would lead to measurement obsolescence.

Supposing to acquire a number of sample N in one observation interval, the streaming process is designed so that the CPU reads an entire set of N samples every cycle, together with their timestamp. For each window of samples, after fixed-point-to-double conversion is carried out, an Hanning windowing function is applied to reduce short-range leakage errors, then the phasor is computed by means of a standard DFT algorithm. In parallel to this process, also the signal frequency is computed by means of a DFT-based interpolating algorithm. For this purpose it has been necessary to make some assumptions regarding the considered electrical system:

- a network steady state working point is considered. This assumption is necessary to neglect all those transient phenomena that would affect the synchrophasor estimation. This hypothesis is not usually verified, indeed the intrinsic function of a grid-connected inverter is to control dynamically the three-phase voltage and current at the PCC. In a more realistic case of a grid-connected converter with PMU capability an estimation algorithm taking into account transient phenomena would be required.

- grid frequency variations are in a range of $[\pm 0.1]$Hz. In M class Phasor Measurement Units the TVE must comply with C37.118 standards in a range of ± 5 Hz. This would imply to implement an algorithm capable of computing with good accuracy electrical quantities at off-nominal frequency. Such algorithm is of course more complicated than the simple DFT application, for example a variable window length would be necessary to correctly estimate the main tone of the signal.

The timestamp provided by the module is given in TAI64 format. International Atomic Time(TAI) is an extraordinarily precise means of time-keeping in a 64 bit timestamp format. One TAI second is defined as the duration of 9192631770 periods of the radiation corresponding to the transition between the two hyperfine levels of the ground state of the cesium atom.Atomic clocks deviate only 1 second in about 20 million years. Thanks to its definition it represents the current international real

No.	Field	Size (bytes)	Comment
1	SYNC	2	Sync byte followed by frame type and version number.
2	FRAMESIZE	2	Number of bytes in frame, defined in 6.2.
3	IDCODE	2	Stream source ID number, 16-bit integer, defined in 6.2.
4	SOC	4	SOC time stamp, defined in 6.2, for all measurements in frame.
5	FRACSEC	4	Fraction of Second and Time Quality, defined in 6.2, for all measurements in frame.
6	STAT	2	Bit-mapped flags.
7	PHASORS	4 × PHNMR or 8 × PHNMR	Phasor estimates. May be single phase or 3-phase positive, negative, or zero sequence. Four or 8 bytes each depending on the fixed 16-bit or floating-point format used, as indicated by the FORMAT field in the configuration frame. The number of values is determined by the PHNMR field in configuration 1, 2, and 3 frames.
8	FREQ	2 / 4	Frequency (fixed or floating point).
9	DFREQ	2 / 4	ROCOF (fixed or floating point).
10	ANALOG	2 × ANNMR or 4 × ANNMR	Analog data, 2 or 4 bytes per value depending on fixed or floating-point format used, as indicated by the FORMAT field in configuration 1, 2, and 3 frames. The number of values is determined by the ANNMR field in configuration 1, 2, and 3 frames.
11	DIGITAL	2 × DGNMR	Digital data, usually representing 16 digital status points (channels). The number of values is determined by the DGNMR field in configuration 1, 2, and 3 frames.
	Repeat 6–11		Fields 6–11 are repeated for as many PMUs as in NUM_PMU field in configuration frame.
12+	CHK	2	CRC-CCITT

Figure 4.5: Dataframe organization according to C37.118

time standard and deviates only 1 second in about 20 million years. This format counts the number of seconds since the beginning of 1970.

Phasor timetagging is carried out selecting the timestamp related to the sample placed in the middle of the window. If the number of samples is an odd number an average of the timestamp corresponding to the $(\frac{N-1}{2})^{th}$ and $(\frac{N+1}{2})^{th}$ samples is performed to obtain a more precise timestamp. Afterwards the timetag is converted from TAI64 format to UTC format. To accomplish this task conversion from second format to "YYYY-MM-DDThh:mm:ssss" format is performed and offset time between TAI and UTC is added.

At last, computed synchrophasors are arranged in dataframes according to C37.118-2011: as it is noticeable in figure 4.5 the Standard specifies the exact position and number of bits for each required information. Each dataframe, together with PMU configurations, command and header messages, is finally sent through Ethernet connection by means of UDP protocol that requires Phasor Data Concentrator IP address to establish a connection channel. For the purpose of this project OpenPDC has been installed in the host computer to simulate a generic PDC.

4.2 Implementation

4.2.1 FPGA and sampling process

During the implementation process it has been necessary to adequate some design choice with hardware limitations and requirements.

The controller, as previously mentioned, is a NI-9035 cRIO. All the compactRIO devices can be programmed using LabVIEW a development environment for a visual programming language from National Instruments. Since the cRIO includes both a Real-time processor and an FPGA, in addition to the standard software

LabVIEW 2015, two packages have been installed to exploit all the features of the board. The most important one is the FPGA module that translate the LabVIEW visual programming language (VPL) into HDL code for FPGA. Being a VPL, LabVIEW enable the user to program and write code for great number of devices and applications, without even having a background of code syntax.

To have an overview of the application implemented on the cRIO board a complete block diagram is provided in 4.6.

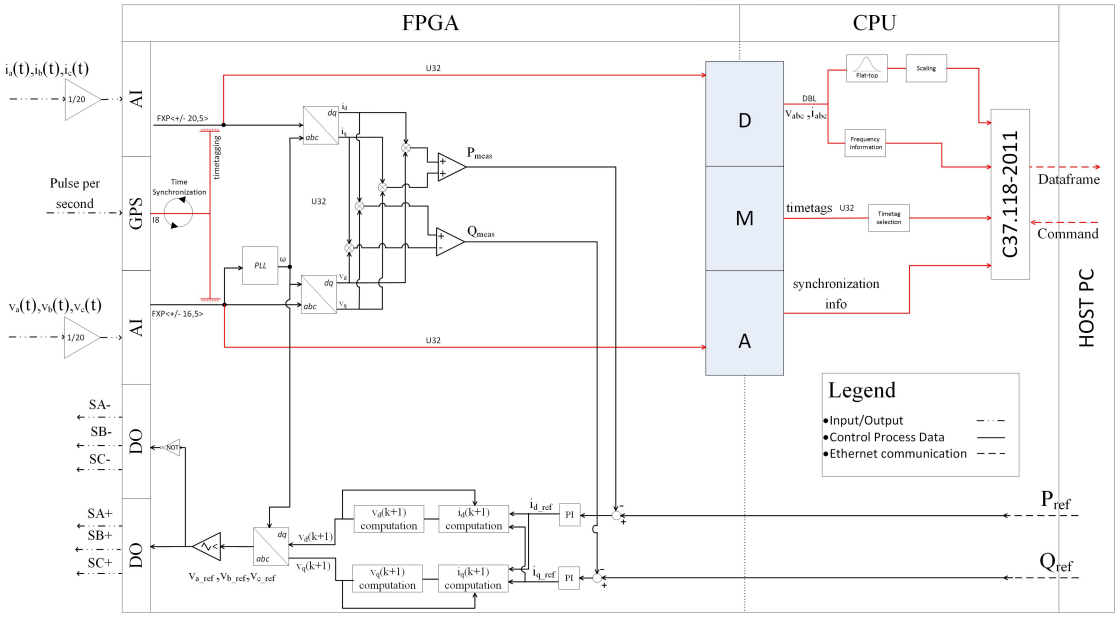

Figure 4.6: NI-9035 hardware configuration

As it can be noticed, two different applications must run in parallel: on the FPGA, data acquisition, raw-data streaming, time synchronization, control system and PWM generation are deployed; the Real-time processor, instead, runs synchrophasor computation, dataframe streaming and manage the communication via Ethernet.

The FPGA is a powerful device because it allows an high level of parallelization separating different tasks in various hardware components, totally decoupling different processes. Thanks to its structure, this device can perform high-speed signal processing, I/O synchronization, and custom triggering or also run advanced control algorithms directly in the FPGA fabric to minimize latency and maximize loop rates. However, there are also some technical issues that arise in dealing with this sort of devices. Probably the problems affecting the most the design process of an FPGA are the extremely high synthesizing time of the HDL code and a limited resources capability, when comparing the performance of this boards with a standard CPU. As a matter of fact, during the first attempts of implementing the smart controller, NI-9002 real-time processor and a NI-9102 FPGA composed the hardware for this project. However, after several tries, it has been observed that the FPGA resources were not sufficient to perform the wanted control algorithm and PMU function. This led to the choice of selecting a more powerful hardware that is the one used for the final system implementation.

The FPGA board of NI-9035 is characterized by an on-board clock running at 40 MHz. This feature has conditioned several design choice. As a matter of fact, the 40 MHz clock is the maximum rate for every operation carried out by the FPGA, including the modules management and so the sampling process. To ensure synchronous sampling condition it is required to sample at an integer multiple frequency of the acquired signal or, more in general, to acquire an integer number of samples over an integer multiple of fundamental period. By consequence, because of the constraint introduced by the clock rate, the sampling frequency must be chosen to be an integer divisor of 40 MHz. Hence, to respect the synchronous sampling condition, it has been chosen to set the sampling frequency at $f_s = 10$ kHz. Considering the DFT algorithm used to compute the phasorial representation of the input signal, the selected sampling frequency implies that the main tone of the signal is no more on the first bin of its discrete fourier transform but on the third. Indeed, the ratio between the sampling frequency and the fundamental of the signal leads to a number of samples per period equal to

$$N_0 = \frac{f_s}{f_0} = \frac{10000}{60} = 166.66 \tag{4.10}$$

thus, if an observation interval $T_O = 3T_0$ is considered, the resulting window will be composed by $N = 500$ samples.

Once the frequency has been chosen, the problem of correctly synchronizing all the controller functions is not trivial and some considerations about the effects of f_s on the control have to be made . It is evident that, in order not to violate Shannon's theorem, the sampling process should proceed at a very high frequency, so high that the spectrum of the sampled signal can be considered negligible after the Nyquist frequency. Therefore, considering that PWM modulation introduces harmonic components in the output current at the switching frequency, a sampling frequency twice the switching frequency should be adopted to correctly sample the signals and to avoid aliasing. However, if the sampling and switching processes are suitably synchronized, the effect of aliasing is the automatic reconstruction of the average value of the sampled signal, which is exactly what has to be controlled[52]. To perform synchronization the typical switching frequency value is generally set to be one half or equal to the sampling frequency. Hence, to respect the 40 MHz constraint imposed by the FPGA clock rate, this consideration led to the consequential choice of generating the PWM by means of a triangular carrier signal at $f_{carrier} = 10kHz$ and unit amplitude. To synchronize the sampling process with the beginning of the PWM period, an interrupt is sent to the PWM generation loop at the occurrence of the first sampling instant.

The value set for the switching frequency is not free of consequences. Indeed, as it is stated by Mohan, N. *et al.* in [74], in case of three-phase inverters the best choice for the frequency modulation ratio, indicating with this term $m_f = \frac{f_{carrier}}{f_0}$, is an integer odd number multiple of 3. Such a mindful decision, in fact, leads to the minimization of the even harmonics (for m_f odd), the harmonics multiple of three ($m_f = 3k$) and the inter-harmonic components(for m_f integer) from the current harmonic content. By consequence, setting $f_{carrier} = 10kHz$ wouldn't comply to any of the careful requirements suggested in [74], being $f_0 = 60Hz$, and find a doable solution to avoid the constraint imposed by the clock rate constitutes the

starting point for future developments.

A fundamental requirement for a correct synchrophasor estimation is a precise synchronization of the measure. Synchronization with time reference signal has been carried out exploiting one of LabVIEW's features: the FPGA Timekeeper API. This set of view uses an internal counter that is continually adjusting how much each clock tick "counts" in terms of nanoseconds. This method, according to National Instrument, will be able to correlate absolute time with system events at an accuracy of around 100 ns which is far above the accuracy required by Synchrophasor Standard. A snapshot of LabVIEW code is shown in figure 4.7

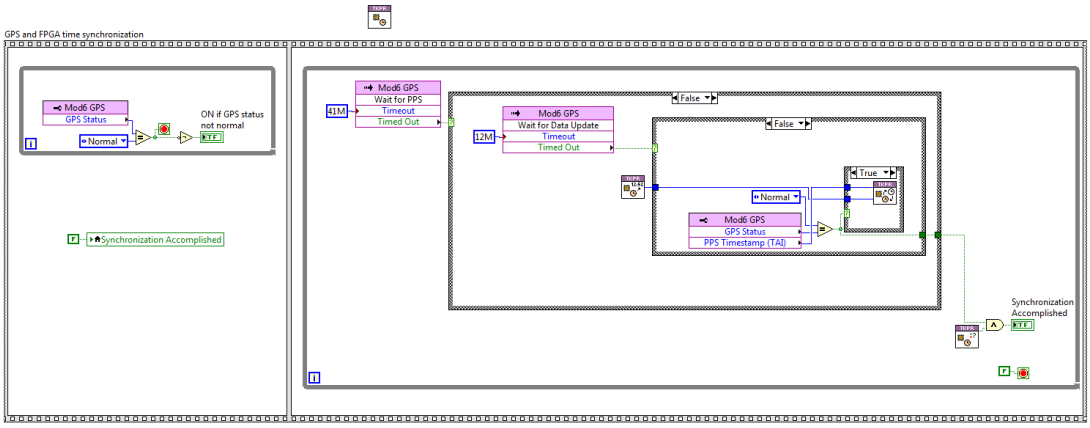

Figure 4.7: FPGA clock synchronization in LabVIEW

The time synchronization loop implements also a boolean flag to warn the user in case of loss of GPS signal. Losing a GPS signal doesn't imply an immediate loss of synchronization since the system is able to keep the synchronization between the FPGA clock and the reference time for several cycles. In any case, the GPS module provides information on the number of "unlocked" seconds enabling the user to exploit this datum to create a boolean logic to tag out-of-synchronization data.

In the scheme of figure 4.6 on page 110 it is possible to see in red lines the data flow for synchrophasor estimation. The streaming process between FPGA and CPU is modeled through the "DMA block". Actually, this block represents the Direct Memory Access(DMA) FIFO used for this task.

If there is the need to stream data between the FPGA and real-time processor, DMA FIFOs do not involve the host processor when reading data off the FPGA; therefore, it is the fastest method for transferring large amounts of data between the FPGA target and the host. The benefits of using DMA communication to transfer data between an FPGA target and a host computer are the following:

- frees the host processor to perform other calculations during data transfer
- save FPGA resources in LabVIEW environment, especially when transferring arrays of data
- automatically synchronizes data transfers between the host and the FPGA target

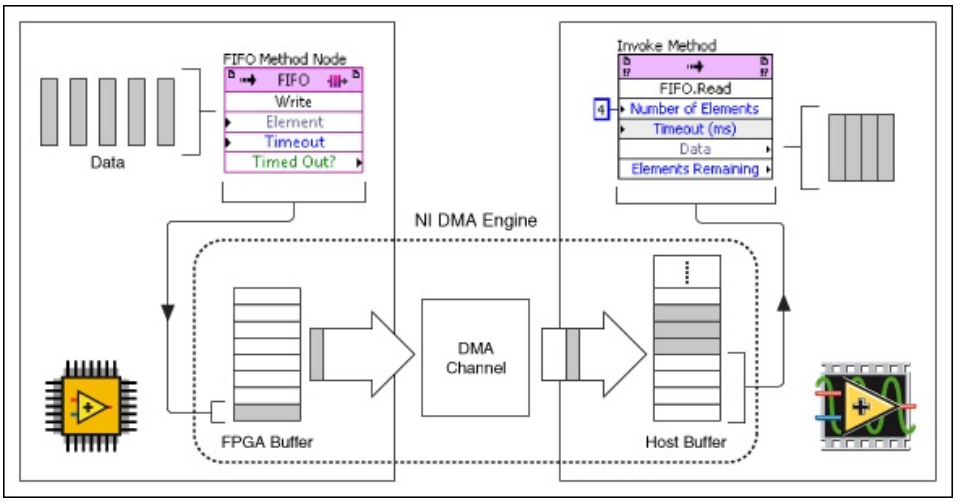

Figure 4.8: Working principle of a Direct Memory Access FIFO

Though DMA FIFOs are a great mechanism for streaming data, they quickly become complicated when streaming data from more than one channel. It is for this reason that countermeasures by means of boolean logic have been implemented to avoid losses and buffer overflows.

4.2.2 Control system

Before discussing the implementation of the control algorithm in LabVIEW, the control system has been simulated and modeled using MATLAB/Simulink. In figure 4.9 on the next page the model is shown.

The model is divided in two parts: upward in the figure the considered electrical system is pictured. As previously said, the DC bus is modeled as a constant voltage source, therefore DC bus voltage dynamics, due to the presence of a capacitance at the DC link, are not modeled. The inverter is considered ideal, hence blanking time effect and internal voltage drops are neglected, leading to an harmonic content of the output variables not affected by these two phenomena. It is worth to notice that the voltage and current measurements have been scaled of a factor of 20. This is done to model the transducers needed to acquire the signals in a compatible range for the C-series modules input. In this case, this scaling factor is to ensure that at the input of the controller, current and voltage signals have an amplitude in the range of ± 10 V.

Figure 4.10 shows the detailed block diagram of the control system. The zero-order hold blocks are set to simulate a sampling acquisition at $f_s = 10$kHz, whereas the delay block introduced before the PWM generation subsystem represents the intrinsic delay of one sampling period that occurs in the deadbeat controls, that has to be modeled to correctly simulate the behaviour of the algorithm. In figure 4.10 on the following page the content of the "control system" subsystem is shown. The diagram is composed by four blocks. The first, starting from left, is including park transformation for currents and voltages and the Phase-Locked-Loop that is locked on the grid voltages and provide the angle $\theta = \omega t$ useful to perform the Park transform in a reference frame rotating at a synchronous speed with the

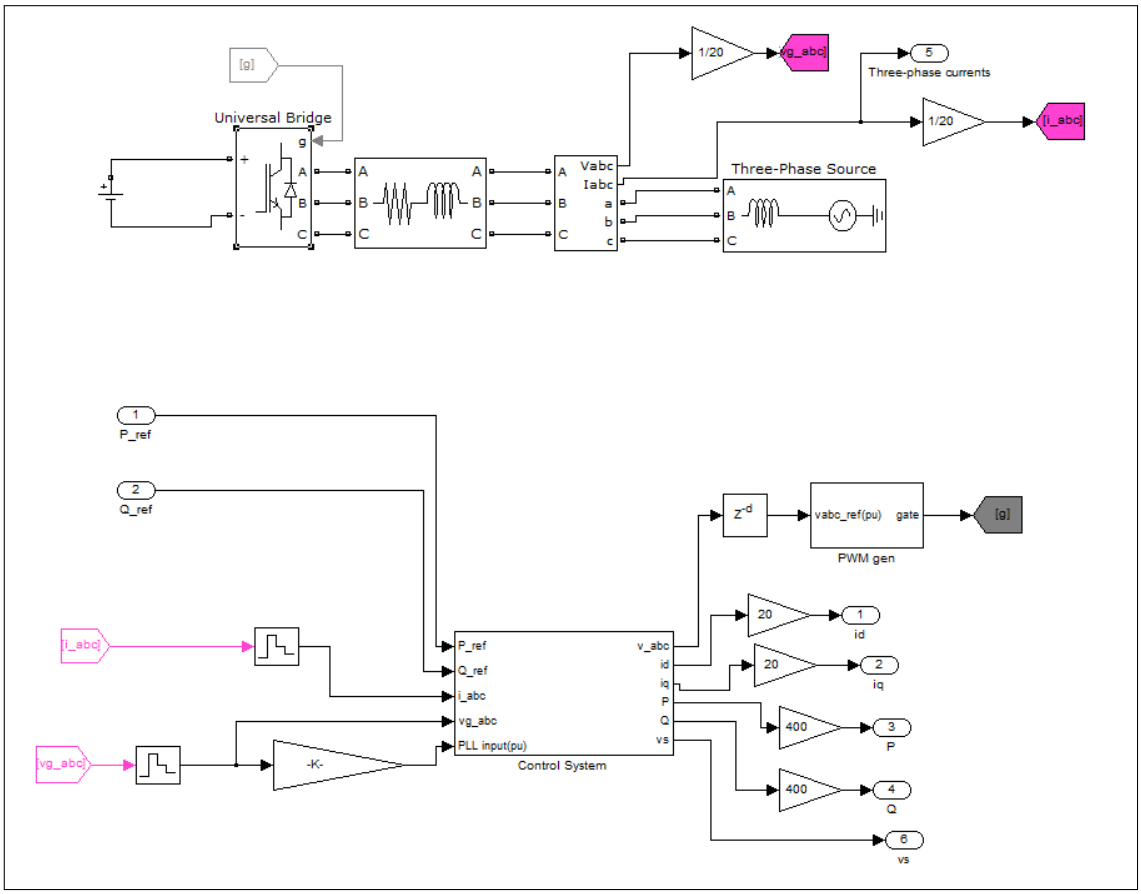

Figure 4.9: Control system Simulink model

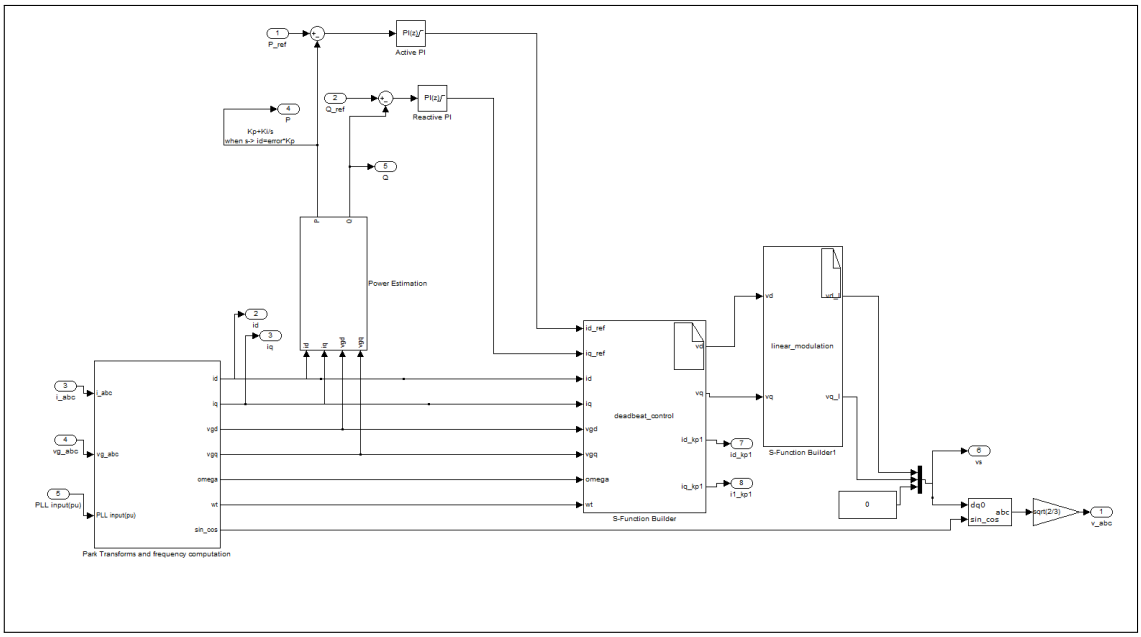

Figure 4.10: Detail of the control subsystem

system electrical quantities. At the output of this block voltages and currents in dq frame are provided, as well as the frequency that will be used in the deadbeat

control equations. The PI power controllers receive the power errors as inputs. The measured power is computed in accordance with the *p-q theory* shown in equation 4.9 in the previous section. The PI controllers implement anti-wind up and saturation functions to avoid saturation of the integral part and actuators that would lead to non-linearity and unstable response of the control outputs(v_d, v_q). To model the deadbeat control and the linear modulation constraints S-function blocks have been exploited. An S-function is a computer language description of a Simulink block written in C++; they are compiled as MEX files using the mex utility. As with other MEX files, S-functions are dynamically linked subroutines that the MATLAB execution engine can automatically load and execute. The code used for the deadbeat algorithm is the following:

```
*id_kp1 = ((*id)*(1-(*Rs)*((*Tsam)/(*Ls)))+(xD[0]-(*vgd))*((*
   Tsam)/(*Ls))+(*omega)*(*iq)*(*Tsam));
*iq_kp1 = ((*iq)*(1-(*Rs)*((*Tsam)/(*Ls)))+(xD[1]-(*vgq))*((*
   Tsam)/(*Ls))-(*omega)*(*id)*(*Tsam));

/*current prediction at instan k+1*/

*vd = (*Rs) * (*id_kp1) + ((*id_ref ) - (*id_kp1)) * ((*Ls)
   /(*Tsam)) - (*omega) * (*iq_kp1) * (*Ls) + (*vgd);
*vq = (*Rs) * (*iq_kp1) + ((*iq_ref ) - (*iq_kp1)) * ((*Ls)
   /(*Tsam)) + (*omega) * (*id_kp1) * (*Ls) + (*vgq);
```

updating the discrete status as follow:

```
if (hypot(*vd,*vq)>(0.5*800*1.22475/20)){

xD[0]= *vd * ((0.5*800*1.22475/20)/hypot(*vd,*vq));
xD[1]= *vq * ((0.5*800*1.22475/20)/hypot(*vd,*vq));

}
else{

xD[0]=*vd;
xD[1]=*vq;

}
```

The presence of two S-functions has been necessary to avoid mistakes in code writing for discrete status updating. Actually, the updating equations are similar to the ones used for ensuring linear modulation apart from the scaling. The fundamental difference in Simulink environment is that the discrete status update store the output values of the control v_d and v_q to feed them back at the next control iteration. On the other hand "linear_modulation" S-function scales the values v_d and v_q during the simulation step of their computation. This solution is maybe not the optimal one but it is surely simple and functional. Lastly the output voltages in dq frame are anti-transformed and used for PWM generation. Using MATLAB/Simulink to simulate the system has made possible to troubleshoot the control before its implementation on the FPGA. This procedure has surely saved a

lot of compilation time that otherwise it would have been wasted. Moreover, the simulation has conditioned also some design choices. For instance, the insertion of the PI power control upstream the deadbeat control has been chosen observing the system response to a constant reference value for i_d and i_q. Keeping i_q constant, a reference step change from 60 A to 80 A for $i_{d_{ref}}$ is shown in figure 4.11.

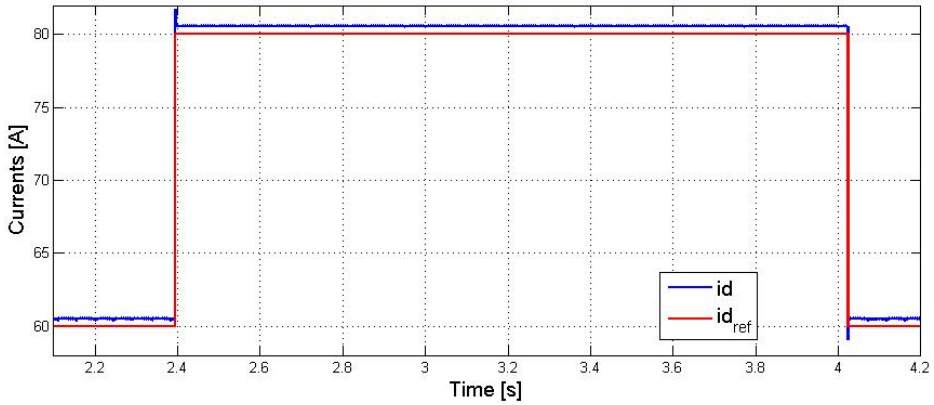

Figure 4.11: Step change in current reference with steady-state error

It is well evident the steady state errors for both the reference values of $id = 60$A and $id = 80$A.

Once the validity of the model and the stability of the control system has been checked, the algorithm has been implemented on LabVIEW. The main problem related with this task is related to number representations in FPGA environments that is usually performed by means of fixed point numbers. A fixed point number is a real data type for a number that has a fixed number of digits after (and sometimes also before) the radix point. Because fixed point operations can produce results that have more bits than the operands, there is possibility for information loss. For instance, the result of fixed point multiplication could potentially have as many bits as the sum of the number of bits in the two operands. When multiplying two fixed point numbers with the same format, for instance with I integer bits, and Q fractional bits, the answer could have up to 2I integer bits, and 2Q fractional bits.In order to fit the result into the same number of bits as the operands, the answer must be rounded or truncated. If this is the case, the choice of which bits to keep is very important. Therefore, in order to save FPGA resources and to avoid overflows and truncations, each operation should be checked in order to verify the congruency of the result. In addition, fixed-point format, due to the way it is defined, cannot represent all the real numbers but only a given set of positive and negative values of two-powers, depending on the number of fractional bits included in the number representation. This naturally leads to mismatch of model parameters that in case of deadbeat controls may worsen the performance.

In light of this and to compensate the presence of possible delays, the outer power loop has been added to the control system. The bandwidth of this latter has been chosen much lower than the deadbeat one; apart from ensuring stability, this choice is justified by the fact that power variations in electrical systems are characterized by time constants much higher than the time constants of electrical

circuits. The coefficients of the PI have been set to $K_p = 0.09$ for the proportional constant and $K_i = 1.3$ for the integral part, leading to a bandwidth of $\frac{K_p}{2\pi K_i} = 2.4$ Hz.

LabVIEW allowed also to build user interfaces for the FPGA and the CPU, letting a continuous interaction with the device during running state. On the FPGA side of the machine, the front panel shows three set of information:

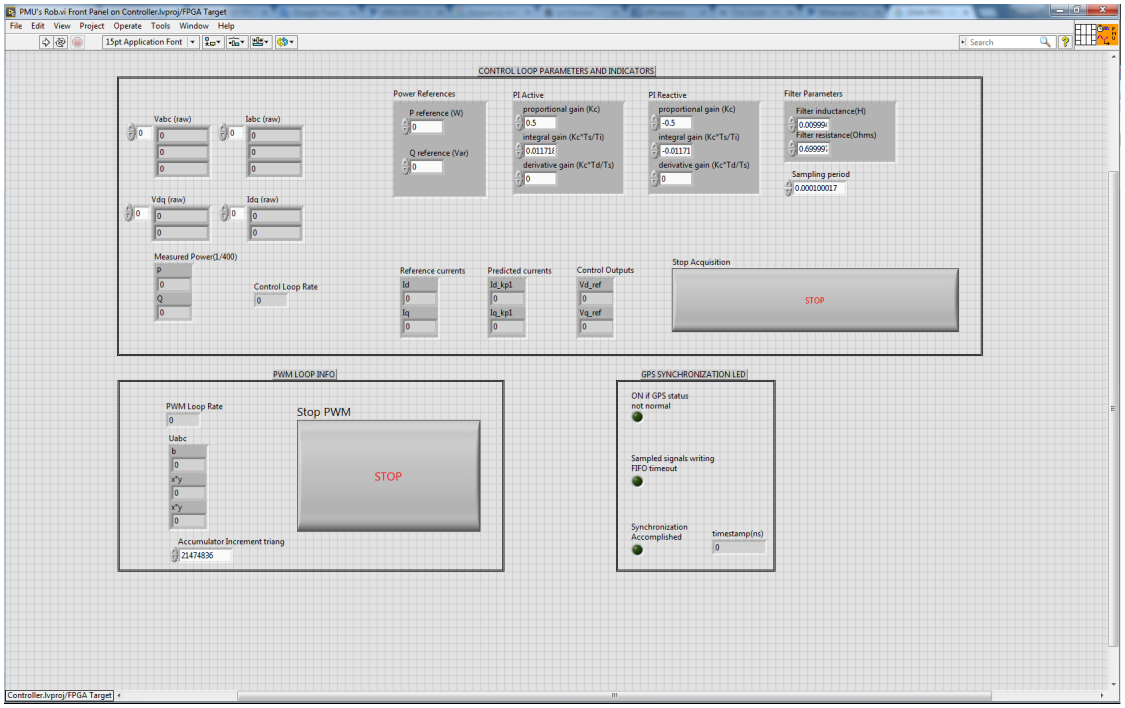

Figure 4.12: FPGA user interface

- as far as the PMU function is concerning, synchronization information and DMA FIFO status are shown through boolean virtual leds. Also the status of the GPS module is shown to notice module's malfunctioning.
- in another block the control system performance and the sampling process can be observed. This is useful for troubleshooting the application with readiness, highlighting each step of the algorithm. In this block also control parameters can be changed in real-time such as PI constants, reference values and also model parameters.
- lastly the PWM generation with its loop rate is scanned. In case of necessity, the switching frequency can be changed.

To better model a smart inverter control, the CPU side user interface has been developed to receive via Ethernet connection power reference values and parameters for the control. Afterwards, exploiting the build-in connection between FPGA and CPU these information are streamed in real-time to the FPGA that put into effect the desired changes. As mentioned in chapter 1 on page 5 a PMU must be able to send not only the measurement dataframe but also other information.

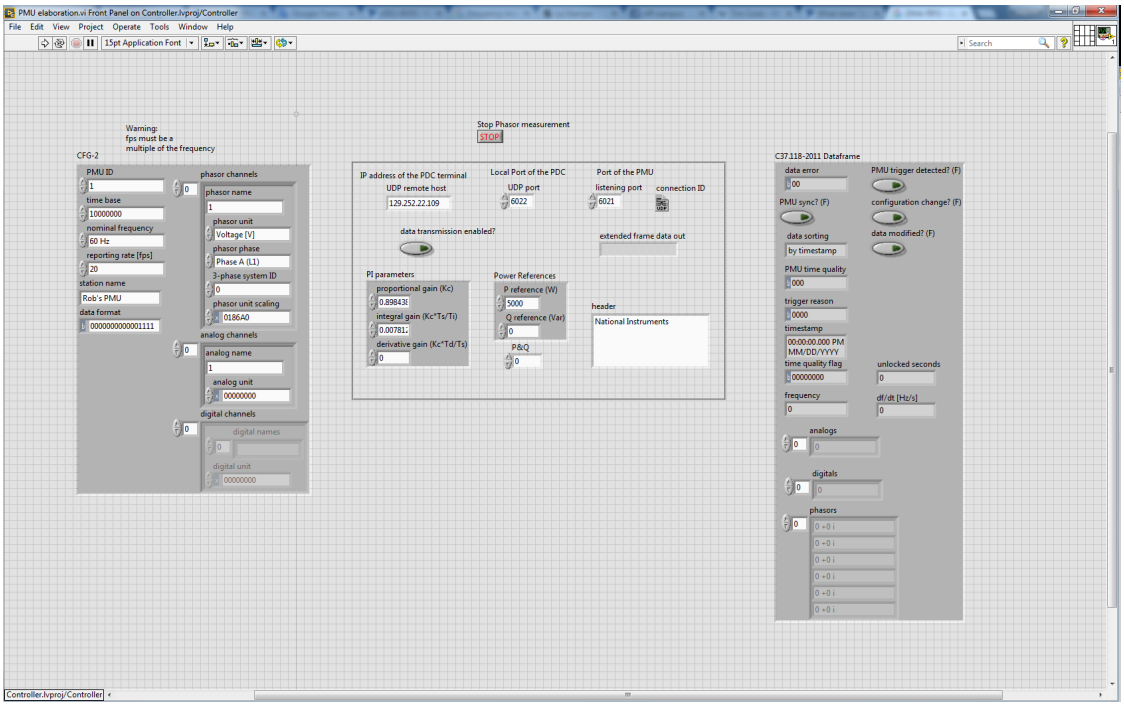

Figure 4.13: CPU user interface

In particular there are three more frames that have to be sent to the PDC: the configuration frame, which provides the characteristic of the PMU such as the measured quantities, the reporting rate, (setted in this case at 20fps), nominal frequency of the system and scaling factors; the header frame that provides PMU details in human-readable format and is analogous to the application banners used in fingerprinting; the command frames that are communication data to send messages to the PDC to which the PMU is connected. To select a given PDC a User Datagram Protocol(UDP) is employed: it is more unreliable than TCP but surely faster. The UDP requires to set port numbers and a receiving IP address to establish the communication. Finally also the dataframe is shown into the front panel so phasors with their timestamps can be visualize on the host computer.

4.3 Experimental validation with HIL

To test the developed prototype and to validate the results obtained during Simulink simulations, real-time simulation techniques have been employed. The simulator used in this work is an OPAL-RT simulator with an I/O expansion unit(OP5607) that uses the Xilinx Virtex-7 FPGA to run the models and provide inputs and outputs. This approach has many advantages, firstly, computation time within each timestep is almost independent of system size because of the parallel nature of FPGA, secondly but most importantly, the simulation time-step can be very small, in the order of 250 nanoseconds.

To facilitate the user and to provide a design tool to be used with comfort, this machine is managed through RT-LAB, a software that not only interface the users to the machine but also enables Simulink models to interact with the real

world in real-time by linking Simulink generated code to highly-optimized runtime libraries. These libraries enable the designer to leverage the full power of modern PC architectures, achieving fixed-step sizes down to a few tens of microseconds and free of jitters.

One of the most interesting features of this machine is the possibility of running simulations with Hardwares in the Loop(HIL). This term identify all those design, testing or modeling procedures that allow an external hardware to communicate with models running in real time. A schematic representation of an Hardware in the Loop is shown below.

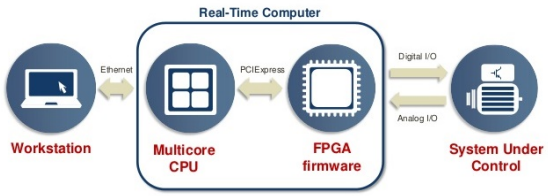

Figure 4.14: CPU user interface

In order to perform simulations that include high dynamic phenomena due to non linear elements such as those characterizing power electronic devices, the simulink model depicted in figure 4.9 has been modified with special blocks, belonging to the RT-EVENTS blockset, provided by OPAL. In particular, as shown in figure 4.15 on the next page, the classical universal bridge block that models the inverter in MATLAB/Simulink is replaced by a RTE-Drive 2-Level Time Stamped Bridge (TSB) block. Moreover, Input/Output signal blocks are added in order to capture PWM signals from the controller by means of an FPGA-based I/O card and to output voltage and current signals. The employment of the FPGA-based I/O card allows to record the times of rising and falling transitions and then forward them to the IGBT model. To make use of transition times, it is necessary to use the RT-EVENTS time-stamped inverter model that implements interpolation for fixed-step simulation of voltage source inverters and PWM generation units.

To sum up, the utilization of real-time simulations with HIL allows to test both the control system and the PMU function of the smart controller, simulating a real grid-connection of the device and, hence, to verify the proper coordination among the processes.

The laboratory has been setup to perform at the same time the PMU and the control testing. When the controller is connected in Hardware in the Loop indeed, the synchrophasors computed by the PMU are sent through Ethernet connection to a remote workstation. Open PDC, a software open source that let the users to customize their own Phasor Data concentrator, is used to acquire and visualize the synchrophasors. The schematic of laboratory setup is shown in figure 4.16 while a photography is visible in figure 4.17. It can be seen that all the employed devices are connected to the same LAN network and that a direct connection exists between the RT simulator and the cRIO board.

Picture 4.18 provides a detailed view of the cRIO-9035 controller connections to OPAL-RT. In details, from left to right, the C-series modules are: DO modules

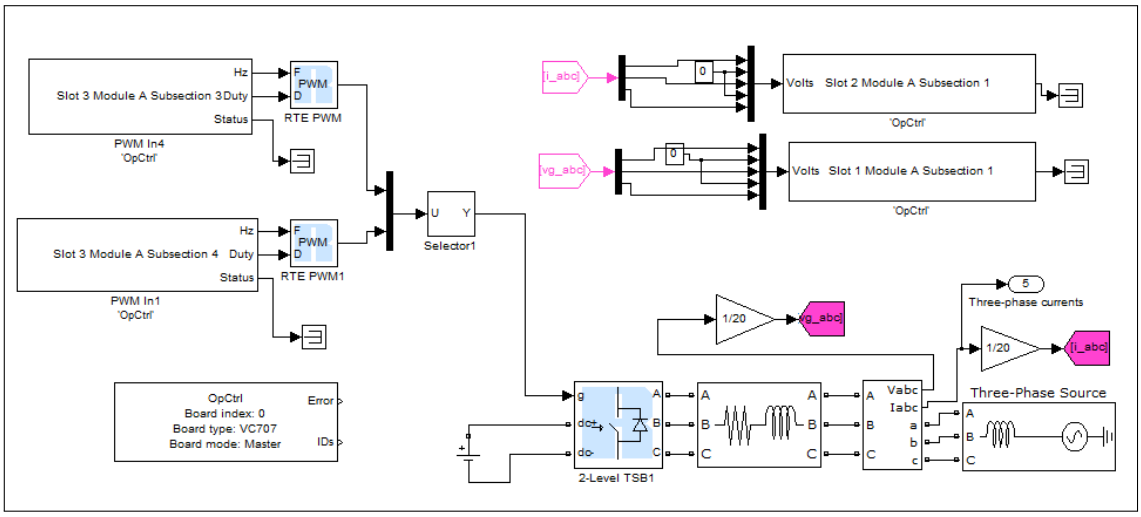

Figure 4.15: Simulink model for real time simulation with Hardware in the Loop

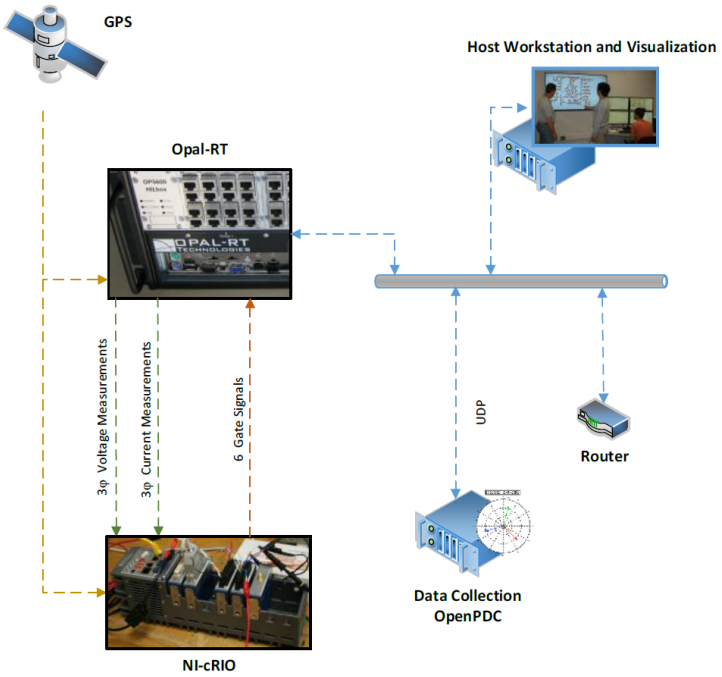

Figure 4.16: Hardware In the Loop testing set-up

sending PWM signals to the simulator, AI modules acquiring voltages and currents signals and the GPS module to retrieve the PPS signal.

4.3.1 Results

In this section some of the HIL simulation results are presented. Every simulation, due to its complexity in management and setting, has been highly time consuming. Because of the time required by the software to synthesize the code for the FPGAs, for OPAL-RT and LabVIEW both, implementation of model variations or code debugging processes, required long time to be carried out and tested, so further

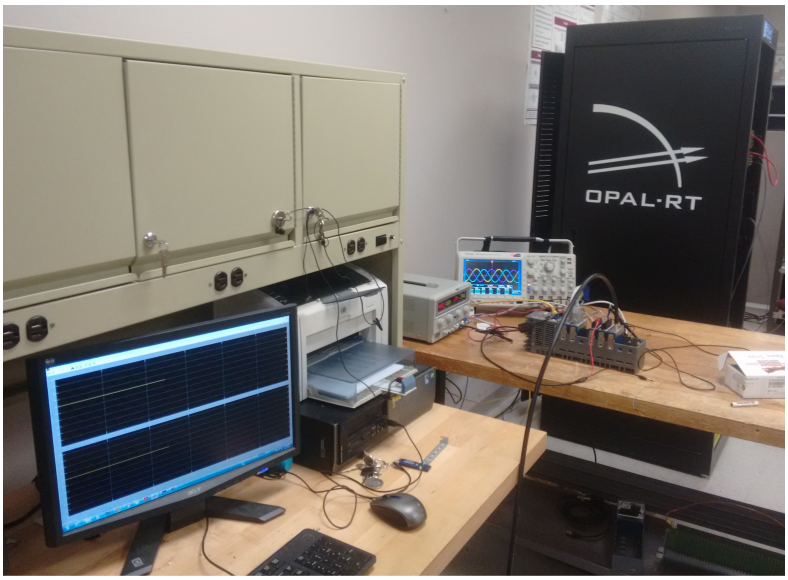

Figure 4.17: Laboratory configuration

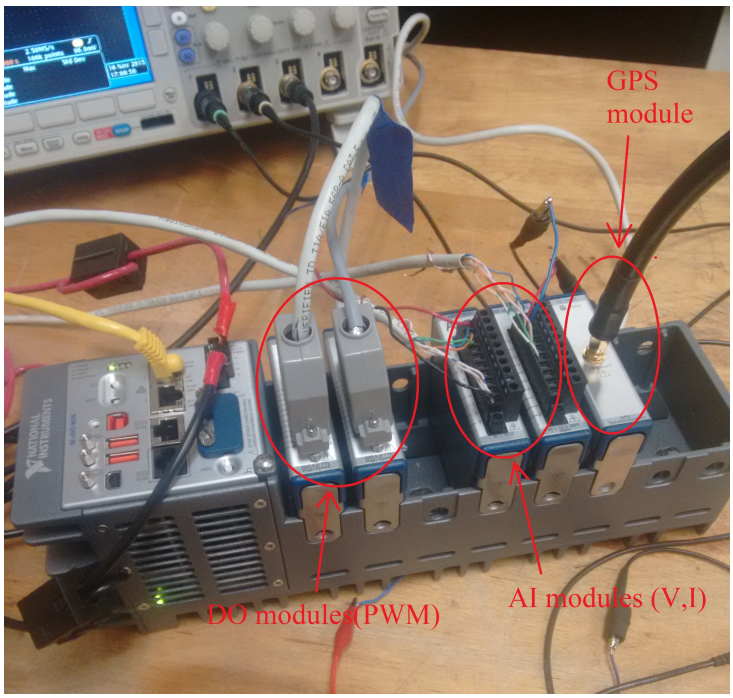

Figure 4.18: NI-cRIO connections to lab testbench

data acquisition and developments of the device are expected in later works.

The first step to verify the correct operation of the control algorithm is to test by means of an oscilloscope that sinusoidal voltages and currents input would produce a correct PWM signal output. If it is not the case, indeed, some error is present in the algorithm design or coding.

Picture 4.19 presents the PWM signals for the upper switches of each leg. The acquired signals are symmetrical with each other, therefore the PWM generation

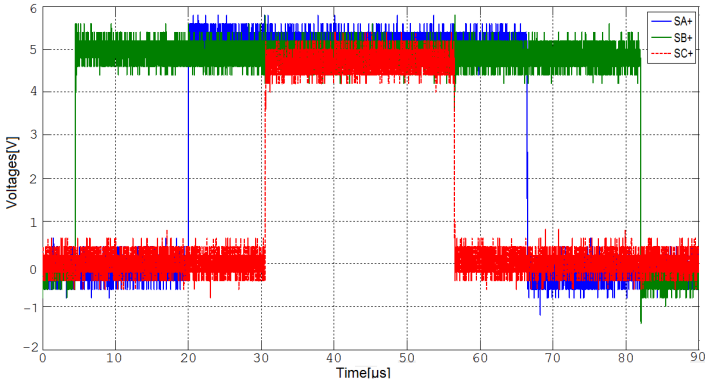

Figure 4.19: PWM generated signal

is correctly accomplished. The same holds for the lower switches considering an opposite voltage level.

Once the PWM generation has been tested, the controller operation in closed-loop must be checked. For this reason, the sinusoidal phase currents are acquired and monitored using again the oscilloscope. Figure 4.20 shows the balanced three-phase currents proving that the controller accomplished its tasks even in closed-loop.

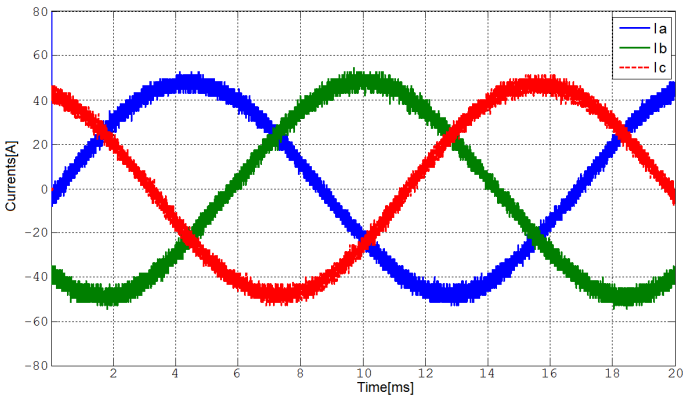

Figure 4.20: Controlled three-phase steady state current

The last of steady-state tests regards the synchrophasor measurement and the DFT algorithm testing. In steady-state, the PMU must be able to measure the voltages and the currents at the PCC in terms of magnitude and phase. As is shown in figure 4.21, the measurement does not change with time, since the measured quantities are in steady-state, proving that DFT algorithm works well. Figures 4.21a and 4.21b do not correspond to the same phasors but are taken at in two different instants.

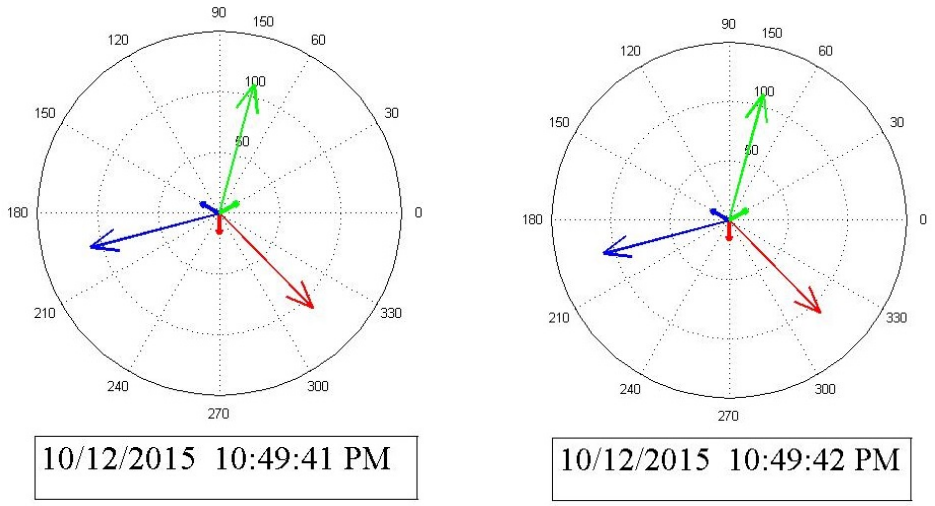

(a) Instant t_1 **(b)** Instant t_2

Figure 4.21: DFT algorithm testing: Constant phasors at two different time instants $t_2 > t_1$

The control algorithm has been tested also giving different power references. In particular, figure 4.22 shows the active power variations in correspondence to a step change from 0 to 5kW and then from 5 kW to 10 kW, keeping the reactive power null. As it can be noticed, the power references are well followed, even though for a zero active power reference the sinusoidal currents and voltages are affected by a non-negligible noise that leads to an higher harmonic distortion of the power. The same behaviour can be seen on the reactive power chart, where step references of Q=5kVar and Q=10kVar are given, maintaining in this case the active power at zero.

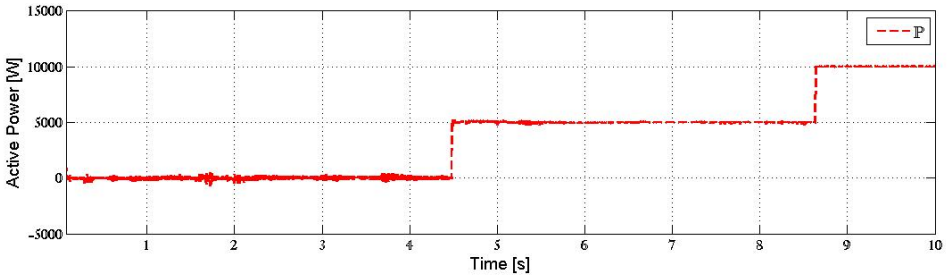

Figure 4.22: Power step change P=5 and 10kW and Q costant

The higher distortion at zero active and reactive power reference is shown also plotting the direct and quadrature component of the injected current. In figure 4.24 a simultaneous power step change for active and reactive power is set. In particular P&Q are set to be equal to 0, 3 and 6 kW and kVar respectively. It can be also noticed that the higher is the reference value the less distorted is controlled quantity.

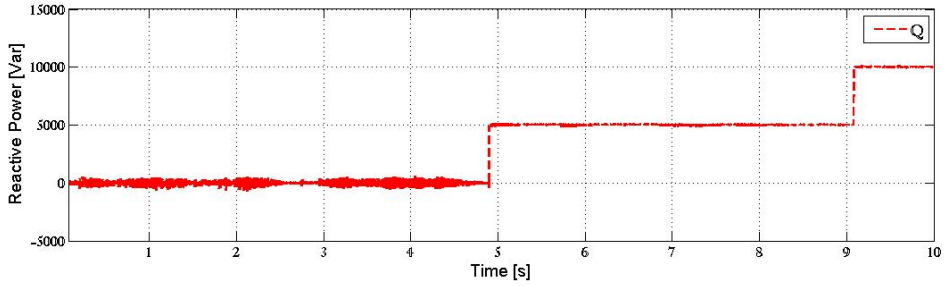

Figure 4.23: Power step change Q=5 and 10kW and P constant

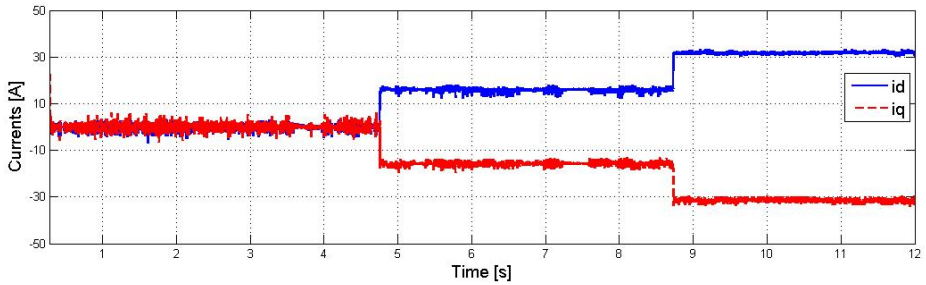

Figure 4.24: Current responses to power step changes: P:3kW and Q=3kVar and P=6kW and Q=6kVar

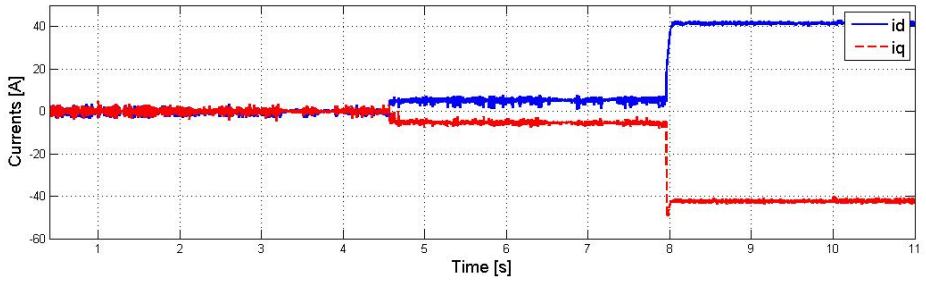

Figure 4.25: Current responses to power step changes: P:1kW and Q=1kVar and P=8kW and Q=8kVar

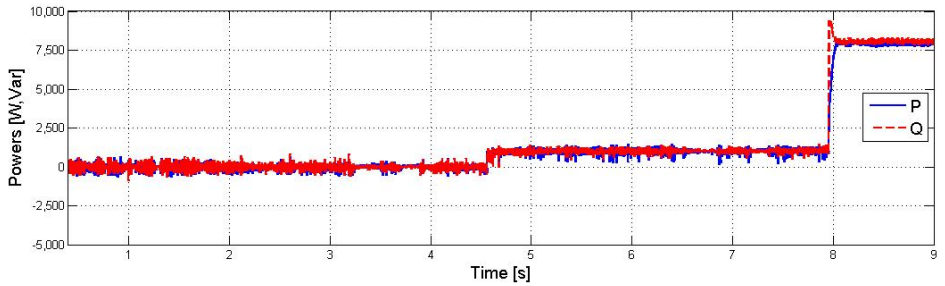

Figure 4.26: Power responses to power step changes: P:1kW and Q=1kVar and P=8kW and Q=8kVar

On the other hand, figures 4.25 and 4.26 show the control system response to different variations. In particular when the active and reactive power references are set to $P = 1kW$ and $Q = 1kVar$ the system responds in a similar manner as

before. However, when the power references are set respectively to $P = 8kW$ and $Q = 8kVar$ the response of the system shows a different transient behaviour. In particular, the direct current is slightly underdumped while the quadrature current is slightly overdumped. This happens because of the saturation of the control action that cannot produce a such big variation of the current. Therefore, the controller tries to follow the references as fast as possible even if it is not possible, producing transient oscillations.

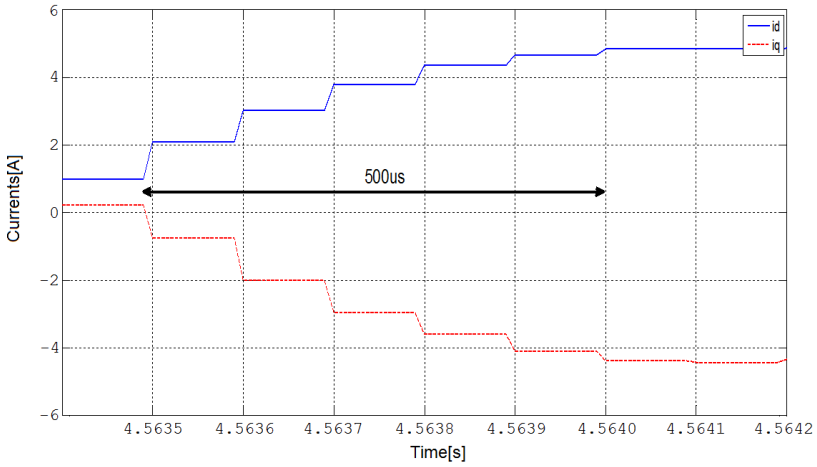

Figure 4.27: Current transient response

The transient response of the controlled current is reported in figure 4.27. As it has been said, the deadbeat control should ensure a zero steady-state error within two sampling periods that in this case corresponds to $200\mu s$. However as it is shown in the picture the direct and quadrature current components reach the steady-state value after 5 sampling period. This is due to the nested loop architecture adopted for the control. Indeed, the external power loop, composed by a PI controller, provides to the deadbeat control a reference current that evolves in an higher time than 2 sampling periods (5 in this case), slowing down the current response according to the chosen bandwidth. Thus, an higher PI bandwidth would lead to a faster transient response of the currents.

The PMU operation has been tested using an host computer as Phasor Data Concentrator. The open-source software Open PDC has been used to simulate the datastreaming process. Figure 4.28 shows a screenshot of the real-time synchrophasors acquisition. The dataframe sent by the PMU are correctly received and visualised by the host PC in terms of magnitudes, phase and detected system frequency, proving that the C37.118-2011 standard is well implemented and that the connection protocols are respected. Open PDC is useful also to test the reporting rate of the PMU that in this case is correctly operating at 20 fps and no under/over flows occur.

To further verify the correct operation of the controller and of the PMU, a real-time display of the streamed data has been implemented on MATLAB. However,

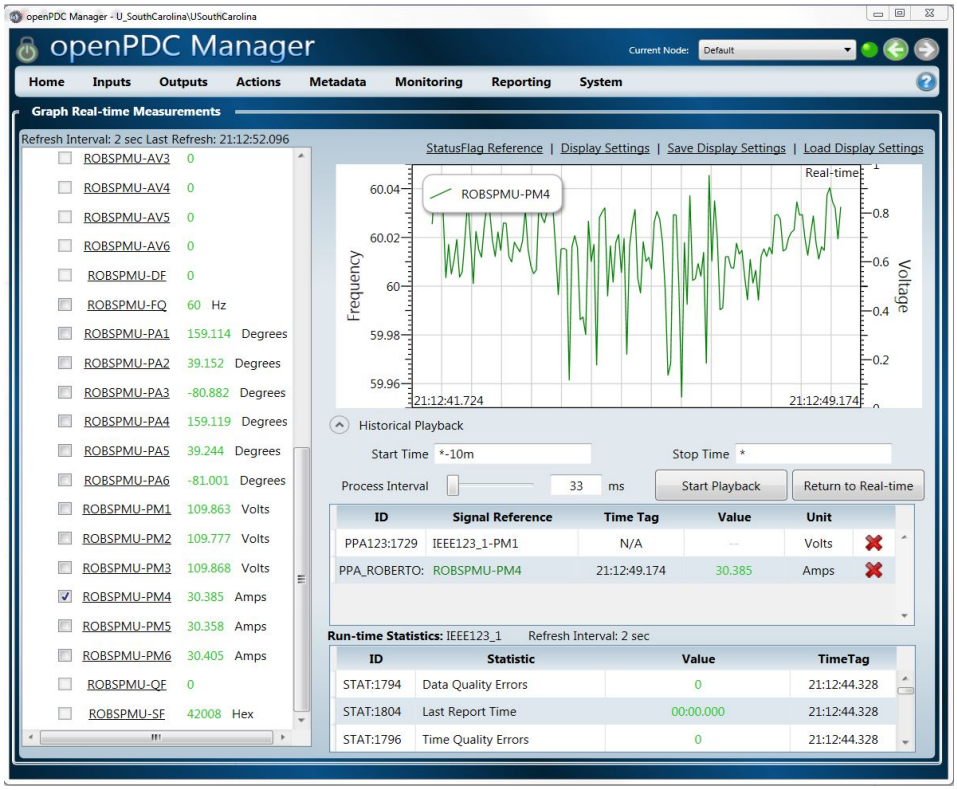

Figure 4.28: Open PDC interface with real-time phasor datastreaming

this program has only been roughly implemented for demonstrative purposes, hence overflow problems have not been solved. The acquired screenshot of the current and voltage phasor representation are shown in figures 4.29 4.30 and 4.31. In particular,

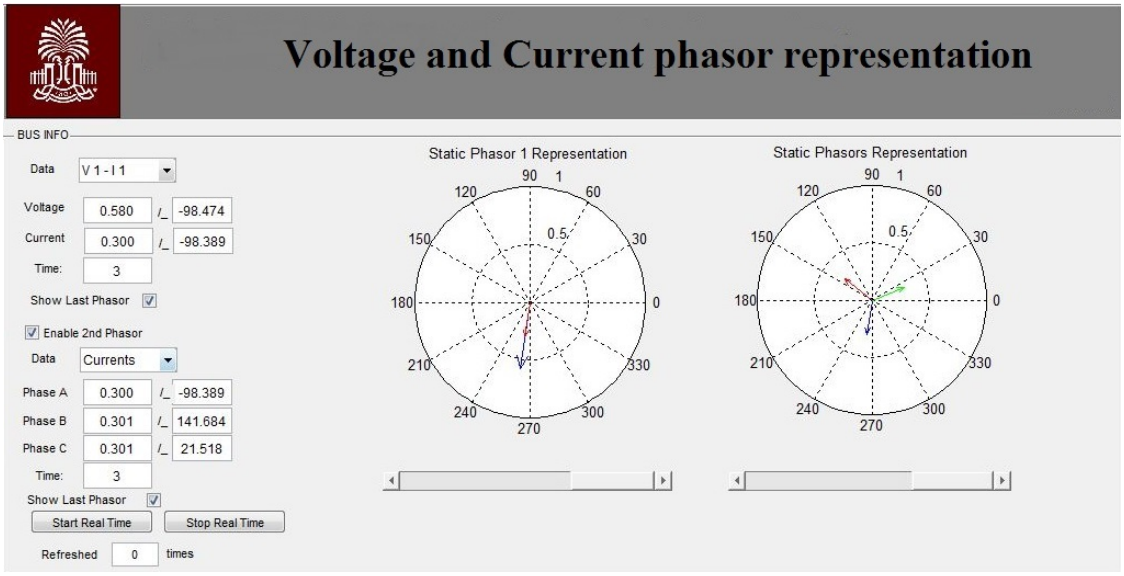

Figure 4.29: Real time phasor visualization for injected power P=10kW and Q=0KW

figure 4.29 shows that when only active power is injected into the grid the three-phase voltages and currents are in phase and the three-voltages are correctly shifted by 120 degrees on the polar plot.

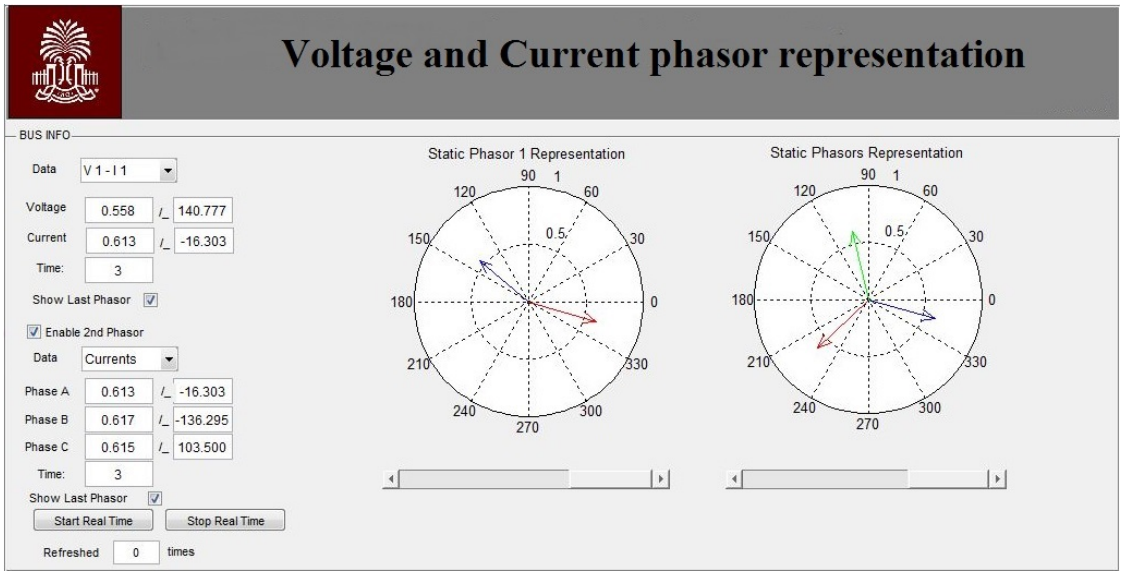

Figure 4.30: Real time phasor visualization for injected power P=3kW and Q=-3KW

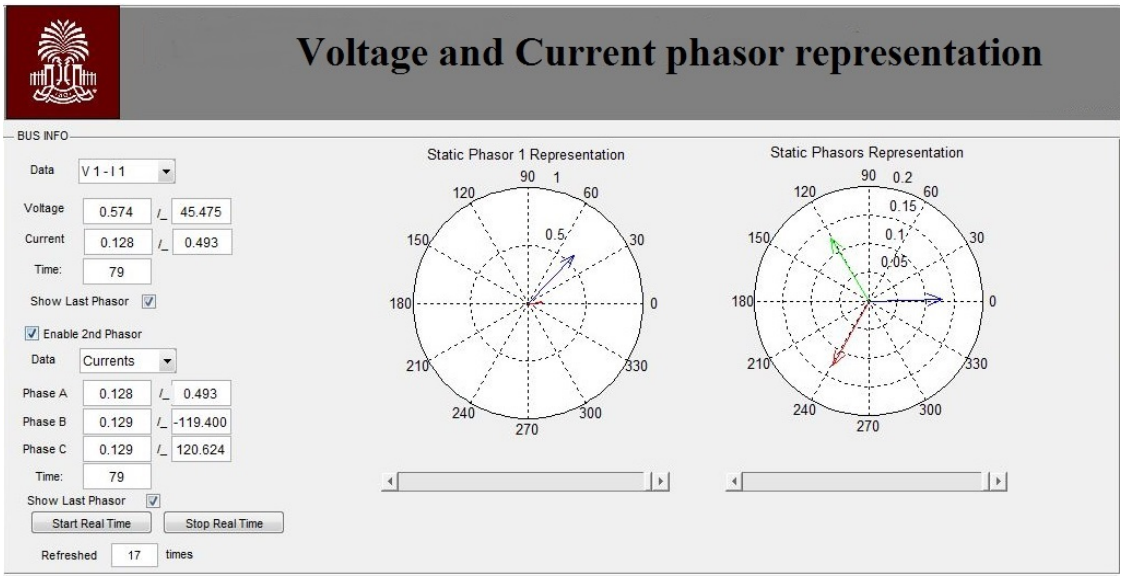

Figure 4.31: Real time phasor visualization for injected power P=3kW and Q=3KW

Figures 4.30 and 4.31 refers to voltages and currents at the point of common coupling to another grid model. Indeed, to test the influence of the injected reactive power variation on the grid voltage a less stiff grid has been simulated. The results are shown in terms of voltage magnitude in the pictures. The voltage magnitudes are divided by 200 only for representation purposes. However, it is still possible to notice the higher voltage magnitude in correspondence to an injected positive reactive power (fig. 4.31) with respect to an injected negative reactive power(fig.4.30).

Even though the implemented PMU seems to work correctly during steady-state conditions, it has not been designed to correctly estimate the phasors during transient conditions. This is visible looking at the figures 4.32 and 4.33 where the

evolution of the current phasor after a reference step-change is reported in terms of magnitude and angle for one of the phases.

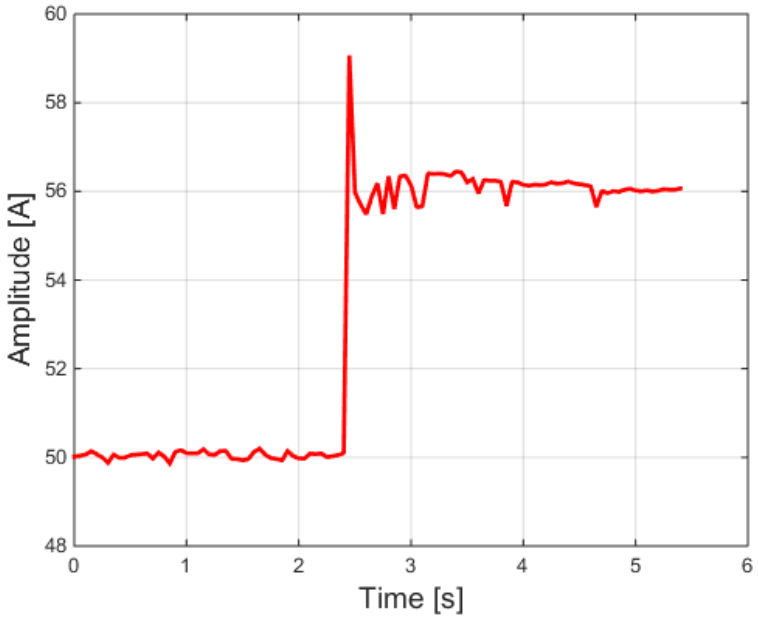

Figure 4.32: Phasor magnitude transient evolution

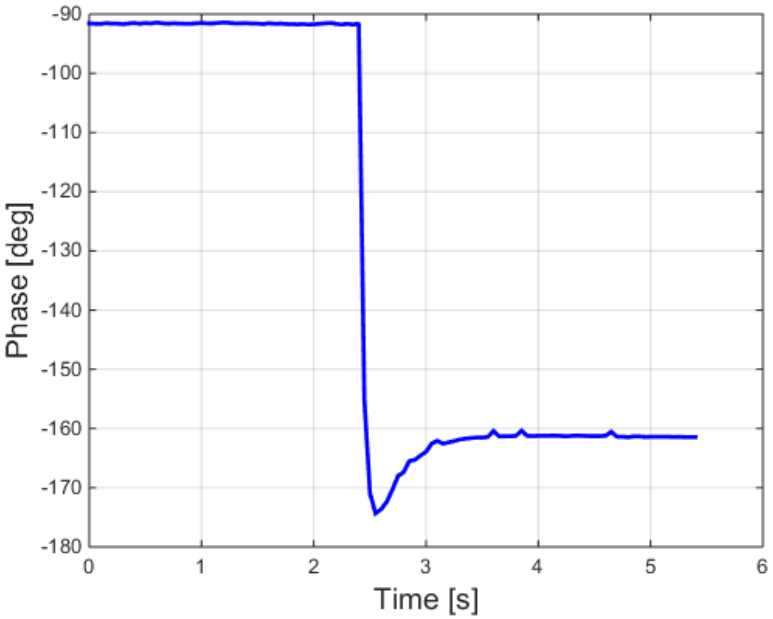

Figure 4.33: Phasor angle transient evolution

As it can be noticed, both the graphs present a period of about 1 second after the step-change in which the evaluated quantity is definitely not constant. In

particular the phase graph present an overshoot before reaching the steady-state value. This period of uncertainty is due to the fixed length of the DFT window that during a transient condition is composed of samples not related to a real sinusoid and, therefore, produces an incorrect result. This leads to the conclusion that, if the converters provides ancillary services with high dynamics, such is the case of harmonic compensation, the synchrophasor estimation will result to be not reliable. However, if slower processes are controlled, such is the case of reactive power compensation, the synchrophasors provide a realistic picture of the system.

Conclusion

The aim of this work was to propose a new concept of controller for power converters in grid-connected applications, capable of providing not only a correct grid synchronization of the injected electrical quantities but also of implementing additional PMU and ancillary service functions. Thanks to these features, the grid-connected converter can become "smart", meaning that, when integrated with a suitable grid architecture such as smart grids, it is able to actively participate to the monitoring and the control of the power system.

For this reason, all the functions that such a controller should be able to perform are analysed in this thesis. In particular, within the first chapter the PMUs have been treated as stand-alone units. It has been highlighted how these devices have gone, and are still going, through a necessary process of standardization that allows the data processing of dataframes collected by PMUs of different manufacturers in Phasor Data Concentrators. This ongoing process has led, as of today, to the IEEE C37.188 Standard. It has been concluded that, even though the algorithms for synchrophasor estimation can be arbitrarily chosen by the designer, the measurements must respect certain constraints given by the Standard, in accordance to the chosen PMU's reference class, in order to be processed in control systems and to be exploited in post-mortem analysis. The most relevant technical challenge regards the synchrophasor estimation during high dynamics transient phenomena that often characterize the power system, particularly in distribution networks. To overcome this difficulty, a dynamic phasor representation can be adopted, leading to the so called Taylor-Fourier transform, but this is paid in terms of computational burden. In addition, in the first chapter it has been pointed out that the only additional hardware in a grid-connected controller consist in a GPS receiver that provides the reference synchronization signal for the PMU measurements.

In the second chapter grid-connected converters have been discussed focusing the attention on grid integration of renewable resources. The key role in grid integration of the power electronics section of these systems has emerged from the text, leading to the conclusion that a future scenario characterized by a massive presence of RESs interfaced to the distribution grid implies a proportional increment of grid-connected converters. This point is paramount for the aim of this thesis since the deployment of PMUs in the distribution grid would be greatly accelerated by their implementation into computational units of power electronics converters. In addition, within the second chapter, to provide the basic knowledge to design power converters control systems, the fundamental functions performed by grid-interface converters have been analysed. In particular, for the sake of this thesis, an in-depth

description of the deadbeat current control and of the grid synchronization process has been reported.

The third chapter has dealt with the provision of ancillary services in renewable energy systems. Almost every grid code nowadays has its requirements to enable the active participation of the consumers to the system stability control, being the presence of distributed generating unit an increasing threat for system reliability and power quality. However, apart from LVRT and HVRT voltage-time profiles, the norms provided by grid codes are, as of today, mainly static requirements given that in dynamic conditions the performances of the renewable energy systems cannot be predicted. Therefore, in a scenario where the equipment of RESs can communicate between each other and with the utility control centre, the ancillary service provision can be further enhanced allowing better power quality and system reliability. This last conclusion let us to state that a converter controller with PMU function, receiving reference signals through its communication channel, can potentially acquire even more charm.

In the last part of this work the design and the implementation of a prototype of the proposed innovative controller is described. To test the device an hardware-in-the-loop approach has been exploited. This technique allows to test not only the converter control action but also synchrophasor estimation algorithm. In fact, the signals acquired through the OPAL-RT simulator are processed by the cRIO board and streamed to a simulated PDC. The results provided in this chapter show that the prototype is able to correctly control the output current, performing a good synchronization and enabling also active and reactive power control. The active and reactive power references are given from an host PC communicating via ethernet to simulate the interaction of the controller with an external control centre. Also the synchrophasor estimation resulted to be well performed, with the simulated PDC displaying, without overflows and underflows, the whole dataframe where each measurement was correctly synchronized with the PPS reference signal. The chosen hardware is a NI-cRIO 9035 board that represents probably the main limitation of this work, being significantly more performing than the computing hardware normally available in a converter. The most challenging task in the implementation of this device has been the simultaneous execution of processes with very different refresh times. It has been solved by decoupling the PMU function and the control system respectively in the FPGA and the CPU of the cRIO board. However, due to the constraint given by the FPGA clock rate, it has not been possible to choose independently the switching frequency and the sampling frequency, leading to the non-optimal choice of setting them to be equal.

As discussed in the first chapter, a possible solution to overcome this problem is to execute the reallocation of the samples. Indeed, this let to choose the sampling frequency independently on the fundamental frequency of the signal, giving, by consequence, one more degree of freedom on the choice of the switching frequency. In addition sample reallocation helps to reduce the number of processed samples for a given DFT window, saving also computational power.

Suggestion for future developments are given also by the analysis of the computed synchrophasor during transient phenomena. As a matter of fact, as it emerged by the results, the implemented PMU cannot achieve good perfomances in computing variable sinusoidal signals. This suggests to improve the chosen algorithm by

considering a dynamic phasor representation that, through the Taylor-Fourier transform, leads to a better estimation of non-sinusoidal signals.

Lastly, also as regards the control system some improvements can be made. First of all, the inverter used in the simulation, being an ideal model, does not include deadtime and internal voltage drop effects that in real conditions are always present and cause a worsening of the inverter harmonic voltage output. Thus they must be taken into account in future works. Secondly, a better external power loop can be designed in order to obtain better and faster transient responses.

To conclude, the implemented prototype can be considered as a starting point to design a real "smart controller". In particular, the PMU function must respect the requirements given by the Standards and must be able to provide also the $ROCOF$ measurement that, because of lack of time, has been neglected in this work. The efforts for a future development of the device are addressed to optimize the computational burden of the implemented functions and to improve the control performances.

Bibliography

[1] H. Farhangi, "The path of the smart grid", *Power and Energy Magazine, IEEE*, vol. 8, no. 1, pp. 18–28, 2010 (cit. on p. 1).

[2] A. Johnson, "The history of the smart grid evolution at southern california edison", in *Innovative Smart Grid Technologies (ISGT), 2010*, Jan. 2010, pp. 1–3. DOI: 10.1109/ISGT.2010.5434757 (cit. on p. 2).

[3] A. G. Phadke, "Synchronized phasor measurements-a historical overview", in *Transmission and Distribution Conference and Exhibition 2002: Asia Pacific. IEEE/PES*, IEEE, vol. 1, 2002, pp. 476–479 (cit. on p. 5).

[4] A. G. Phadke and J. S. Thorp, *Synchronized phasor measurements and their applications*. Springer Science & Business Media, 2008 (cit. on pp. 5, 26).

[5] A. Phadke and J. Thorp, "History and applications of phasor measurements", in *Power Systems Conference and Exposition, 2006. PSCE '06. 2006 IEEE PES*, Oct. 2006, pp. 331–335. DOI: 10.1109/PSCE.2006.296328 (cit. on p. 6).

[6] A. Carta, "Sincronizzazione dei sistemi di misura distribuiti nelle reti elettriche.", 2008 (cit. on p. 8).

[7] S. Buttayak, A. Wornpuen, N. Promparn, N. Charbkaew, and T. Bunyagul, "Design of phasor data concentrator for phasor monitoring system", in *Sustainable Utilization and Development in Engineering and Technology (STUDENT), 2012 IEEE Conference on*, Oct. 2012, pp. 102–107. DOI: 10.1109/STUDENT.2012.6408374 (cit. on p. 9).

[8] (2015). Global Position System website gps description, [Online]. Available: http://www.gps.gov/systems/gps/ (visited on 11/01/2015) (cit. on p. 10).

[9] P. Kovár, P. Kacmarik, and F. Vejrazka, "Interoperable gps, glonass and galileo software receiver", *Aerospace and Electronic Systems Magazine, IEEE*, vol. 26, no. 4, pp. 24–30, Apr. 2011, ISSN: 0885-8985. DOI: 10.1109/MAES.2011.5763340 (cit. on pp. 11, 12).

[10] S. Gopi, *Global positioning System: Principles and applications*. Tata McGraw-Hill Education, 2005 (cit. on p. 12).

[11] (2015). Glonass official website, [Online]. Available: https://www.glonass-iac.ru/en/archive/GENRAL.php (visited on 11/01/2015) (cit. on p. 12).

[12] B. Dickerson, "Substation time synchronization", *Protection, Automation and Control World*, vol. 33, pp. 39–45, 2007 (cit. on pp. 12, 14).

[13] (2015). Galileo official website, [Online]. Available: http://www.gsa.europa.eu/galileo/why-galileo (visited on 11/01/2015) (cit. on p. 13).

[14] "Ieee standard for synchrophasor measurements for power systems", *IEEE Std C37.118.1-2011 (Revision of IEEE Std C37.118-2005)*, pp. 1–61, Dec. 2011. DOI: 10.1109/IEEESTD.2011.6111219 (cit. on pp. 14, 16–18).

[15] "Ieee guide for synchronization, calibration, testing, and installation of phasor measurement units (pmus) for power system protection and control", *IEEE Std C37.242-2013*, pp. 1–107, Mar. 2013. DOI: 10.1109/IEEESTD.2013.6475134 (cit. on p. 14).

[16] J. Depablos, V. Centeno, A. Phadke, and M. Ingram, "Comparative testing of synchronized phasor measurement units", in *Power Engineering Society General Meeting, 2004. IEEE*, Jun. 2004, 948–954 Vol.1. DOI: 10.1109/PES.2004.1372972 (cit. on p. 15).

[17] "Ieee standard for synchrophasers for power systems", *IEEE Std 1344-1995(R2001)*, pp. i–, 1995. DOI: 10.1109/IEEESTD.1995.93278 (cit. on p. 15).

[18] "Ieee standard for synchrophasors for power systems", *IEEE Std C37.118-2005 (Revision of IEEE Std 1344-1995)*, pp. 1–57, 2006. DOI: 10.1109/IEEESTD.2006.99376 (cit. on p. 15).

[19] K. Martin, G. Brunello, M. Adamiak, G. Antonova, M. Begovic, G. Benmouyal, P. Bui, H. Falk, V. Gharpure, A. Goldstein, Y. Hu, C. Huntley, T. Kase, M. Kezunovic, A. Kulshrestha, Y. Lu, R. Midence, J. Murphy, M. Patel, F. Rahmatian, V. Skendzic, B. Vandiver, and A. Zahid, "An overview of the ieee standard c37.118.2 ;synchrophasor data transfer for power systems", *Smart Grid, IEEE Transactions on*, vol. 5, no. 4, pp. 1980–1984, Jul. 2014, ISSN: 1949-3053. DOI: 10.1109/TSG.2014.2302016 (cit. on p. 16).

[20] "Ieee standard for synchrophasor data transfer for power systems", *IEEE Std C37.118.2-2011 (Revision of IEEE Std C37.118-2005)*, pp. 1–53, Dec. 2011. DOI: 10.1109/IEEESTD.2011.6111222 (cit. on p. 16).

[21] K. Martin, "Synchrophasor measurements under the ieee standard c37.118.1-2011 with amendment c37.118.1a", *Power Delivery, IEEE Transactions on*, vol. 30, no. 3, pp. 1514–1522, Jun. 2015, ISSN: 0885-8977. DOI: 10.1109/TPWRD.2015.2403591 (cit. on pp. 17, 21).

[22] "Ieee standard for synchrophasor measurements for power systems – amendment 1: Modification of selected performance requirements", *IEEE Std C37.118.1a-2014 (Amendment to IEEE Std C37.118.1-2011)*, pp. 1–25, Apr. 2014. DOI: 10.1109/IEEESTD.2014.6804630 (cit. on p. 17).

[23] K. Martin, "Synchrophasor measurements under the ieee standard c37. 118.1-2011 with amendment c37. 118.1 a", (cit. on p. 18).

[24] P. Castello, "Algorithms for the synchrophasor measurement in steady-state and dynamic conditions", 2014 (cit. on p. 25).

[25] P. Castello, M. Lixia, C. Muscas, and P. A. Pegoraro, "Impact of the model on the accuracy of synchrophasor measurement", *Instrumentation and Measurement, IEEE Transactions on*, vol. 61, no. 8, pp. 2179–2188, 2012 (cit. on p. 26).

[26] D. Belega, D. Macii, and D. Petri, "Fast synchrophasor estimation by means of frequency-domain and time-domain algorithms", *Instrumentation and Measurement, IEEE Transactions on*, vol. 63, no. 2, pp. 388–401, 2014 (cit. on p. 26).

[27] D. Belega, D. Macii, and D. Petri, "Fast synchrophasor estimation by means of frequency-domain and time-domain algorithms", *Instrumentation and Measurement, IEEE Transactions on*, vol. 63, no. 2, pp. 388–401, Feb. 2014, ISSN: 0018-9456. DOI: 10.1109/TIM.2013.2279000 (cit. on pp. 26, 28).

[28] S. Kincic, B. Wangen, W. Mittelstadt, M. Fenimore, M. Cassiadoro, V. VanZandt, and L. Perez, "Impact of massive synchrophasor deployment on reliability coordination and reporting", in *Power and Energy Society General Meeting, 2012 IEEE*, Jul. 2012, pp. 1–8. DOI: 10.1109/PESGM.2012.6343929 (cit. on p. 28).

[29] U. D. of Energy - Electric Delivery and E. Reliability, "American recovery and investment act 2009 - factors affecting pmu installation costs", *Smart Grid investment program 2014*, 2014 (cit. on p. 28).

[30] M. Wache and D. Murray, "Application of synchrophasor measurements for distribution networks", in *Power and Energy Society General Meeting, 2011 IEEE*, Jul. 2011, pp. 1–4. DOI: 10.1109/PES.2011.6039337 (cit. on p. 29).

[31] S. Chakrabarti and E. Kyriakides, "Optimal placement of phasor measurement units for power system observability", *Power Systems, IEEE Transactions on*, vol. 23, no. 3, pp. 1433–1440, 2008 (cit. on p. 30).

[32] J. De La Ree, V. Centeno, J. Thorp, and A. Phadke, "Synchronized phasor measurement applications in power systems", *Smart Grid, IEEE Transactions on*, vol. 1, no. 1, pp. 20–27, Jun. 2010, ISSN: 1949-3053. DOI: 10.1109/TSG.2010.2044815 (cit. on p. 31).

[33] B. Singh, N. Sharma, A. Tiwari, K. Verma, and S. Singh, "Applications of phasor measurement units (pmus) in electric power system networks incorporated with facts controllers", *International Journal of Engineering, Science and Technology*, vol. 3, no. 3, 2011 (cit. on p. 31).

[34] Y. Zhang and A. Bose, "Design of wide-area damping controllers for interarea oscillations", *Power Systems, IEEE Transactions on*, vol. 23, no. 3, pp. 1136–1143, 2008 (cit. on p. 31).

[35] (2014). Renewable power generation cost in 2014, [Online]. Available: http://www.irena.org/documentdownloads/publications/irena_re_power_costs_2014_report.pdf (visited on 01/01/2016) (cit. on p. 34).

[36] J. Arai, K. Iba, T. Funabashi, Y. Nakanishi, K. Koyanagi, and R. Yokoyama, "Power electronics and its applications to renewable energy in japan", *Circuits and Systems Magazine, IEEE*, vol. 8, no. 3, pp. 52–66, Third 2008, ISSN: 1531-636X. DOI: 10.1109/MCAS.2008.928420 (cit. on p. 35).

[37] F. Blaabjerg, F. Iov, T. Terekes, R. Teodorescu, and K. Ma, "Power electronics - key technology for renewable energy systems", in *Power Electronics, Drive Systems and Technologies Conference (PEDSTC), 2011 2nd*, Feb. 2011, pp. 445–466. DOI: 10.1109/PEDSTC.2011.5742462 (cit. on pp. 35, 41).

[38] R. Passey, T. Spooner, I. MacGill, M. Watt, and K. Syngellakis, "The potential impacts of grid-connected distributed generation and how to address them: A review of technical and non-technical factors", *Energy Policy*, vol. 39, no. 10, pp. 6280–6290, 2011 (cit. on p. 36).

[39] J. M. Carrasco, L. G. Franquelo, J. T. Bialasiewicz, E. Galván, R. C. P. Guisado, M. Á. M. Prats, J. I. León, and N. Moreno-Alfonso, "Power-electronic systems for the grid integration of renewable energy sources: A survey", *Industrial Electronics, IEEE Transactions on*, vol. 53, no. 4, pp. 1002–1016, 2006 (cit. on pp. 37, 41).

[40] R. Wiser, Z. Yang, M. Hand, O. Hohmeyer, D. Infield, P. H. Jensen, V. Nikolaev, M. O'Malley, G. Sinden, and A. Zervos, "Wind energy", *IPCC special report on renewable energy sources and climate change mitigation*, pp. 535–608, 2011 (cit. on p. 37).

[41] T. Ackermann *et al.*, *Wind power in power systems*. Wiley Online Library, 2005, vol. 140 (cit. on p. 38).

[42] R. Teodorescu, M. Liserre, and P. Rodriguez, *Grid converters for photovoltaic and wind power systems*. John Wiley & Sons, 2011, vol. 29 (cit. on pp. 38, 43).

[43] A. Hansen, F. Iov, F. Blaabjerg, and L. Hansen, "Review of contemporary wind turbine concepts and their market penetration", *Wind Engineering*, vol. 28, no. 3, pp. 247–263, 2004 (cit. on p. 38).

[44] U. M. Choi, K. B. Lee, and F. Blaabjerg, "Power electronics for renewable energy systems: Wind turbine and photovoltaic systems", in *Renewable Energy Research and Applications (ICRERA), 2012 International Conference on*, Nov. 2012, pp. 1–8. DOI: 10.1109/ICRERA.2012.6477249 (cit. on pp. 41, 45).

[45] S. Kouro, J. I. Leon, D. Vinnikov, and L. G. Franquelo, "Grid-connected photovoltaic systems: An overview of recent research and emerging pv converter technology", *Industrial Electronics Magazine, IEEE*, vol. 9, no. 1, pp. 47–61, 2015 (cit. on p. 41).

[46] F. Blaabjerg, M. Liserre, and K. Ma, "Power electronics converters for wind turbine systems", *Industry Applications, IEEE Transactions on*, vol. 48, no. 2, pp. 708–719, Mar. 2012, ISSN: 0093-9994. DOI: 10.1109/TIA.2011.2181290 (cit. on p. 43).

[47] F. Blaabjerg and K. Ma, "Future on power electronics for wind turbine systems", *Emerging and Selected Topics in Power Electronics, IEEE Journal of*, vol. 1, no. 3, pp. 139–152, Sep. 2013, ISSN: 2168-6777. DOI: 10.1109/JESTPE.2013.2275978 (cit. on p. 43).

[48] J. R. Dreher, F. Marangoni, L. Schuch, M. L. d. S. Martins, and L. D. Flora, "Comparison of h-bridge single-phase transformerless pv string inverters", in *Industry Applications (INDUSCON), 2012 10th IEEE/IAS International Conference on*, Nov. 2012, pp. 1–8. DOI: 10.1109/INDUSCON.2012.6453349 (cit. on p. 46).

[49] B. Ge, H. Abu-Rub, F. Z. Peng, Q. Lei, A. T. de Almeida, F. J. Ferreira, D. Sun, and Y. Liu, "An energy-stored quasi-z-source inverter for application to photovoltaic power system", *Industrial Electronics, IEEE Transactions on*, vol. 60, no. 10, pp. 4468–4481, 2013 (cit. on p. 46).

[50] H. W. Low, "Control of grid connected active converter: Design of control strategies for grid synchronization", 2013 (cit. on p. 52).

[51] R. Teodorescu, F. Blaabjerg, M. Liserre, and P. C. Loh, "Proportional-resonant controllers and filters for grid-connected voltage-source converters", *IEE Proceedings - Electric Power Applications*, vol. 153, no. 5, pp. 750–762, Sep. 2006, ISSN: 1350-2352. DOI: 10.1049/ip-epa:20060008 (cit. on p. 53).

[52] S. Buso and P. Mattavelli, "Digital control in power electronics", *Lectures on Power Electronics*, vol. 1, no. 1, pp. 1–158, 2006 (cit. on pp. 57, 111).

[53] E. Martinot *et al.*, *Renewables 2015: Global status report*. Worldwatch Institute Washington, DC, 2015 (cit. on p. 67).

[54] O. Alsayegh, S. Alhajraf, and H. Albusairi, "Grid-connected renewable energy source systems: Challenges and proposed management schemes", *Energy Conversion and Management*, vol. 51, no. 8, pp. 1690–1693, 2010 (cit. on p. 69).

[55] M. Molinas, "The role of power electronics in distributed energy systems", in *Proc. Symposium on Distributed Energy Systems*, 2008 (cit. on p. 69).

[56] I. Kuzle, D. Bosnjak, and S. Tesnjak, "An overview of ancillary services in an open market environment", in *Control Automation, 2007. MED '07. Mediterranean Conference on*, Jun. 2007, pp. 1–6. DOI: 10.1109/MED.2007.4433835 (cit. on p. 70).

[57] W. Tan, "Load frequency control: Problems and solutions", in *Control Conference (CCC), 2011 30th Chinese*, Jul. 2011, pp. 6281–6286 (cit. on p. 72).

[58] Y. G. Rebours, D. S. Kirschen, M. Trotignon, and S. Rossignol, "A survey of frequency and voltage control ancillary services mdash;part i: Technical features", *IEEE Transactions on Power Systems*, vol. 22, no. 1, pp. 350–357, Feb. 2007, ISSN: 0885-8950. DOI: 10.1109/TPWRS.2006.888963 (cit. on p. 72).

[59] C. Rehtanz and J. J. Zhang, "New types of facts-devices for power system security and efficiency", in *Power Tech, 2007 IEEE Lausanne*, Jul. 2007, pp. 293–298. DOI: 10.1109/PCT.2007.4538332 (cit. on p. 73).

[60] R. Pearmine, Y. h. Song, T. G. Williams, and A. Chebbo, "Identification of a load-frequency characteristic for allocation of spinning reserves on the british electricity grid", *IEE Proceedings - Generation, Transmission and Distribution*, vol. 153, no. 6, pp. 633–638, Nov. 2006, ISSN: 1350-2360. DOI: 10.1049/ip-gtd:20050404 (cit. on p. 74).

[61] W. Sun, C. C. Liu, and L. Zhang, "Optimal generator start-up strategy for bulk power system restoration", *IEEE Transactions on Power Systems*, vol. 26, no. 3, pp. 1357–1366, Aug. 2011, ISSN: 0885-8950. DOI: 10.1109/TPWRS.2010.2089646 (cit. on p. 74).

[62] W. Sun, C. C. Liu, and S. Liu, "Black start capability assessment in power system restoration", in *Power and Energy Society General Meeting, 2011 IEEE*, Jul. 2011, pp. 1–7. DOI: 10.1109/PES.2011.6039752 (cit. on p. 75).

[63] C. E. Italiano, *Cei 0-21: Reference technical rules for connecting users to the active and passive lv distribution companies of electricity*, 2011 (cit. on pp. 79, 81).

[64] C. Norm, "Cei 0-16: Regola tecnica di riferimento per la connessione di utenti attivi e passivi alle reti at ed mt delle imprese distributrici di energia elettrica", *Comitato Elettrotecnico Italiano, Mailand*, 2012 (cit. on p. 81).

[65] K. D. Brabandere, B. Bolsens, J. V. den Keybus, A. Woyte, J. Driesen, and R. Belmans, "A voltage and frequency droop control method for parallel inverters", *IEEE Transactions on Power Electronics*, vol. 22, no. 4, pp. 1107–1115, Jul. 2007, ISSN: 0885-8993. DOI: 10.1109/TPEL.2007.900456 (cit. on p. 85).

[66] E. Demirok, P. C. González, K. H. B. Frederiksen, D. Sera, P. Rodriguez, and R. Teodorescu, "Local reactive power control methods for overvoltage prevention of distributed solar inverters in low-voltage grids", *IEEE Journal of Photovoltaics*, vol. 1, no. 2, pp. 174–182, Oct. 2011, ISSN: 2156-3381. DOI: 10.1109/JPHOTOV.2011.2174821 (cit. on p. 85).

[67] A. Camacho, M. Castilla, J. Miret, R. Guzman, and A. Borrell, "Reactive power control for distributed generation power plants to comply with voltage limits during grid faults", *Power Electronics, IEEE Transactions on*, vol. 29, no. 11, pp. 6224–6234, 2014 (cit. on p. 86).

[68] G. Angeli, G. Superti-Furga, and E. Tironi, "Harmonic damping by means of dg front-end converter. part i: Theory and algorithm", in *Harmonics and Quality of Power, 2008. ICHQP 2008. 13th International Conference on*, Sep. 2008, pp. 1–5. DOI: 10.1109/ICHQP.2008.4668834 (cit. on p. 89).

[69] S. D'Arco, L. Piegari, and P. Tricoli, "Harmonic compensation with active front-end converters based only on grid voltage measurements", in *Renewable Power Generation Conference (RPG 2014), 3rd*, Sep. 2014, pp. 1–6. DOI: 10.1049/cp.2014.0935 (cit. on p. 89).

[70] S. W. Kang and K. H. Kim, "Sliding mode harmonic compensation strategy for power quality improvement of a grid-connected inverter under distorted grid condition", *IET Power Electronics*, vol. 8, no. 8, pp. 1461–1472, 2015, ISSN: 1755-4535. DOI: 10.1049/iet-pel.2014.0833 (cit. on p. 90).

[71] W. Bower and M. Ropp, "Evaluation of islanding detection methods for utility-interactive inverters in photovoltaic systems", *Sandia report SAND*, vol. 3591, p. 2002, 2002 (cit. on pp. 93, 94).

[72] D. Dong, J. Li, D. Boroyevich, P. Mattavelli, and Y. Xue, "A novel anti-islanding detection algorithm for three-phase distributed generation systems", in *Applied Power Electronics Conference and Exposition (APEC), 2012 Twenty-Seventh Annual IEEE*, Feb. 2012, pp. 761–768. DOI: 10.1109/APEC.2012.6165905 (cit. on p. 95).

[73] H. Akagi and A. Nabae, "The p-q theory in three-phase systems under non-sinusoidal conditions", *European Transactions on Electrical Power*, vol. 3, no. 1, pp. 27–31, 1993 (cit. on p. 105).

[74] N. Mohan and T. M. Undeland, *Power electronics: Converters, applications, and design*. John Wiley & Sons, 2007 (cit. on p. 111).

[75] H. A. Kazem, "Harmonic mitigation techniques applied to power distribution networks", *Advances in power electronics*, vol. 2013, 2013.

[76] L. Ma, T. Kerekes, R. Teodorescu, X. Jin, D. Floricau, and M. Liserre, "The high efficiency transformer-less pv inverter topologies derived from npc topology", in *Power Electronics and Applications, 2009. EPE '09. 13th European Conference on*, Sep. 2009, pp. 1–10.

[77] Z. Chen, J. Guerrero, and F. Blaabjerg, "A review of the state of the art of power electronics for wind turbines", *Power Electronics, IEEE Transactions on*, vol. 24, no. 8, pp. 1859–1875, Aug. 2009, ISSN: 0885-8993. DOI: 10.1109/TPEL.2009.2017082.